Dissertation

submitted to the

Combined Faculties for the Natural Sciences and for Mathematics

of the Ruperto-Carola University of Heidelberg, Germany

for the degree of

Doctor of Natural Sciences

Presented by: B.Sc. Shiying Lu

Born in: Suzhou, Jiangsu, P.R.China

Oral-examination: February 16th, 2018

Gene Programs of Spinal Cord Cells Mediating Pain States:

Identification of Protein targeting to glycogen as an induced gene in spinal cord astrocytes upon peripheral pain

Referees:

Dr. Kyung-min Noh

Prof. Dr. Stephan Frings

Acknowledgement

I would like to thank my supervisors Prof. Dr. Jan Siemens, Prof. Dr. Rohini Kuner and Dr. Paul Heppenstall for giving me the opportunity to participate in the SFB 1158 project and the guidance throughout my project. I especially thank Prof. Dr. Jan Siemens for the indispensable support and the stimulating ideas, and for sharing with me the enthusiasm for scientific research. I also thank my thesis advisory committee members Dr. Kyung-min Noh, Prof. Dr. Stephan Frings, and Dr. Wolfgang Huber for the support and critical inputs. It has been a memorable and inspiring experience.

I am grateful to Dr. Hagen Wende for the many pivotal discussions throughout my project. I thank Dr. Wanessa du Fresne von Hohenesche and Dr. Hong Wang for sharing invaluable advices and tips, steering my curiosities for science, and the many happy memories we share. I also thank the current and past members of the University of Heidelberg Institute of Pharmacology and EMBL Genecore for your great help.

For this thesis, I would like to thank Dr. Hagen Wende and Prof. Dr. Jan Siemens for the comments, Dr. Wanessa du Fresne von Hohenesche for proofreading and Dr. Maria Bottermann for translating the abstract.

I thank all the wonderful people in my life for the many laughters I deeply cherish and for making me who I am today.

Abstract

Nociceptive pain signals are relayed in the spinal cord as they are transmitted from the periphery to higher brain centers. The neuronal populations in the spinal cord that transmit peripheral stimuli are very heterogeneous. This has hampered the identification of interneuron subtypes involved in pain processing and the characterization of their functional connectivities. In this study, I obtained a transcriptomic profile of spinal cord cells specifically activated by a peripheral painful stimulus using the recently developed phospho-ribosome profiling technique, and identified Protein targeting to glycogen (*Ptg*) as a pain-induced gene in spinal astrocytes. *Ptg* is known to play an important role in glycogenesis. I observed elevated spinal cord glycogen levels in response to different painful stimuli and proposed a correlation between the magnitude and duration of glycogen elevation with the persistency of different pain models. Moreover, manipulation of *Ptg* expression and glycogen metabolism led to altered pain sensitivity. My study points toward a new perspective of the role of astrocytes in pain processing and a potential link between changes in the metabolic state and pain processing in the spinal cord.

Zusammenfassung

Nozizeptische Schmerzsignale werden im Rückenmark vom peripheren Nervensystem an höhere Hirnzentren übertragen. Die Neuronenpopulationen im Rückenmark, die diese peripheren Signale übermitteln, sind heterogen was die Identifikation von Interneuron-Subtypen involviert in Nozizeption sowie die Charakterisierung ihres neuronalen Netzes erschwert. In der vorgelegten Studie habe ich mit der neu-entwickelten „phospho-ribosome profiling“ Methode das Transkriptomprofil von durch periphere Schmerzsignale aktivierte Rückenmarkszellen erhalten und Ptg (Protein targeting to glycogen) als ein schmerzinduziertes Gen in Astrozyten identifiziert. Ptg spielt eine wichtige Rolle in der Glykogenese und ich konnte ein erhöhtes Glykogenlevel als Reaktion auf verschiedene schmerzauslösenden Stimuli feststellen, sowie eine Korrelation zwischen dem Ausmaß und der Dauer des erhöhten Glykogenlevel und der Dauer verschiedener Schmerzmodelle. Außerdem habe ich demonstriert, dass Manipulation von Ptg-Expression und Glykogenstoffwechsel zu veränderter Schmerzsensitivität führt. Daher unterstützt meine Studie eine neue Sichtweise auf die Rolle von Astrozyten in der Nozizeption und eine potentielle Verbindung zwischen Veränderungen im Stoffwechsel und der Schmerzverarbeitung im Rückenmark.

Abbreviations

ANLS: astrocyte-neuron lactate shuttle
CCI: chronic constriction injury
CFA: complete freud's adjuvant
CNS: central nervous system
DAB: 1,4-dideoxy-1,4-imino-d-arabinitol
DNA: deoxyribonucleic acid/ cDNA: complementary DNA
DRG: dorsal root ganglion
GABA: gamma-aminobutyric acid
GYS: glycogen synthase
IEG: immediate early gene
IN: interneuron
iIN: inhibitory interneuron
IP: immunoprecipitation
α-KG: alpha-ketoglutaric acid
MCT: monocarboxylate transporter
NA: noradrenalin
OAA: oxaloacetic acid
PCR: polymerase chain reaction/qPCR: quantitative PCR
PN: projection neuron
PNS: peripheral nervous system
pS6: phosphorylated ribosome subunit S6
RNA: ribonucleic acid/ mRNA: messenger RNA
RT: room temperature
SNI: spared nerve injury
TCA: tricarboxylic acid cycle
TRP: transient receptor potential
TN: transmission neuron
VIP: vasoactive intestinal peptide

List of Figures and Tables

Table of contents

1. Introduction

I will first introduce pain as a physiological modality as well as the pathological forms of pain. Next I will summarize how nociceptive signals are transduced, with an emphasis on the current knowledge of spinal cord neuronal circuits and glial cells involved in pain processing. Furthermore I will introduce a technique called phospho-ribosome profiling that I employed in my thesis to identify spinal cord cells mediating pain.

1.1 What is pain?

First of all, pain and nociception are two different concepts. Pain is the feeling, or the perception of pinching, aching, stabbing, throbbing, as well as the unbearable or miserable sensations rising from a part of our body (Woolf & Salter, 2000). Nociception is the sensory process that provides the signals that trigger the conscious experience of pain (Bear et al., 2007).

The uncomfortable feeling of pain indicates that damage is happening or is about to happen (Bear et al., 2007) and it is therefore essential for survival: pain functions as a very useful early warning device that alerts our body against many harmful environmental stimuli and triggers protective responses almost instantly (S. Hunt, P. & Mantyh, 2001; Julius & Basbaum, 2001). Most of the time, pain is just a nuisance and goes away after a while. Other times it can be devastating. When pain is too intense or lingers for too long, additional physical symptoms emerge: nausea, weakness or drowsiness. Prolonged pain may even cause emotional effects such as anger and depression (Bear et al., 2007).

Pain is not homogeneous and is commonly classified into physiological and pathological pain (Woolf & Salter, 2000).

- **Physiological pain**

Physiological pain is the acute, 'useful' pain, as it triggers protective withdraw or escape responses. Unlike many other somatosensations, painful feelings can be evoked by many different stimuli. Physiological pain results from noxious stimuli such as (i) thermal: heat ≥ 43°C or extreme cold, (ii) mechanical: intense pressure or force, (iii) chemical: e.g. concentrated acid or pungent agents (Dubin & Patapoutian, 2010). In any case, the pain goes away as the stimulus fades and the wound heals. Physiological pain also usually responds well to opioid or non-steroidal anti-inflammatory drug medications.

- **Pathological pain**

There are two types of pathological pain: **inflammatory pain** initiated by tissue damage/inflammation and **neuropathic pain** by nervous system lesions. Both inflammatory and neuropathic pain are characterized by hypersensitivity at the site of tissue damage and in adjacent normal tissue. In both cases, pain may be elicited by normally non-painful stimuli (allodynia) or noxious stimuli may evoke a greater and more prolonged pain (hyperalgesia) (Woolf & Salter, 2000; Gangadharan & Kuner, 2013).

Inflammation is an adaptive response, eliciting physiological responses that promote wound healing. Inflammatory pain hypersensitivity usually returns to normal if the disease process is controlled (Medzhitov, 2008). Neuropathic pain, on the other hand, persists long after the initiating event has healed.

If pain persists longer than 6 months, it is classified as chronic pain. Chronic pain no longer serves a biological function and is now considered no longer a symptom of diseases but a disease itself (Basbaum et al., 2009). Chronic pain affects up to 30% of the adults in the world, and there is no adequate medication to improve patients' conditions (Woolf & Salter, 2000).

1.2 The pain pathway: peripheral nervous system

The perception of pain involves the peripheral and the central nervous systems (PNS and CNS) (Damann et al., 2008). The painful stimulus is first detected in the periphery, by nociceptors.

A needle pinch, like the gentle brush from the spring breeze or the rising temperature under the sun, is felt through our skin. In order to accurately sense all these stimuli, skin is heavily innervated by various somatosensory neurons. Among them, nociceptors sense the high threshold, pain-inducing stimuli (Bove & Swenson, 2007; Y. Liu & Ma, 2011).

Nociceptors, like other somatosensory neurons, are pseudo-unipolar neurons. This means the cell body (soma) sits in the dorsal root ganglia (DRG), with two branches of one single axon projecting to both the skin (peripheral) and the spinal cord (central). The axons of somatosensory neurons are classified as Aß-, Aδ-, or C-fibers, which have different degrees of myelination: the thickly myelinated Aß fibers, the thinly myelinated Aδ fibers, and the un-myelinated C fibers (Fig. 1A) (Bear et al., 2007). Nociceptors comprise of either Aδ or C fibers. The Aδ nociceptive fibers detect the fast, sharp, precise-localized ‘fast pain’ and un-myelinated nociceptive C fibers convey the second wave of longer-lasting and poorly localized ‘slow pain’. The third type of fiber, Aß fibers, sense mechanical stimulation (Bear et al., 2007; Bove & Swenson, 2007).

- **Types of nociceptors**

As pain could be induced by excessive mechanical, thermal or chemical stimuli, nociceptors are accordingly classified by the sensory modalities that they respond to. However, unlike mechanoreceptors or thermoreceptors which respond only to mechanical or thermal stimulus, a large group of nociceptors is polymodal, i.e. they

respond to a combination of thermal, mechanical and/or chemical stimuli: HTM (high-threshold mechanical) nociceptors respond to both mechanical and chemical stimuli, as well as heat greater than 50°C (Basbaum et al., 2009); or CMH (C-fiber mechano-heat-responsive) nociceptors detect both noxious heat and excessive pressure (Perl, 2007). There are in addition also a group of silent nociceptors, which respond to none of these modalities under normal conditions, but can be activated when injury and inflammation occur (Schmidt et al., 1995).

- **Activation of nociceptors**

How do nociceptors 'sense' the noxious stimuli? Nociceptors express a unique repertoire of ion channels and receptors (Benarroch, 2015).

The largest group of noxious stimulus detectors is the transient receptor potential (TRP) channel family, among which (i) TRPV1 is activated by capsaicin and heat, and (ii) TRPA1 is activated presumably by mechanical stimulus (Mickle et al., 2016) and has been reported as a key chemical sensor. Many pungent chemicals such as formalin, the most commonly used agent to assay chemical nociception in rodent, activate TRPA1 (Patapoutian et al., 2009). In addition to these two better studied TRP channels, roles of many more nociceptive TRP channels are being revealed.

In addition to TRP channels, subtypes of voltage-gated Ca^{2+} and Na^{+} channels, K^{+} channels, acid sensing ion channels, hyperpolarization-activated cyclic nucleotide-gated channels, TMEM16 channels, as well as 5-HT_3 receptors and P2X family receptors have be shown to be triggered by various noxious stimuli (Benarroch, 2015).

The activated channels or receptors convert noxious mechanical, thermal, chemical stimuli into electrical activities at the peripheral terminals of nociceptors (Damann et al., 2008). The electrical signals then travel from the peripheral branch of the axon to the central branch, towards the central nervous system.

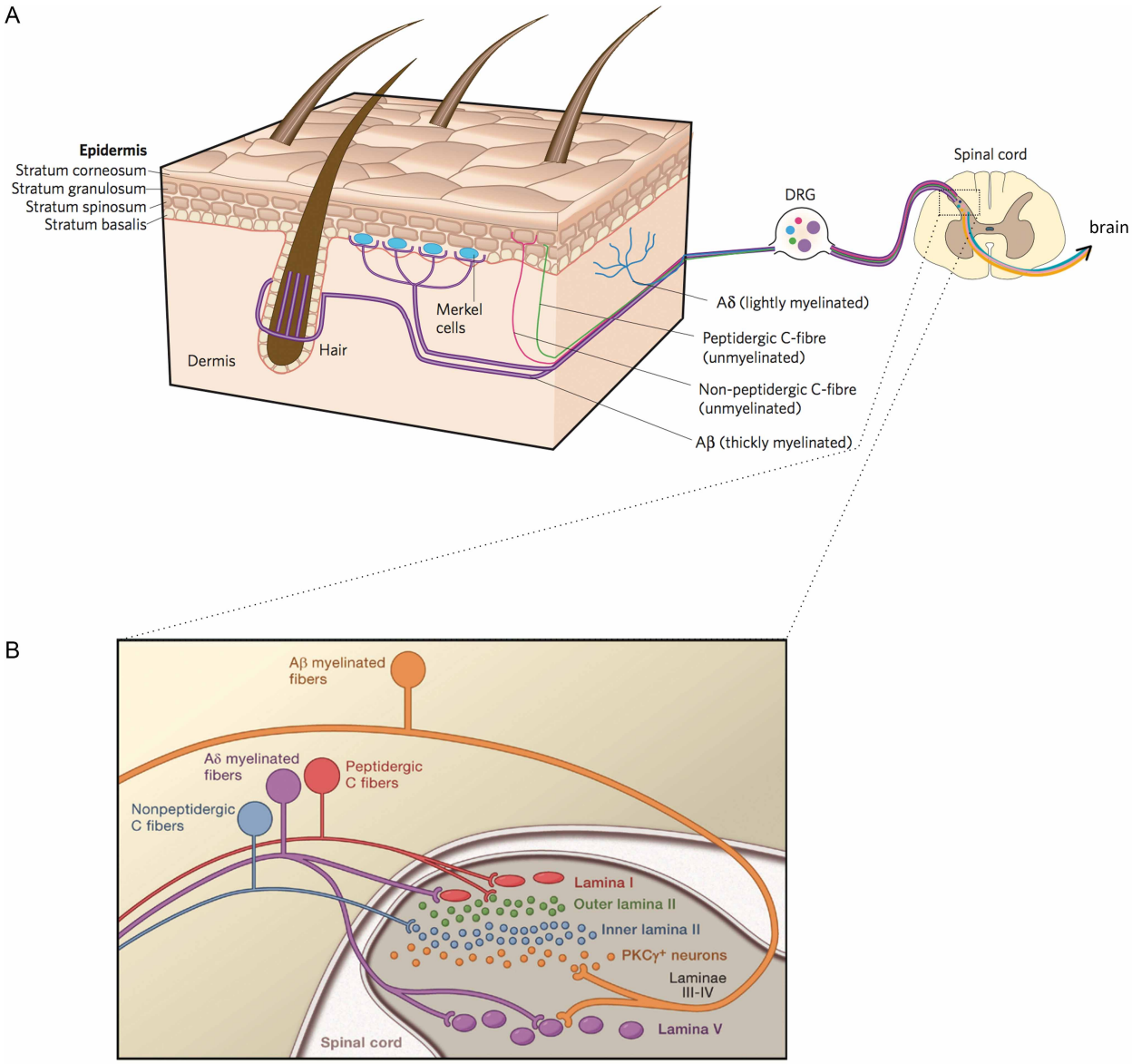

Figure 1: The pain pathway
1A: The pain pathway: primary sensory neurons innervate the skin via various types of sensory afferents: thickly myelinated Aß fibers sense mechanical stimuli, thinly myelinated Aδ fibers detect pain and temperature, and un-myelinated C fibers are responsible for pain, temperature and itch. The fibers project first to spinal cord in a lamina-specific fashion and then further to the brain. Adapted from (Lumpkin & Caterina, 2007).
1B: Connections between primary afferents and the spinal cord. Aß fibers (orange) project to deeper laminae III and IV, Aδ fibers (purple) project to both outer lamina II and lamina V, peptidergic C fibers (red) project to superficial lamina I, and non-peptidergic C fibers (blue) project to inner lamina II. Adapted from (Basbaum et al., 2009).

1.3 The pain pathway: central nervous system

Of the central nervous system (CNS), spinal cord is the first relay station of peripheral stimuli and the processed information then enters the higher brain center. As I aim to gain more knowledge of pain precessing at the spinal cord through my project, I will put an emphasis on summarizing the current knowledge on spinal cells (neurons and glia) involved in pain processing.

1.3.1 Spinal cord neurons in pain processing

The spinal cord is the first relay station in the processing of noxious stimuli from the periphery. Axons of different somatosensory neurons project into the spinal cord dorsal horn, where nociceptive information is integrated along with other somatic sensory information.

The central branches of the somatosensory neuron axons enter the dorsal horn of the spinal cord and synapse on the dorsal horn cells (Bear et al., 2007). Information processing in the dorsal spinal cord is segregated: different axon fibers project to different layers of the dorsal spinal cord (Fig. 1B). Nociceptive Aδ- and C-fibers project to the superficial dorsal layers (laminae I and II) while the non-nociceptive Aδ- and mechanoreceptive Aß- fibers project to the deeper dorsal layers (laminae III-V) (Basbaum et al., 2009). The dorsal horn neurons are comprised of a large variety of interneurons (IN) and a smaller group of projection neurons (PN) (Todd, 2010).

Interneurons are named so because their axons remain in the spinal cord and arborize locally. There are two main types of interneurons: (i) excitatory interneurons, which utilize glutamate as their neurotransmitters, i.e. glutamatergic; and (ii) inhibitory interneurons, which use gamma-aminobutyric acid (GABA) alone or a

combination of GABA and glycine as their main neurotransmitters. Interneurons are also classified by their dendritic morphologies: islet, central, vertical and radial (Grudt & Perl, 2002). This morphological classification however remains a very crude one as morphological features do not necessarily correlate with molecular and functional diversities, which are only starting to be revealed.

Excitatory interneurons have been shown to be diverse in terms of marker expression and the functional properties of some of these different neuron types have already been analyzed. Calretinin (*Calb2*)-expressing neurons for instance spread over laminae I and II, and are suggested to transmit only light acute mechanical pain (Duan et al., 2014b). Protein kinase C gamma (*Pkc-γ)*-expressing neurons are expressed in lamina I and inner lamina II, and has been proposed to mediate mechanical allodynia (Koch et al., 2017). Somatostatin (*Som*)-expressing neurons are one of the most abundant excitatory interneurons (~60%) (Gutierrez-Mecinas et al., 2016; Todd, 2017) and are found from laminae I to III. These *Som*-expressing neurons have been shown to be involved in acute mechanical pain. Ablation of *Som*-expressing neurons leads to the loss of both static and dynamic allodynia upon inflammatory pain, while transient activation of *Som*-expressing neurons results in immediate nocifensive responses (Duan et al., 2014b; Christensen et al., 2016). *MafA*-expressing neurons are localized mainly in laminae III and IV (Del Barrio et al., 2013) but also scatter into laminae I and II (Appendix). Altered mechanical pain threshold has been observed in *MafA*-knock-out mice after inducing chronic pain (Appendix). Cholecystokinin (*Cck*)-expressing neurons are localized mainly in the deeper dorsal horn. The ablation of *Cck*-expressing neurons leads to a transient insensitivity to noxious cold (Haueter, 2016).

Subgroups of inhibitory interneurons have been identified and their functions in pain processing studied. Dynorphin (*Dyn*)-expressing neurons are enriched in superficial laminae (Xu et al., 2008). Spinal *Dyn*-ablated mice are reported to show spontaneous development of both static and dynamic mechanical allodynia (Duan et al., 2014b). Glycine transporter 2 (*Glyt2*)-expressing neurons spread through the

deeper dorsal horn laminae III-V (Zeilhofer et al., 2012). Ablation or silencing of spinal *Glyt2*-expressing neurons results in an abnormally exaggerated sensitivity to mechanical, heat and cold stimuli and the development of spontaneous pain. Conversely, activation of the same neurons alleviated neuropathic hyperalgesia (Foster et al., 2015).

Projection neurons are mainly located in lamina I but are also found scattered through laminae II–VI. The projection neurons project to the brain. Although the brain areas to which their ascending axons project to have been largely mapped, the heterogeneity of the lamina I projection neurons remains an obstacle to categorize them into discrete groups. The Neurokinin 1 receptor (*Nk1r*) is expressed by many lamina I projection neurons (~80%) and ablation of *Nk1r*-expressing neurons prevents the development of both mechanical and thermal hyperalgesia (Mantyh et al., 1997; Todd, 2010; Weisshaar & Winkelstein, 2014).

In addition of lamina specific markers, combinations of markers have also been reported to define subpopulations of spinal cord neurons, such as in the study by Del Barrio and colleagues (Del Barrio et al., 2013), in which a set of nine transcription factors (Fig.2A) was used to define nine different inhibitory and excitatory interneuron populations. These recent studies on dorsal horn lamina-specific neuron populations and their roles in pain processing have resulted in a dramatic improvement in our understanding of pain processing at the spinal level (Todd, 2017).

- **Spinal cord pain circuit**

Spinal cord neurons are not only extremely heterogenous themselves, they also form sophisticated circuits in pain processing. Ronald Melzack and Patrick Wall proposed the *gate theory of pain* in the 1960s to explain the interaction between the excitatory and inhibitory circuits in spinal cord pain processing (Ronald & Patrick, 1965).

The *gate theory of pain* hypothesizes that nociceptive transmission neurons (TN) of the spinal dorsal horn are activated not only by high-threshold Aδ/C nociceptors,

but also by low-threshold Aß mechanoreceptors. However, this input from Aß mechanoreceptors is gated by feed-forward activation of inhibitory interneurons (iIN) (Fig.2B). Therefore, (i) when there is only high-threshold painful stimulus, the nociceptive TN is activated. In addition, as iIN is inhibited by painful stimulus, maximal nociceptive signals ascend to the brain. (ii) When there is only low-threshold mechanical stimulus, activation of iIN prevents low-threshold mechanical stimulus from activating the pain transmitting TN. (iii) If there are simultaneous inputs from high-threshold Aδ/C nociceptors and low-threshold Aß mechanoreceptors, activated iIN suppresses the activity of TN, thus reducing the nociceptive signals rising to the brain. This is why it feels good to rub the skin around a bruise. To sum this up, spinal nociceptive transmission neurons are gated by inhibitory interneurons through feed-forward inhibition (Duan et al., 2014b; Peirs et al., 2015).

Since the proposal of the *gate theory of pain*, numerous studies have tried to test the key argument of the theory. This theory first of all correctly predicted that disinhibition (the injured state) could be a reason for the development of mechanical allodynia, i.e. pain by innocuous mechanical stimuli (Zeilhofer et al., 2012; Prescott et al., 2014). And several electrophysiological studies have since revealed the existence of a circuit linking input to lamina III by mechanosensitive Aß fibers with lamina I projection neurons (Torsney & MacDermott, 2006; Takazawa & MacDermott, 2010). However, the precise make up of the spinal cord pain circuit is only starting to be discovered (Duan et al., 2014a). Below I summarize the main recent findings in spinal pain circuits:

Lamina III glycinergic (*Glyt2*$^{+}$) neurons are believed to represent one group of the above-described iIN. They are inhibitory interneurons and are innervated by Aß fibers. Ablation of *GlyT2*$^{+}$ neurons leads to hyperalgesia, while activation of them effectively alleviates neuropathic pain, indicating a role of *Glyt2*$^{+}$ neurons in gating pain. Paired patch-clamp recordings showed that inner lamina II *Pkc-γ*$^{+}$ interneurons are gated by these glycinergic inhibitory interneurons through feed-forward inhibition. In the original *gate theory of pain*, TN was proposed to comprise solely of projection

neurons, but this study suggests that TNs can also be lamina II interneurons (Lu et al., 2013; Foster et al., 2015).

Som$^+$ excitatory interneurons and *Dyn*$^+$ inhibitory interneurons are another pair identified as the TN and IN in the gate theory, respectively. *Som*$^+$ neurons receive both low-threshold Aß mechanical and high-threshold Aδ/C nociceptive inputs. Upon ablation of dorsal spinal cord *Dyn*$^+$ neurons, *Som*$^+$ excitatory neurons are activated by low-threshold mechanical stimulus. *Dyn*$^+$ inhibitory neurons thus act to prevent low-threshold mechanical stimulus from activating *Som*$^+$ excitatory neurons, i.e. *Dyn*$^+$ inhibitory neurons gate *Som*$^+$ excitatory neurons (Duan et al., 2014b).

Two additional IN groups have been identified: (i) lamina III inhibitory interneurons expressing parvalbumin (*Pv*$^+$) gate *Pkc-γ*$^+$ excitatory interneurons. PV$^+$ neurons have been proposed to modulate hypersensitivity especially in inflammatory and neuropathic pain (Petitjean et al., 2015); and (ii) lamina III-V inhibitory interneurons with neonatal expression of receptor tyrosine kinase (*Ret*$^+$) gate both *Som*$^+$ and *Pkc-γ*$^+$ excitatory interneurons. These transient *Ret* expressing neurons are involved in modulating mechanical pain as well as inflammatory and neuropathic pain (Cui et al., 2016; Koch et al., 2017).

In a subsequent study, a lamina III to I circuit involved in persistent mechanical pain (neuropathic and inflammatory) transmission was mapped (Peirs et al., 2015). A group of Lamina III excitatory interneurons with transient postnatal *Vglut3* expression receives Aß input and synapses to the more dorsal lamina II excitatory interneurons expressing *Pkc-γ* and *Calb2*, which act to refine the excitability of the circuit. The lamina II vertical cells then integrate these signals and send an output to the lamina I nociceptive *Nk1r*$^+$ projection neurons (Peirs et al., 2015). Dorsal horn ablation of this transient *Vlgut3*$^+$ interneuron population reduces the brush-evoked dynamic mechanical hypersensitivity, but not the filament-evoked punctate hypersensitivity (Cheng et al., 2017).

To briefly summarize the above-mentioned spinal cord pain circuits, with a focus on mechanical pain processing, TN (*Som*$^+$ /*Pkc-γ*$^+$/*Calb2*$^+$ neurons) are gated via feed-forward activation of IN (*GlyT2*$^+$/*Dyn*$^+$/*PV*$^+$/*Ret*$^+$ neurons), preventing the activation of nociceptive TN by low-threshold mechanical inputs. The exact interaction and segregation of the four IN populations are not yet clear (Duan et al., 2017). And under persistent mechanical pain, transient *Vlgut3*$^+$ interneurons are activated to convey mechanical hyper-sensitivities. Despite the tremendous progress, we still have many gaps to fill for a generally accepted scheme that covers all the spinal dorsal horn neurons and their circuits.

1.3.2 Spinal cord glia in pain processing

The nervous systems mainly consist of two cell types, the neurons and the glia. The role of neurons, primary or spinal, has been the main focus of pain research. For quite a long time, the predominant thinking in the pain field was that pain was purely a matter of miscommunication between neurons (Miller, 2005). There has been emerging evidence suggesting the involvement of glia in pain hypersensitivity. Originally considered as supporting cells to neurons, glial cells have now been shown to actively communicate with neurons and contribute to many aspects of neuronal functions including pain processing (Kohno, 2010; Chiang et al., 2012). Glial cells make up over 70% of the CNS cells and are divided into astrocytes, oligodendrocytes and microglia (Fig.2C).

Astrocytes are named after their star shape. They are the most abundant glial cell type, making up 40% to 50% of all glia cells (Aldskogius & Kozlova, 1998). There are two main categories of astrocytes: (i) Protoplasmic astrocytes in the gray matter with a morphology of several stem branches and many finely branching processes in a

uniform globoid distribution, and (ii) Fibrous astrocytes in white matter and have many long fiber-like processes (Fiacco et al., 2009). Astrocytes are known to fulfill many functions including the maintenance of the homeostasis, metabolic support for neurons, and maintenance of the blood-brain barrier (Sofroniew & Vinters, 2010).

Microglia are the resident macrophages in the CNS, as they act as the first and main form of active immune defense. In resting states, microglia are ramified with thin branches. Once reactive i.e. activated, they become amoeboid with thick and short branches (Ru-Rong Ji & Wen, 2006).

Oligodendrocytes are the myelinating cells in the CNS. Their main functions are to provide support and insulate CNS axons with the myelin sheath.

- **Spinal astrocytes and microglia in pain processing**

Astrocytes are the only glial cells to form networks with themselves and are closely associated with neurons. Each astrocyte is estimated to be in contact with 300 to 600 neuronal dendrites (Halassa et al., 2007). This close contact makes astrocytes capable of responding to neurotransmitters. In addition, upon peripheral tissue damage or inflammation, spinal dorsal horn astrocytes become reactive and release gliotransmitters, which in turn regulate nociceptive neuronal activities (Chiang et al., 2012). Spinal astrocytes undergo biochemical, translational, transcriptional, and morphological changes when they become reactive. Some changes occur within minutes after receiving peripheral nociceptive stimuli, such as increasing intracellular Ca^{+} level and phosphorylation of signaling molecules, e.g. p-JNK. Translational modifications and transcriptional regulations happen after tens of minutes to one hour. Morphological change such as astrocyte hypertrophy may occur only hours or even days later (Gao & Ji, 2010).

Microglia have been shown to be the quickest responder to peripheral nerve injury (Kreutzberg, 1996). In most cases, microglial reaction precedes astrocytic reaction and

likely leads to astrocyte reaction, though the activity of the two are not always linked (Hald et al., 2009; Gao & Ji, 2010).

Activation of spinal astrocytes and microglia has been reported in many pain models:

Inflammatory pain:

Astrocyte activation was found in formalin-induced pain, preceding microglia activation. It is suggested that astrocytes modulate the formalin-induced hyperalgesia via astrocytic-neuronal heterotypic gap junctions (M. Qin et al., 2006). In complete freud's adjuvant (CFA)-induced pain, gene expression studies showed elevated microglial markers through all phases (acute, subacute and chronic) of the inflammation. While on the contrary, up-regulation of astrocytic markers was observed only during the subacute and chronic phases (Raghavendra et al., 2004). Upon zymosan-induced pain, blocking glial metabolism resulted in a marked, but reversible, attenuation of the persistent thermal and mechanical hyperalgesia (Meller et al., 1994).

Neuropathic pain:

Astrocyte activation has been shown in various neuropathic pain models, e.g. spared nerve injury (SNI) and chronic constriction injury (CCI). It is suggested that astrocytes are involved in the maintenance phase of chronic neuropathic pain, rather than during the onset (Garrison et al., 1991; Tanga et al., 2006). Microglia, on the other hand, are quickly activated after peripheral nerve injury and are involved in both the onset and the maintain of chronic neuropathic pain (Hains & Waxman, 2006).

Although the involvement of astrocytes and microglia in pain processing is widely proven, and we are starting to unravel the modulators and pathways of glia-neuron interaction (Guan et al., 2016; Lim et al., 2017), there remains many missing links in the mechanism of glia-neuron interaction in pain processing to be discovered.

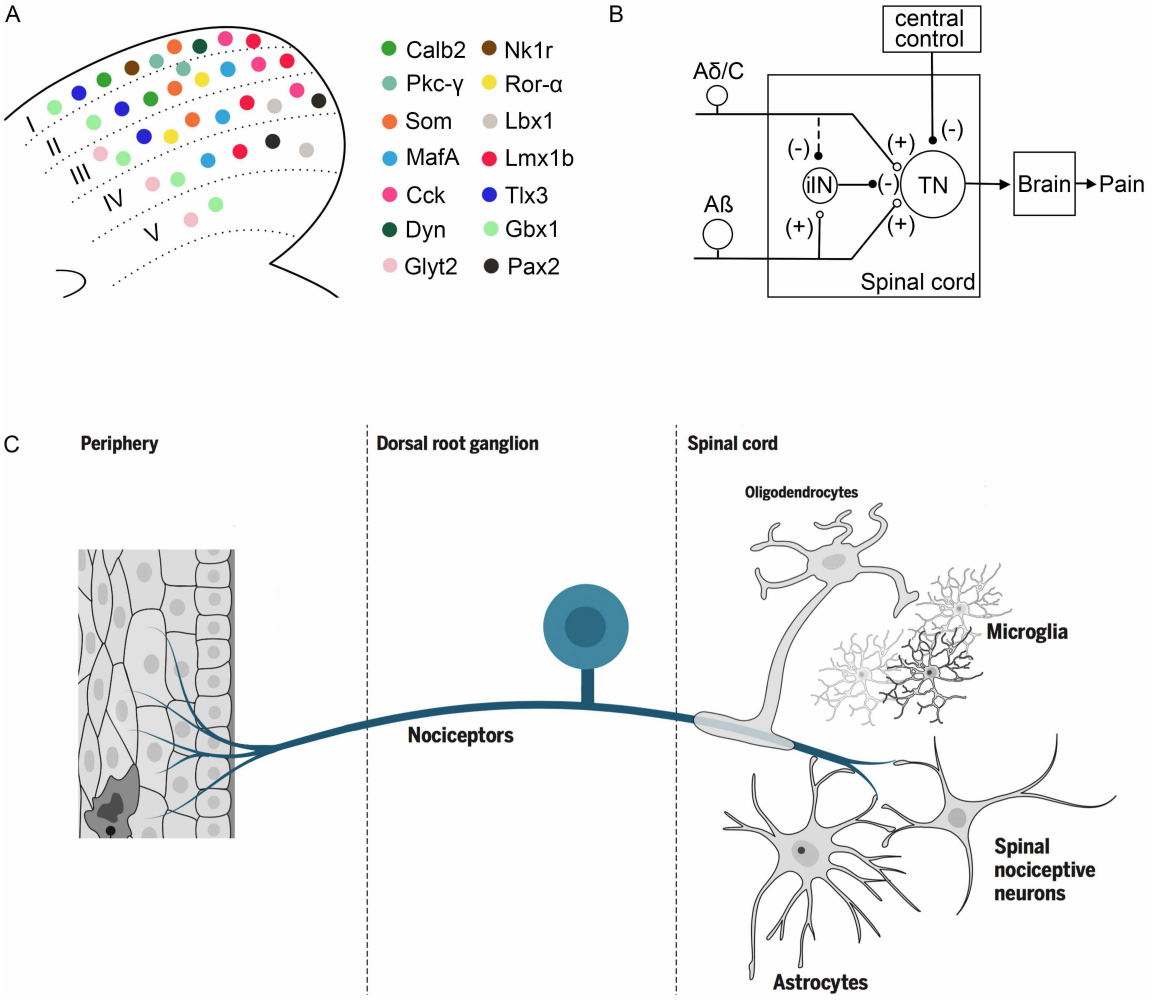

Figure 2: Spinal cord pain processing
2A: Lamina distribution of few known dorsal spinal cord-specific genes.
2B: Gate theory of pain. Spinal transmission neurons (TN) are gated by inhibitory interneurons (iIN) through feed-forward inhibition: TN is activated by both nociceptive Aδ/C fibers and mechanosensitive Aß fibers, and inhibited by the neighboring iIN. iIN is activated by mechanosensitive Aß fibers and inhibited by nociceptive Aδ/C fibers. Therefore, when there is only nociceptive signal, iIN is silent and maximal signal is sent to the brain from TN; when there is a combination of nociceptive and mechanical stimuli, iIN is activated, which in turn reduces the signal sent by TN. Adapted from (Duan et al., 2014a).
2C: Glial cells are in vicinity of neurons and hold important functions in the central nerve system (CNS) including spinal cord, shown here. Astrocytes are the most abundant of the glial cells and are in closest communication with neurons, serving diverse functions from maintaining homeostasis to metabolic support. Microglia are the resident macrophage of CNS and oligodendrocytes are the myelinating cells in the CNS. Adapted from (Ru-Rong. Ji et al., 2016).

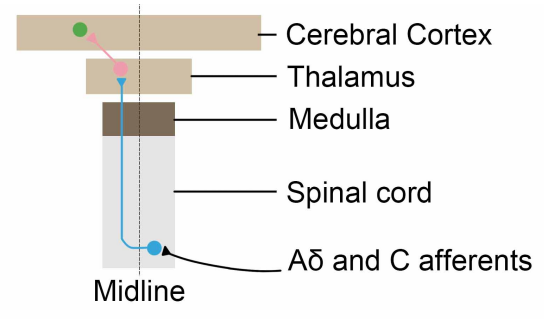

Figure 3: The spinothalamic pathway
The spinothalamic pathway. Spinal cord neurons, which receive nociceptive signals from primary Aδ/C fibers, decussate immediately and ascend to thalamus without synapsing. The thalamic neurons then project to cerebral cortex, where nociceptive signals are translated to the perception of pain. Adapted from (Bear et al., 2007).

1.3.3 Pain processing at higher brain centers

Nociceptive information is conveyed from the spinal cord to the brain via the spinothalamic pathway (Fig.3). The axons of spinal projection neurons decussate immediately to the opposite side of the spinal cord, i.e. nociceptive information travels contra-laterally, and ascend through the spinothalamic tract running along the ventral surface of the spinal cord. As the name spinothalamic indicates, the spinothalamic fibers project up the spinal cord and go through first medulla, pons and midbrain without synapsing, until they reach the thalamus. From the thalamus, nociceptive information is projected to various areas of the cerebral cortex (Bear et al., 2007; Segerdahl et al., 2015). Activation of nociceptors can lead to the conscious experience of pain. However, pain can be felt without activity in nociceptors i.e. the brain may experience pain without receiving any input from peripheral nociceptors (Bear et al., 2007; Dubin & Patapoutian, 2010).

Characterization of both the brain regions that are involved in pain processing and the peripheral nociceptors has been the main focus of pain research. While research in the last decade has tremendously enriched our knowledge about spinal cord pain processing, we still have many gaps to fill.

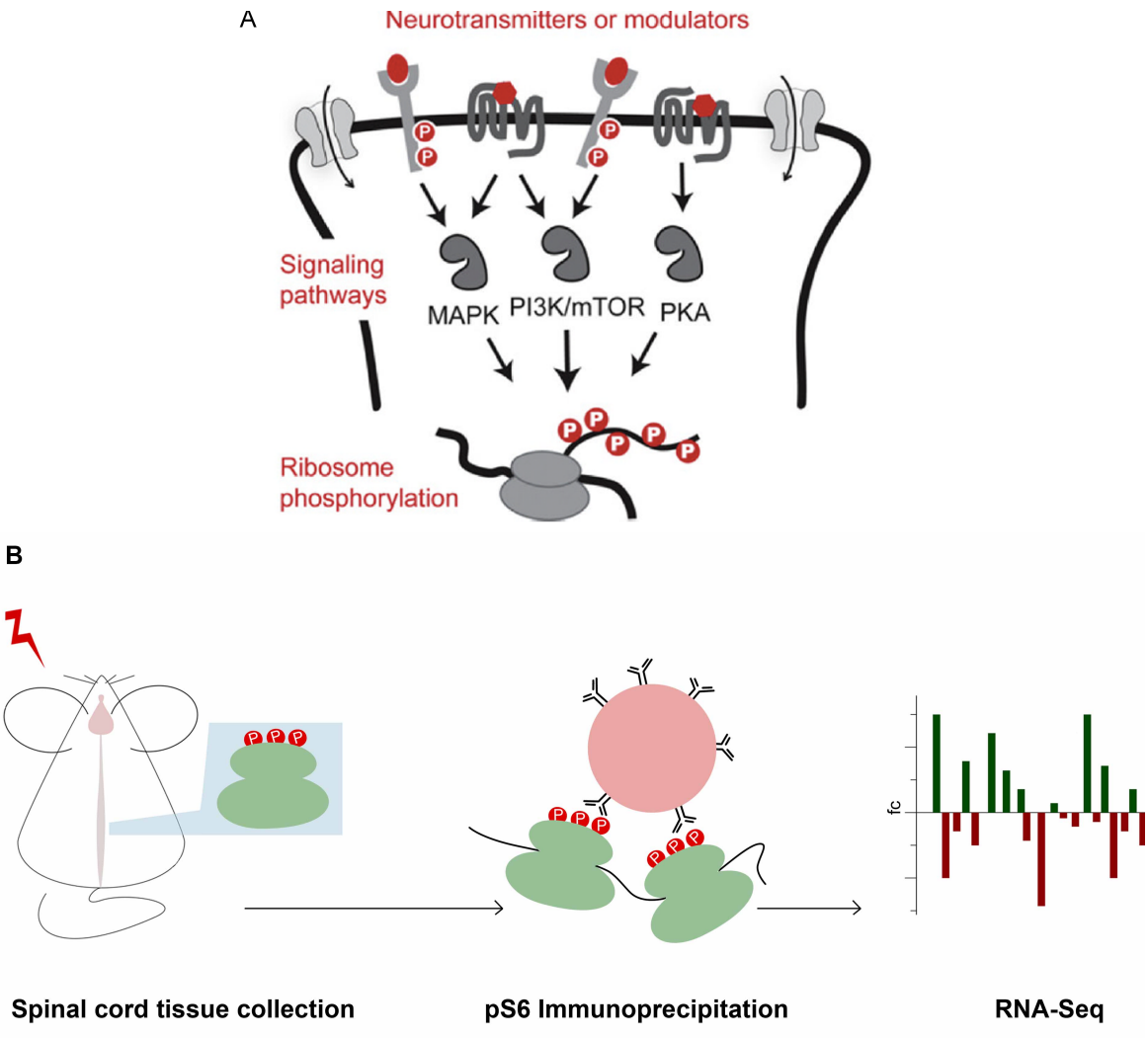

Figure 4: Ribosome phosphorylation and phospho-ribosome profiling
4A: Neurotransmitters and modulators activate a set of signaling pathways. Ribosomal protein S6 is downstream of these pathways and is phosphorylated in an activity-dependent fashion. Adapted from (Knight et al., 2012).
4B: Phospho-ribosome profiling experiment scheme: Mice are administrated a peripheral painful stimulus. Upon receiving the nociceptive signals, spinal cord pain processing cells are activated and subsequently show enhanced S6 phosphorylation (pS6). pS6 immunoprecipitation (IP) is performed to enrich for the phospho-ribosome bound mRNA from these activated cells. Subsequent transcriptome analysis of the collected mRNA reveals the molecular profiles of the activated cells.

1.4 Phospho-ribosome profiling

In spinal pain processing research, studies of neurons have been mainly based on electrophysiology and the manipulation of cell populations with known distinct dorsal spinal cord expression patterns (see section 1.3). Till date, there remains gaps in our knowledge about the molecular and functional diversity of spinal cord cells.

During my PhD, I aimed to expand our understanding of spinal pain processing from an activity-dependent angle i.e. to look for the cell populations responsible for a certain defined nociceptive response, rather than the 'phenotypical and behavioral characterization of a defined cell population' approach that has been employed in the aforementioned studies.

A recently developed technique by Knight and colleagues allows the transcriptomic analysis of cells that are specifically activated by certain stimulus (Knight et al., 2012). This technique, termed phospho-ribosome profiling, takes advantage of the activity-dependent phosphorylation process of the ribosomal protein S6 (pS6), which is downstream of PI3-K/mTOR, MAPK and PKA signaling pathways. These same pathways lead to the expression of known activity-dependent genes such as *c-Fos* (Fig.4A). Antibodies against the phosphorylated S6 episode can therefore be used to capture ribosomes from cells that have been activated by a given stimulus. Using pS6 immunoprecipitation, the mRNA bound to these ribosomes can be isolated. Thereby, mRNA from the activated cells is selectively enriched. Population markers or stimuli-specific gene inductions can subsequently be revealed by mRNA sequencing. Phospho-ribosome capturing has been successfully employed to identify hypothalamic neuronal populations activated by salt challenge or fasting and stimuli-specific odorant receptor expressions in olfactory neurons (Knight et al., 2012; Jiang et al., 2015). I reasoned that this technique would provide me a link between functions and molecular profiles of the spinal cells activated during pain processing.

1.5 Objectives

Despite the tremendous progress that has been achieved in the recent years, there are still many interesting questions in the pain field, especially (1) what stable markers are there that distinguish spinal cell populations specifically activated during (chronic) pain processing? and what are the exact mechanism of these cells in the spinal pain circuits? (2) what are the genetic programs that are specifically altered in spinal cells activated by peripheral painful stimuli? which particular cell types contribute to these transcriptional changes and how might the altered gene expression affect structural changes that are involved in pain processing and the development of chronic pain states?

To address these questions, I employed the phospho-ribosome profiling technique for the advantages of (i) the phosphorylation of ribosome is activity dependent, and (ii) the mRNA bound to the phosphorylated ribosomes carry the molecular profiles of the activated cells. I would obtain transcriptomic profile of spinal cells specifically activated by peripheral pain.

As we already know, pain is very heterogeneous, and so are spinal cell populations. While tremendous progress has been made in deciphering the molecules and mechanisms that mediate the activities of peripheral nociceptors, we are only at the start to understand the interneurons and projection neurons in the dorsal spinal cord, let alone the recently emerging spinal glial cells.

With the help of resources such as the Allen Brain Atlas, we can now look up the expression patterns of numerous genes in the nervous systems, including spinal cord. As previously summarized, progress has been made in investigating the roles of certain spinal dorsal horn neuron populations in pain processing. These studies were mainly performed by selectively and specifically ablating or activating spinal neurons which express certain marker genes, followed by pain-related behavioral

characterization. In my study, I aim to extend our understanding of spinal pain processing from a different angle, to look for genes which mark spinal cell population and genes whose expressions are specifically altered in spinal cells activated by peripheral painful stimuli.

I took formalin-induced acute pain as the pain model to start with. I first established and optimized the phospho-ribosome profiling protocol in spinal cord tissue, as the original study by Knight and colleagues was performed in hippocampus and using different stimuli (Knight et al., 2012). After the modifications were finalized, I performed pS6 immunoprecipitation and the subsequent deep sequencing of the collected phospho-ribosome-bound mRNA (experiment scheme illustrated in Fig.4B). Following sequencing data analysis, I verified a list of selected candidates by means of qPCR and *in situ* hybridization staining. I then focused my study on one of the verified candidates, Protein targeting to glycogen (*Ptg)*, and studied its involvement in spinal pain processing.

2. Result

2.1 Establishing spinal cord phospho-ribosome profiling

In my project, I aimed to use phospho-ribosome profiling to identify stable markers of spinal cells and specifically altered gene expressions involved in pain processing. To do this, I first characterized the activity-dependent phosphorylation of the ribosomal subunit S6 (pS6) in the spinal cord in the context of painful stimulation of the hind paw.

2.1.1 Comparison of S6 phosphorylation with c-Fos expression in the dorsal spinal cord upon formalin-induced acute pain

The expression of the immediate early gene *c-Fos* has classically been used as a marker for neuronal activity (S. P. Hunt et al., 1987; Morgan & Curran, 1991). *c-Fos* was also shown to be induced in dorsal spinal cord neurons upon formalin-induced acute pain (Harris, 1998). Therefore, I examined *c-Fos* mRNA expression in the dorsal spinal cord upon formalin-induced acute pain and compared it to S6 phosphorylation (pS6) in order to confirm the validity of pS6 as an activity marker in the spinal cord. I first characterized the rostral-caudal expression pattern of *c-Fos* in the spinal cord after formalin injection into the hind paw. Lumbar spinal cord tissue was collected 2 hours after unilateral intraplantar formalin injection into the hind paw and *c-Fos* mRNA was visualized by *in situ* hybridization (Fig.5A). Strong *c-Fos* mRNA was detected through the spinal dorsal horn ipsilateral to the formalin injection, while weak expression was also observed in the deep layers (laminae III and deeper) of the contralateral side i.e. *c-Fos* mRNA is strongly and specifically induced in ipsilateral (stimulated) laminae I-III.

The somatosensory inputs from the hind limb are processed at lumbar spinal cord levels. Rostral-caudally, there are 6 sections of lumbar cord (L1 being the most rostral section and L6 the most caudal) (Bear et al., 2007). When I examined the rostro-caudal distribution of *c-Fos* upon formalin injection in the hind paw, I observed *c-Fos* mRNA expression through out L2 to 6, peaking at L3 and L4 .

Next, I performed immunofluorescent stainings of c-FOS and pS6 on spinal cord cross sections using the formalin-induced acute pain model. Since both c-FOS and pS6 antibodies available to me at the time were raised in rabbits, co-staining of the two was unfortunately not possible. Nevertheless, comparing their protein expression on consecutive sections revealed similar patterns in superficial laminae I to III, marked by the solid white line (Fig.5B). Although pS6 was widely distributed in the deeper dorsal layer and ventral spinal cord, its expression in the superficial dorsal horn was specific to the formalin stimulation and therefore could be used as an activity marker for the spinal cells activated by formalin-induced acute pain.

2.1.2 Spatial distribution and time kinetics of spinal pS6

2.1.2.1 Spatial distribution

Both *c-Fos* and pS6 were specifically induced in the superficial dorsal horn. I therefore asked whether they would also share the same rostro-caudal distribution. Hence, I performed whole mount immunofluorescent staining to visualize pS6 across the lumbar spinal cord. Z-stack images were taken through the superficial dorsal horn and a maximal projection image of the pS6 expression profile was generated (Fig.5C). Ipsilateral specific pS6 expression was observed through L3 to L6, with maximal intensity at L4. This spatial distribution was confirmed by stainings of spinal cord cross-sections of L3 to 6 (Fig.5D).

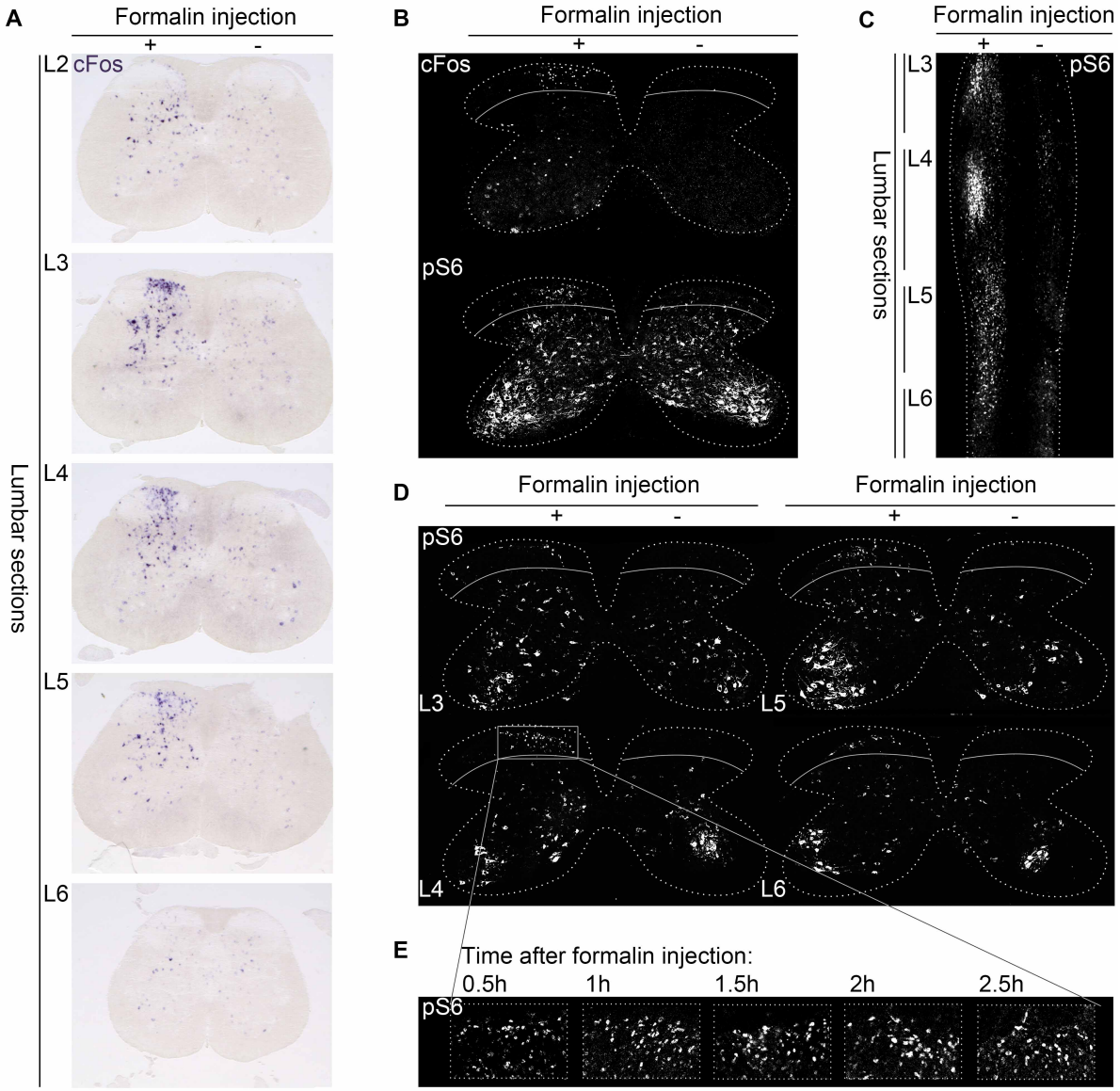

Figure 5: pS6 marks spinal cord cells activated by peripheral painful stimulus

5A: *c-Fos* mRNA expression (*in situ* hybridization) in dorsal spinal cord 2 hours after intraplantar formalin injection. The expression spread through lumbar section L2 to 6 and was specific to the ipsilateral (side of injection) spinal cord in superficial laminae I-III.

5B: Expression patterns of c-FOS (up, immunofluorescence) and pS6 (down, immunofluorescence) at L4 spinal cord, 2 hours after intraplantar formalin injection. Similarly as c-FOS, pS6 showed specific expression in the superficial laminae I-III (above the solid line). In deeper dorsal and ventral horns, pS6 expression were found in both ipsilateral and contralateral sides.

5C: Spatial distribution of pS6 (whole mount immunofluorescence) in L3 to 6 spinal cord, 2 hours after intraplantar formalin injection. Maximal projection image of z-stack images of the dorsal horn is shown here.

5D: pS6 expression (immunofluorescence) on lumbar spinal cord cross sections. L3 and 4 showed maximal pS6 expression at the superficial dorsal horn, corresponding to the whole mount staining shown in 5C.

5E: Time course of pS6 expression (immunofluorescence) in superficial dorsal horn. pS6 expression increased from 0.5 to 1 hour after formalin injection. Between 1 to 2 hours after injection, similar number of pS6 expression cells and similar signal intensity were observed. The expression declined slightly at 2.5 hours.

2.1.2.2 Time course

So far I could show that pS6 is expressed 2 hours after formalin injection, but is this the time when pS6 expression reaches its peak, or exhibits the best ipsi- to contra-lateral contrast? It has previously been shown that *c-Fos* expression is induced within 5 minutes of neuronal activation and reaches its peak within 20 minutes (Harris, 1998); In order to determine when pS6 expression would reach its peak, I checked pS6 levels at different time points after stimulation (Fig.5E). In the area of interest i.e. the superficial laminae I-III, I found an increased pS6 expression from 0.5 to 1 hour after stimulation. The pS6 expression did not significantly change between 1 and 2 hours after formalin injection and showed a small decline after 2.5 hours. As I am interested in finding stable markers, I reasoned that although pS6 expression levels did not significantly change between 1 and 2 hours after stimulation, the 2-hour time point might provide me a more stabilized transcriptome. Therefore, the time point of 2 hours post formalin injection was used in following experiments.

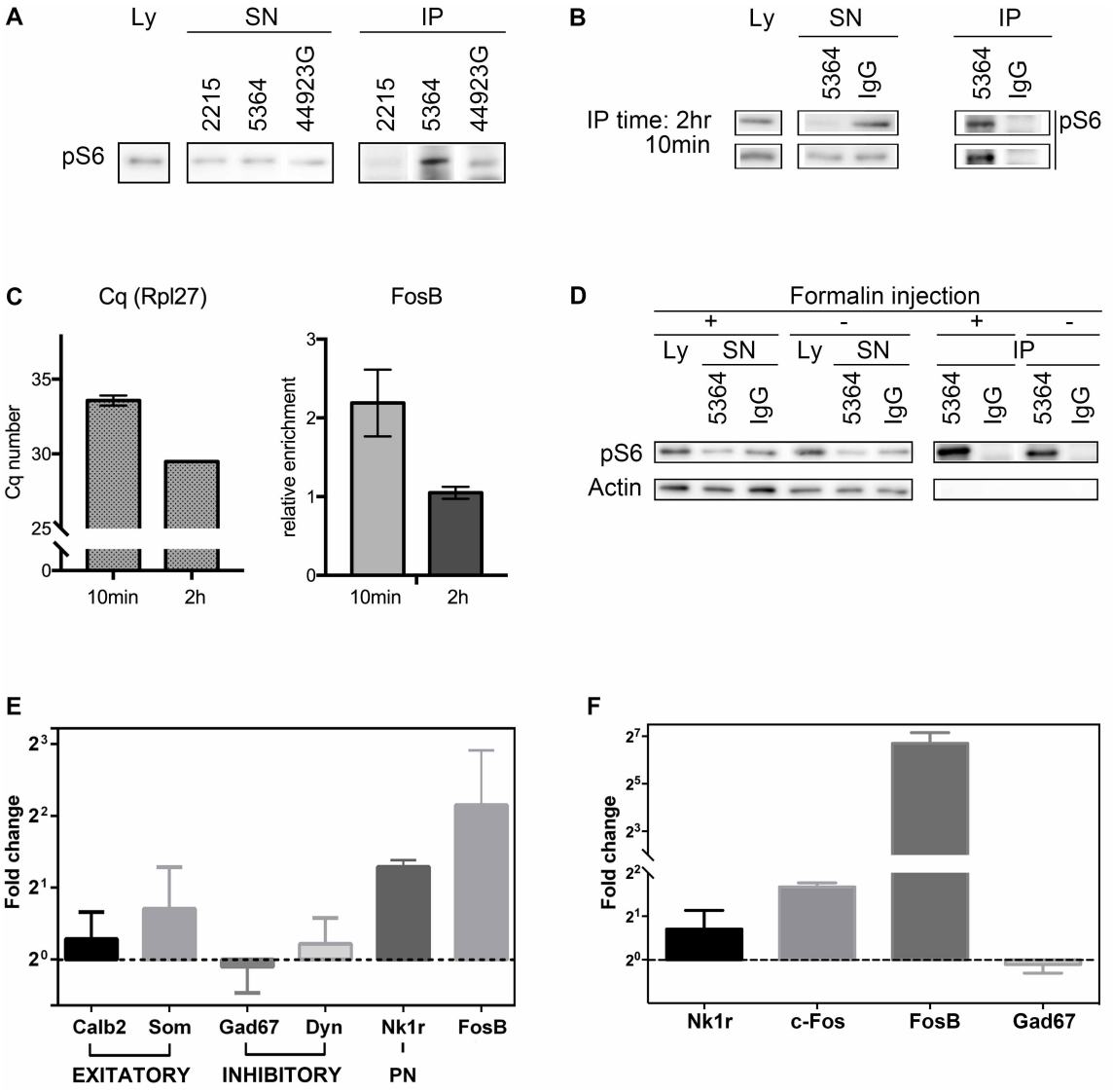

Figure 6: Optimization of pS6 immunoprecipitation in spinal cord tissue
6A: Testing antibodies (Cell Signaling polyclonal antibody #2215, Cell Signaling monoclonal antibody #5364 and Invitrogen polyclonal antibody #44923G) for pS6 immunoprecipitation. Lysate (Ly), the three supernatants (SN) after antibody incubation and the respective immunoprecipitation eluates (IP) were loaded on one western blot gel. All three tested antibodies reduced pS6 amount in the supernatant after immunoprecipitation (SN) while #5364 showed best enrichment (IP).
6B: Testing antibody incubation time for pS6 immunoprecipitation: 2 hours (up) vs. 10 minutes (down). Both incubation lengths reduced pS6 in SN and showed increased pS6 level in IP, while IgG control did not bind any pS6.
6C: qPCR testing of mRNA collected by 2-hour or 10-minute pS6 immunoprecipitation. Longer incubation time yielded 17 times (ΔCq=4.085) more house keeping gene *Rpl27* than the shorter incubation time, while 2 times more *FosB* was enriched with the shorter 10-minute IP (normalized to house keeping gene *Rpl27*, N=2).
6D: pS6 immunoprecipitation of ipsilateral (+) and contralateral (-) dorsal spinal cord. A 10-minute antibody incubation was performed. pS6 was detected in both ipsi- and contra-lateral lysates, reduced in SN and enriched in IP. IgG control did not bind any pS6.
6E: qPCR test of pS6-bound mRNA collected in the immunoprecipitation from 6D. Among the genes tested, *Nk1r* showed a stable enrichment (fc 2.439±0.166). *Som* and *FosB* also showed enrichment but greater variance among samples (N=3).
6F: qPCR test of the cDNA library before sequencing. *Nk1r* showed a slight enrichment while *c-Fos* and *Fos-B* showed significant and consistent enrichment (N=3).

2.2 Enrichment of phospho-ribosomes from pain-activated spinal cells

2.2.1 Optimization of pS6 immunoprecipitation protocol

I showed by immunofluorescent staining that pS6 expression (1) specifically marks activated cells in superficial dorsal horn, and (2) is at its peak 2 hours after peripheral formalin injection. I next moved on to test conditions for pS6 immunoprecipitation (IP).

2.2.1.1 Comparison of different pS6 antibodies

The initial pS6 immunofluorescent stainings in section 2.1 were performed using the Cell Signaling polyclonal antibody #2215, which is the antibody used by Knight and colleagues in their original phospho-ribosome profiling study (Knight et al., 2012). I included two more antibodies for IP testing: Cell Signaling monoclonal antibody #5364 and Invitrogen polyclonal antibody #44923G. I performed three immuno-precipitations in parallel using the three antibodies, respectively with the same spinal cord tissue lysate (lumbar sections L2-6, ipsilateral to formalin injection). I started with the IP condition of 2-hour antibody incubation at 4˚C.

I loaded the tissue lysate, three supernatants (lysates after IP), and the respective IP eluates on one western blot gel to check for changes in pS6 level. The blot was incubated with antibody #2215 (Fig.6A, the antibody labels refer to the one used in IP). Comparing to pS6 level in the lysate, all three antibodies were able to decrease pS6 levels, as shown by the weaker bands in supernatants; while antibody #5364 showed the most enrichment of pS6. The pS6 bands of the three supernatants may be too weak to detect their differences, the bands in IP nevertheless reflect the amount of

pS6 each antibodies enriched. Antibody #5364 was used for further IP experiments and western blot detections.

2.2.1.2 Comparing pS6 IP incubation time

Knight and colleagues reported that immunoprecipitations performed for more than 10-minutes at room temperature (RT) increased unspecific binding (Knight et al., 2012). Therefore, I compared 2-hour (4˚C) and 10-minute (RT) IP in parallel to compare both the quantity of pS6 enriched, as well as the quantity and quality of collected ribosome-bound mRNA. Again I ran western blots to determine the pS6 levels in the lysate, supernatants and eluates of the two different IPs. Both 2-hour and 10-minute incubation decreased pS6 levels in the supernatant, and enriched for pS6 in the eluates (Fig.6B). The 2-hour incubation reduced more pS6 from supernatants, but the two incubation lengths resulted in similar pS6 amounts in the eluates. This suggests that there are no significant difference in the amount of pS6 enriched by IP incubation of different lengths. In addition, although IgG control incubation slightly reduced pS6 in supernatants in both conditions, no pS6 was pulled down, indicating the enrichment is specific. Therefore I went forward to examine the mRNA collected by the two IP durations.

Freshly transcribed mRNA is pulled down together with phospho-ribosomes, and they bear the molecular identities of those activated cells to whom the phospho-ribosome belong to. As pS6 is the mean to enrich for mRNA from activated cells and it is the mRNA collected that I am interested in, I then performed qPCR experiments with eluates from both IPs to determine the amount and to check the quality of the mRNA collected (Fig.6C, left). The housekeeping gene *Rpl27*, a ribosome subunit encoding gene, was used as an indication of the amount of total mRNA collected. The 2-hour incubation resulted in more than 17 times more of *Rpl27* than the 10-minute IP,

suggesting that more mRNA was collected with longer incubation times. However, if taking *Rpl27* as the indicator for total mRNA amount, the expression of *FosB*, an immediate early gene of the *Fos* family, is two times higher in the 10-minute IP compared to the 2-hour IP (Fig.6C, right). These data indicate that although the 2-hour incubation collected more mRNAs, the 10-minute IP achieved a higher enrichment of mRNA from activated cells. Hence, I decided to use the 10-minute room temperature immunoprecipitation in the future.

2.2.2 Immunoprecipitation of phospho-ribosomes from the spinal cord after formalin-induced acute pain

After testing different conditions, I finalized a pS6 immunoprecipitation protocol, namely a 10-minute room temperature incubation with Cell signaling monoclonal antibody #5364. As previously shown in section 2.1, I could show specific pS6 expression in superficial dorsal horn of lumbar spinal cord L3-6, 2 hours after formalin injection. I adopted a dissection scheme to separate superficial dorsal horn from the rest of the spinal cord to further enhance the signal-to-noice ratio, as I have observed pS6 expression also in ventral spinal cord (FIg.5D). With this dissection scheme, I was able to isolate laminae I-III dorsal horn spinal cord from lumbar section L2-6, ipsilateral and contralateral to formalin injection respectively, as the input for pS6 immunoprecipitation.

Next, I performed pS6 immunoprecipitation with the collected tissue lysates using the above protocol. Westernblotting of the samples showed that, first of all, pS6 was detected in both ipsi- and contra-lateral lysates. Although previous immunofluorescent staining had shown clear ipsi- to contra-lateral contrast of pS6 expression in laminae I-III, here I observed pS6 signals from both sides on the western blot, suggesting that

either deeper dorsal lamina layers (where contralateral pS6 expression was also found) were also collected, or the anti-pS6 antibody showed different specificity in recognizing pS6 on tissue section as in lysates. Nonetheless, consistent with results shown above, pS6 levels were reduced in the post-IP supernatants and an enrichment of pS6 was detected in the IP eluates on both sides. The IgG control IPs did not pull down pS6, suggesting there was no unspecific binding of the pS6 to the magnetic beads used in the experiment (Fig.6D). Next, I went to analyze the mRNA that were collected by pS6 IP.

2.2.3 qPCR validations of pre-sequencing samples

To test the molecular information that the obtained mRNA encode and whether there was enrichment of transcripts from activated cells, I performed qPCR on a subset of transcripts known to mark subpopulations of neurons involved in spinal pain processing: the excitatory interneuron markers *Calb2* and *Som*, the inhibitory interneuron markers *Gad67* and *Dyn*, the projection neuron marker *Nk1r* and the immediate early transcript *FosB* (Fig.6E). I expected to see enrichment of those transcripts in the ipsilateral sample, which are stably expressed or induced in pain-activated neurons. Indeed, I observed enrichment of *Som*, *Nk1r* and *FosB*, but not *Gad67* and *Dyn* in ipsilateral sample. *Nk1r* showed the most consistent enrichment (fc 2.439±0.166) while *Som* and *ForB* levels varied more among samples.

I then repeated the pS6 IP and this time, amplified the collected mRNA into a cDNA library for sequencing following the protocol developed by Picelli and colleagues (Picelli et al., 2014). Before I proceeded to sequencing, I tested the cDNA library again with qPCR. Since I had more samples to test in this experiment, I only tested the mRNA expression of *Nk1r*, *c-Fos*, *FosB* and *Gad67* (Fig.6F), in order to fit all the samples in one 96-well plate. In contrast to the consistent enrichment of *Nk1r*

previously observed, I found great variance in *Nk1r* expressions in these samples (fc 1.627±0.566) and possible reasons will be discussed in the later section. Nevertheless, enrichment of *FosB* as well as non-changed expression of *Gad67* were detected, which are consistent with the previous qPCR shown in Fig.6E. In addition, I could show a consistent enrichment of *c-Fos* in the ipsilateral samples (fc 3.19±0.216), reflecting the induction shown by previous *in situ* hybridization stainings (Fig.5A). I subjected the cDNA library to sequencing on an Illumina next-generation sequencing platform.

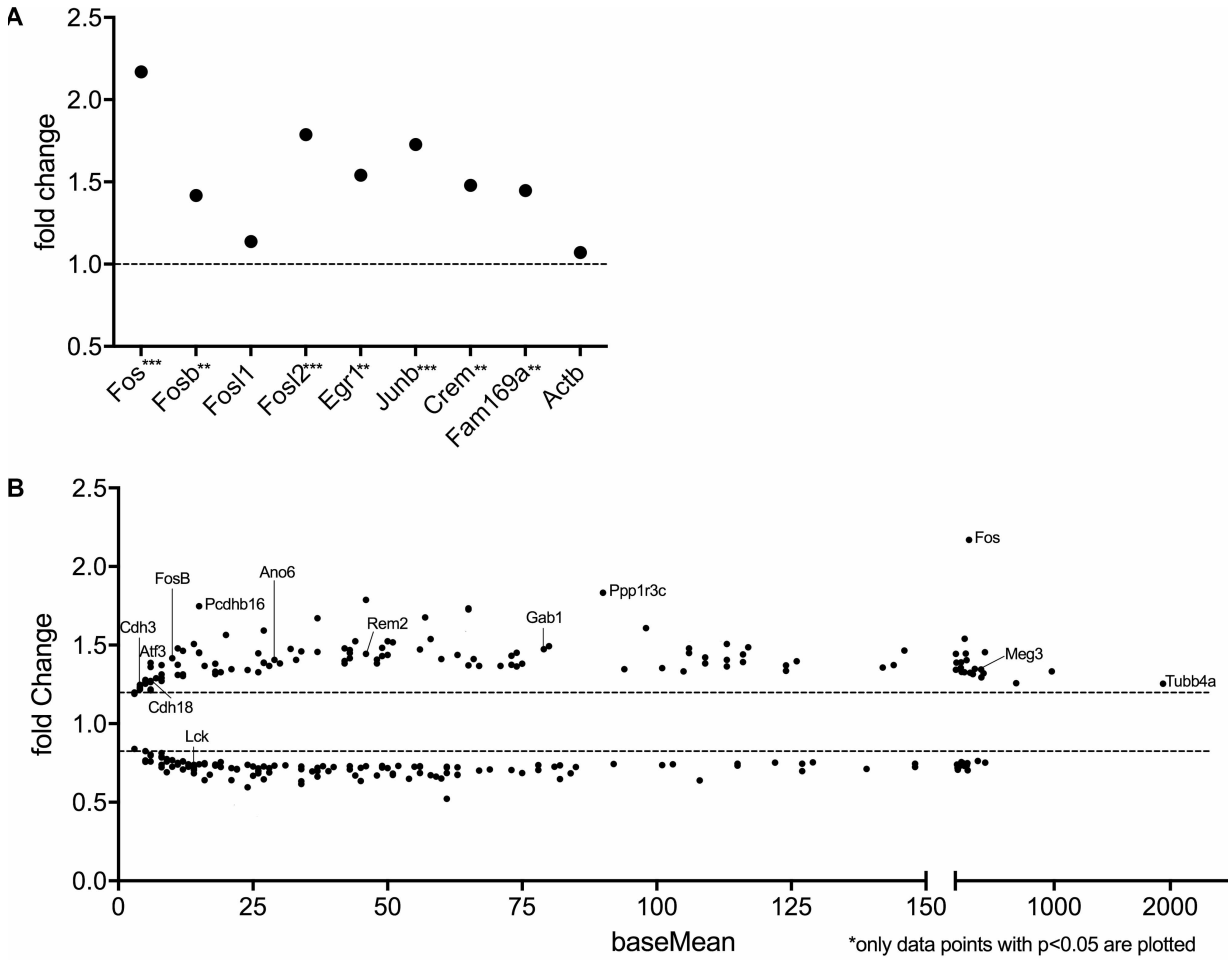

Figure 7: Transcriptome of spinal cord cells activated by formalin-induced acute pain
7A: Fold changes of a selected listed of immediate early genes (IEGs). All IEGs listed, except *Fosl1*, showed significant enrichment while housekeeping gene Actb showed none (N=3, $p<0.05$, Deseq2).
7B: Significantly changed genes (N=3, $p<0.05$, Deseq2) upon formalin-induced acute pain. The fold change of the genes were plotted against their expression level (baseMean). A total of 134 enriched and 136 de-enriched genes were found, with the majority being lowly (0-150 normalized counts) to medium level (150-300 normalized counts) expressed. *c-Fos* was the gene with the highest fold change (fc 2.169) and the most highly expressed enriched-gene was *Tubb4a* (normalized counts 1938), a tubulin beta chain protein. A selected list of differentially expressed genes is summarized in Table 1.

2.3. Transcriptome of spinal cord cells activated by formalin- and capsaicin-induced acute pain

2.3.1 Transcriptome of spinal cells activated by formalin-induced acute pain

The MiSeq platform was chosen for its cost-effectiveness, relative short running time, and the adequate sequence depth (25 million per run) for my experiment purpose to identify robust population markers. The sequencing was performed by EMBL Genecore. After I received the sequencing reads, I first checked their qualities using FastQC and then performed the sequencing data analysis following the workflow developed by Love and colleagues using R (Love et al., 2015) and obtained a list of significantly changed genes ($p<0.05$) i.e. genes which are differentially expressed in ipsi (stimulated)- and contra (control)-lateral samples.

- **Immediate early gene expression, as internal quality control**

I first checked for the presence of immediate early genes (IEGs) among the enriched transcripts. Immediate early genes are among the first genes to be induced once cells are activated and as pS6 immunoprecipitation enriches for transcripts from activated cells, IEGs should be enriched in the ipsilateral samples, when compared to the contralateral samples. A set of immediate early genes was indeed found (Fig.7A): *c-Fos*, *FosB*, *Fosl2*, as well as *Egr1*, *Junb*, *Crem* and *Fam169a* were significantly enriched (ipsilateral/contralateral) with the exception of *Fosl1*. In the case of *c-Fos* and *FosB*, the sequencing results reflect the pre-sequencing qPCR. Although these genes reveal no new information about cellular identity upon formalin-induced acute pain, they were a good indication that the sequencing worked as it was able to detect the known ipsilateral induction of IEGs.

- **Differentially expressed genes in the spinal cord following formalin-induced pain**

I found in total 270 differentially (ipsilateral/contralateral) expressed genes ($p<0.05$). The fold change of the genes were plotted against their expression level (baseMean, Fig.7B). Of the 270, there were 134 enriched and 136 de-enriched genes, with the majority being lowly (0-150 normalized counts) to medium level (150-300 normalized counts) expressed genes. *c-Fos* showed the highest fold change (fc 2.169) and *Tubb4a*, a tubulin beta chain protein, had the highest expression (normalized counts 1938).

In the qPCR of the non-amplified cDNA (Fig.6E), I could show enrichment of *Nk1r*, *Som* and *FosB* in the ipsilateral samples. *FosB* enrichment was found both by qPCR of the amplified cDNA library and in the above list of immediate early genes; however, neither *Nk1r* nor *Som* were on the list of differentially expressed genes. I did not test *Som* in the amplified cDNA library, but in the case of *Nk1r*, I found a discrepancy between the non-amplified and amplified cDNA. In contrast to the consistent 2-fold enrichment I detected in the non-amplified cDNA (Fig.6E), the *Nk1r* expression varied greatly amongst biological replicates after the amplification step (as shown by the large error bar in Fig.6F, and it is not in the list of differentially expressed genes with a significance of $p<0.05$). I think the following procedural differences in the sample preparation step of the pre-sequencing test sample and the actual sequencing library could possibly account for the discrepancy: (1) I used Superscript III for the non-amplified sample but Superscript II for the amplified library preparation. Superscript III produces more cDNA from smaller mRNA fragments while Superscript II is more prone to reverse transcribe full length, intact mRNA, making it the preferred reverse transcriptase for cDNA library preparation. In addition, Superscript III has the working temperature of 55ºC, much higher than the 42ºC of Superscript II. As mRNA secondary structure changes by temperature (Schuster et al., 1994), Superscript III might have a better access to some transcripts e.g. *Nk1r* than Superscript II does. (2) The additional amplification step is a process

with an inevitable bias towards the more abundantly expressed genes. *Nk1r* was detected at high cycle numbers in the qPCR using non-amplified cDNA, which indicates its low expression level and potentially explains its variance after the amplification step.

Which are the differentially expressed genes? Table 1 shows a list of 10 selected genes with high statistical significance and known neuronal functions or CNS expression. Apart from *c-Fos*, *Pcdhb16* and *Ppp1r3c* were the top two enriched genes with also highest significance. *Pcdhb16* belongs to a cadherin family specifically expressed in central nervous system and is believed to be involved in the establishment and function of specific cell-cell neural connections (Junghans et al., 2008). *Ppp1r3c*, protein phosphatase-1 regulatory subunit 3C, is better known by the more indicative name of Protein targeting to glycogen (*Ptg*). PTG protein guides Protein Phosphatase-1 (PP1) to Glycogen Synthase (GYS), resulting in the de-phosphorylation and activation of the latter. Studies of *Ptg* have shown that it is a main regulator of glycogen synthesis in brain astrocytes (Falkowska et al., 2015). All ten genes except *Ptg* have known neuronal involvement, although not all in the pain context. Functions aside, I continued to verify these 10 genes using qPCR to confirm if they were indeed enriched or de-enriched in the activated cells of dorsal spinal cord by formalin-induced acute pain. But before I went on with the verification experiments, I performed another phospho-ribosome profiling. All the above-described experiments were conducted using the formalin pain model, and in order to have a better understanding whether the identified differentially expressed genes are specific to formalin-induced pain or they are general to peripheral painful stimuli, I performed the same profiling and sequencing experiment using another widely used acute pain model, the capsaicin-induced pain model.

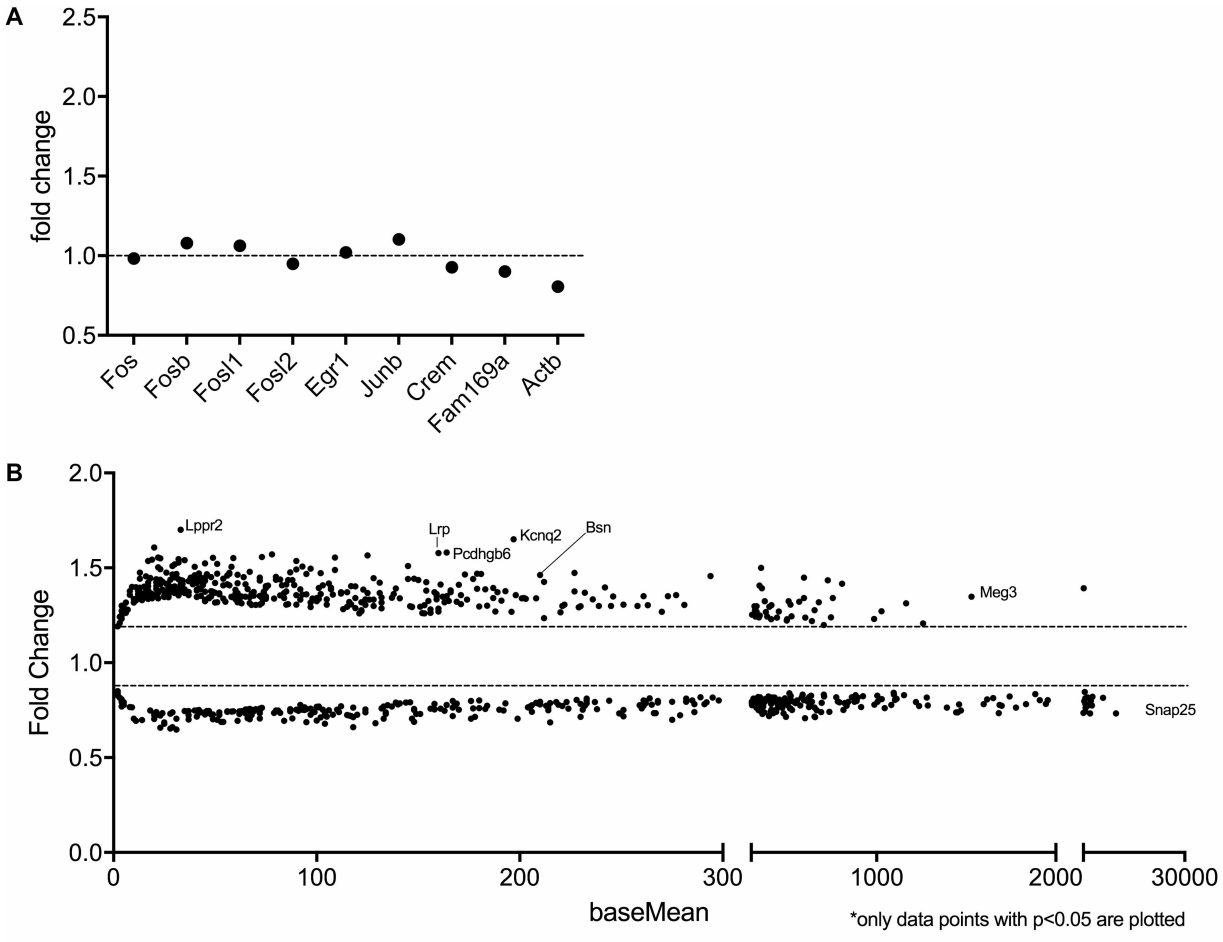

Figure 8: Transcriptome of spinal cord cells activated by capsaicin-induced acute pain.
8A: Fold changes of a selected listed of immediate early genes (IEGs). Unlike in 7A, no IEGs were found enriched (N=3, p value by Deseq2).
8B: Significantly changed genes (N=3, $p<0.05$, Deseq2) upon capsaicin-induced acute pain. The fold change of the genes were plotted against their expression level (baseMean). There were in total 818 differentially expressed genes, with 424 enriched and 394 de-enriched. *Snap25*, a SNARE protein, had the highest normalized counts of 33199. A selected list of differentially expressed genes is summarized in Table 2.

2.3.2 Transcriptome of spinal cells activated by capsaicin-induced acute pain

Apart from formalin, capsaicin is another commonly used substance to induce chemical pain. I therefore repeated the above-described phospho-ribosome profiling experiment to obtain the transcriptome of spinal cells activated by capsaicin-induced acute pain. I first used same pS6 IP and cDNA library preparation protocols as before, however, I was not able to get a good amount of amplified cDNA. Therefore I doubled the amount of pS6 antibody used during the antibody incubation step and collected the mRNA, which was then subjected to library preparation, sequencing and data analysis following the same protocol as above described.

- **Immediate early gene expression, as internal quality control**

I again first checked for the presence of immediate early genes (IEGs) in the analyzed list of differentially expressed genes ($p<0.05$). However, none of the genes in Fig.7A were found to be differentially expressed (Fig.8A). It was puzzling, but I reasoned that since capsaicin-induced pain is often considered as a milder, shorter-lasting model of acute pain (LaMotte et al., 2011), the expression pattern of IEGs could be different from that of formalin-induced pain.

- **Differentially expressed genes in the spinal cord following capsaicin-induced pain**

Surprisingly I observed considerably more differentially expressed genes identified in the sequencing of transcripts from cells activated by capsaicin-induced pain, 818 in total (Fig.8B). 424 of these genes were enriched and 394 de-enriched. The baseMean of this experiment also spun a much larger scale, with the highest normalized count of 33199 assigned to *Snap25*, a SNARE protein. This indicates that my sequencing depth was much higher than in the formalin pain experiment. The double amount of pS6

antibody used in the immunoprecipitation could be one element contributed to the higher amount of mRNA collected.

The top 10 enriched and de-enriched genes are listed in Table 2, with their known functions and fold changes. The most highly enriched gene was *Lppr2*, a membrane protein belonging to the PA-phosphatase related phosphoesterase family. It is known to show dynamic expression regulation during brain development and neuronal excitation (Cohen et al., 2015), which would potentially point to a involvement in pain processing. The most highly de-enriched gene was *Thg1l*, a mitochondria protein, whose mutation has been reported to result in cerebellar ataxia and developmental delay (Edvardson et al., 2016). Among these ten genes, two have been shown to be involved in pain processing: *Btbd17* has been reported to be up-regulated following spinal cord injury (Koehn et al., 2016) and *Lrp1* has been studied in the context of microglia activation and neuroinflammation (Yang et al., 2016).

- **Comparison of RNAseq results of the formalin and capsaicin pain models**

After I obtained the transcriptome from capsaicin pain-activated spinal cells, I compared it with the transcriptome of formalin pain-activated spinal cells. I found a surprisingly low number of differentially expressed genes in common: a total of 7 overlapping genes with $p<0.05$, and 56 if the significance cut-off is extended to 0.1.

In addition to analyze the sequencing data with DESeq2, I also performed t-tests directly on the count numbers (normalized to total reads per sample) and obtained lists of differentially expressed genes in formalin and capsaicin pain models. Using t-tests, I found 24 overlapping genes between the two pain models. Comparing the list of 56 by DESeq analysis and the list of 24 by t-tests, I identified 5 common genes (listed in Table 3 with their known functions and fold changes from both sequencing experiments). These 5 genes, together with the 10 genes from Table 1, were chosen as candidates for the verification experiments.

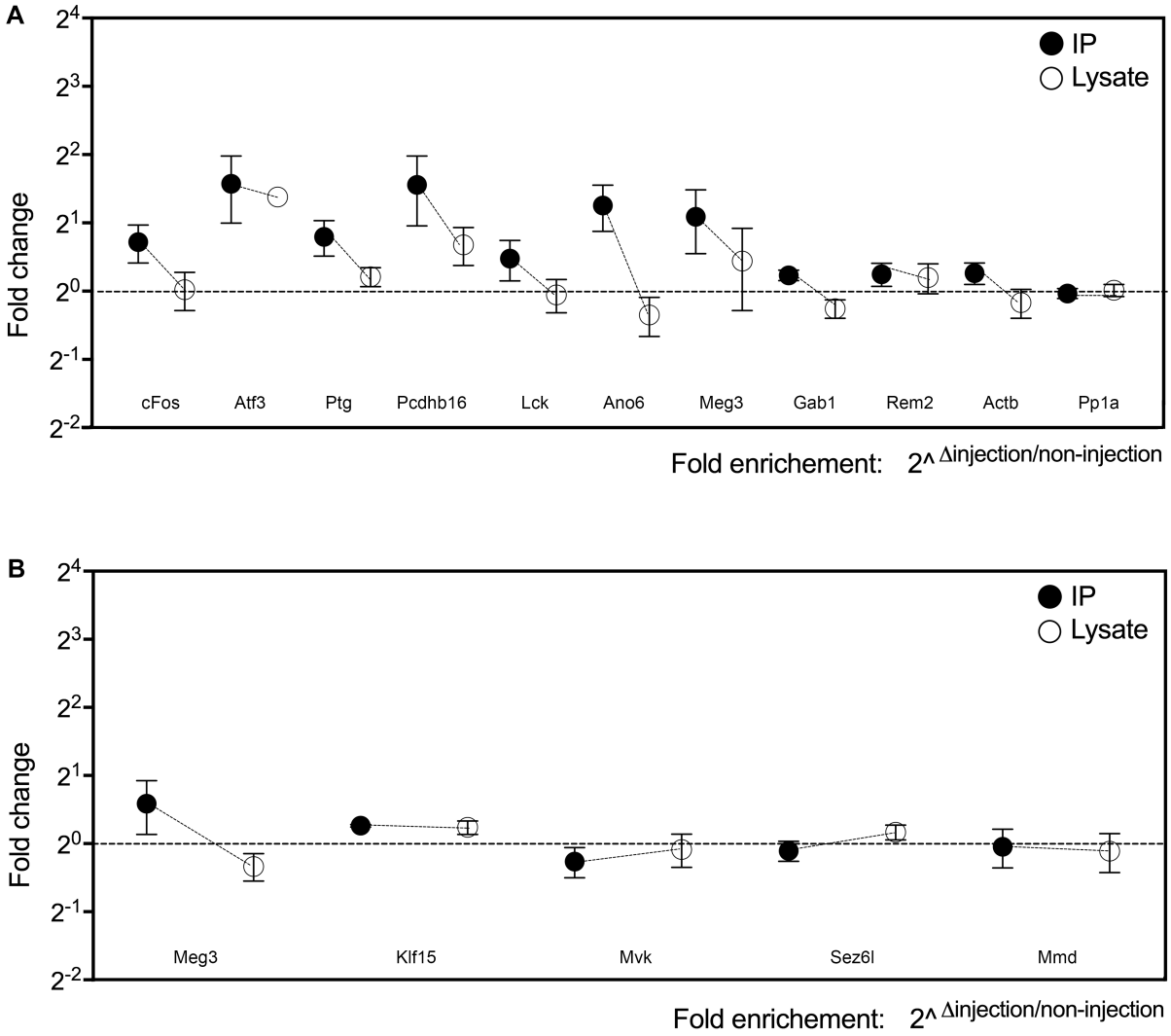

Figure 9: qPCR verification of the sequencing results
9A: Formalin-induced acute pain: fold changes of candidates in immunoprecipitation-enriched samples (IP) and non-enriched lysates, respectively (N=3 or 4). Immediate early gene *Atf3* was enriched in both immunoprecipitation-enriched samples and non-enriched lysates. *c-Fos*, *Ptg*, *Pcdhb16*, *Ano6* and *Meg3* were enriched in IP samples only. *Lck*, *Gab1* and *Rem2* showed minor enrichment. The enrichment was however no greater than that of house keeping genes *Actb* and *Pp1a*, and was thus considered as normal fluctuation.
9B: Capsaicin-induced acute pain: fold changes of candidates in IP and lysate samples (N=3 or 4). None of the tested candidates showed clear enrichment.

Table1: Selected list of differentially expressed genes in spinal cord cells following formalin-induced acute pain

Gene name	Known functions	Fold change
Atf3	• Transcription factor • Known interactor of TRPV1 • Injury marker	1.386
Ppp1r3c (PTG)	• Protein phosphatase-1 regulatory subunit • Targeting PP1 to glycogen synthase	1.833
Pcdhb16	• Protocadherin • Establishment and function of specific cell-cell neural connections	1.747
Lck	• Tyrosine kinase • Known brain expression, function yet unclear	0.739
Ano6	• Cation channel • High reservation to Ano1, a chloride channel in nociceptive DRG neurons	1.406
Meg3	• linc RNA • Neuron apoptosis	1.345
Gab1	• Neurite outgrowth	1.474
Rem2	• Negative regulator of dendritic complexity	1.444
Cdh3	• Layer specific expression in spinal cord	1.235
Cdh18	• CNS specific cadherin • Known involvement in synaptic adhesion, axon outgrowth and guidance	1.271

Atf (Bas-Orth et al., 2017), Ppp1r3c (Falkowska et al., 2015), Pcdhb16 (Junghans et al., 2008), Lck (Omri et al., 1996), Ano6 (Cho et al., 2012; Jacobsen et al., 2013), Meg3 (R. Qin et al., 2013), Gab1 (Korhonen et al., 1999), Rem2 (Ghiretti et al., 2014), Cdh3 (Abraira et al., 2017), Cdh18 (J. Lin et al., 2014)

Table2: Top 10 differentially expressed genes in spinal cord cells following capsaicin-induced acute pain

Gene name	Known functions	Fold change
Lppr2	• Known involvement in brain development and neuronal excitation	1.701
Kcnq2	• Potassium channel unit • Speculated involvement in neuronal excitability	1.650
Btbd17	• Up-regulated after spinal cord injury	1.607
Pcdhgb6	• CNS specific protocadherin • Known involvement in synaptic adhesion, axon outgrowth and guidance	1.582
Lrp1	• Suppresses microglial activation after neuroinflammation	1.579
Thg1l	• Mitochondrial protein whose mutation is linked to cerebellar ataxia and developmental delay	0.648
Shox2	• Marks a subpopulation excitatory spinal interneurons involved in locomotion	0.654
Zfp472	• Zink finger protein	0.661
Spp1	• Expressed by spinal motor neuron	0.661
Hells	• Regulates self-renewal/proliferation of neural stem cells.	0.678

Table 3: Overlapping candidates from formalin (For) and capsaicin (Cap) sequencings

Gene name	Known functions	Fold change (For/Cap)	
Meg3	• linc RNA • Known involvement in cancer	1.345	1.348
Klf15	• Transcription factor • Known involvement in neuronal stem cell differentiation and glycogenesis	1.457	1.336
Mvk	• Mevalonate kinase, a peroxisome enzyme	1.357	1.368
Sez6l	• Seizure 6-like • Known involvement in lung cancer	1.309	1.368
Mmd	• Monocyte To Macrophage Differentiation Associated • suggested to be an ion channel	1.494	1.247

Lppr (Cohen et al., 2015), Kcnq2 (Soh et al., 2014), Btbd17 (Koehn et al., 2016), Pcdhgb6 (Kuhn et al., 2016), Lrp1 (Yang et al., 2016), Thg1l (Edvardson et al., 2016), Shox2 (Dougherty et al., 2013), Spp1 (Yamamoto et al., 2011), Hells (Han et al., 2017); Klf15 (Takashima et al., 2010; Ohtsuka et al., 2011), Mvk (Siemiatkowska et al., 2013), Sez6l (Gorlov et al., 2007), Mmd (Q. Liu et al., 2012).

2.4 Verification of sequencing results

2.4.1 verification by qPCR

In order to verify that the sequencing experiments faithfully identified the differentially expressed transcripts, I performed qPCR to determine the changes of candidates mRNA. I repeated pS6 IP as previously described and collected mRNA from both IP eluates and lysates. cDNA was synthesized with Superscript III and subjected to qPCR.

2.4.1.1 qPCR verification of formalin sequencing candidate genes

I started with the set of 10 transcripts descried in Table 1 as they were detected with high significance and therefore constitutes my best candidates. As they were identified in the spinal cells activated by formalin-induced pain, I continued with the formalin pain model in this qPCR verification experiment. In addition to the genes listed in Table 1, I also included immediate early gene *c-Fos*. *Actb* and *Pp1a* were used as housekeeping genes.

It is important to distinguish between the two conditions that would result in enrichment in the IP samples: 1) the gene is induced in the pS6-positive cells by the given stimulation, or 2) the gene is stably but specifically expressed in the pS6-positive cells. The lysates were included in this case to distinguish between the two possibilities. If the gene is induced, the induction should also be detectable in plain lysates, although the fold change could be diluted by the non-activated cells around. If the gene is stably expressed in a group of cells, there would be no difference in the ipsi- to contra-lateral lysate samples.

Of the genes tested, *c-Fos*, *Atf3*, *Ptg*, *Pcdhb16*, *Lck*, *Ano6* and *Meg3* showed enrichment in IP samples (Fig.9A). Enrichment of *Atf3* was also detected in the lysate. Therefore *Atf3* expression is induced by formalin-induced acute pain. As *c-Fos* expression is clearly induced by formalin pain as previously shown by *in situ* hybridization (Fig.5A), it was surprising that no *c-Fos* enrichment was detected in the lysate. It is possible that the number of *c-Fos* positive neurons is relatively small compared to the total amount of cells, and the induction is masked in lysate. On the other hand, *Pcdhb16* and *Meg* showed enrichment in the lysate, indicating they could be induced genes, although the samples bore relatively high variation. *Gab1* and *Rem2* showed similar variations as the housekeeping genes *Actb* and *Pp1a*, and thus were considered not enriched. *Cdh3* and *Cdh18* qPCR failed to detect the transcripts. This qPCR result suggests that *c-Fos*, *Atf3*, *Ptg*, *Pcdhb16*, *Lck*, *And6* and *Meg3* were indeed enriched by pS6 immunoprecipitation.

2.4.1.2 qPCR verification of the overlapping candidates from formalin and capsaicin sequencings

The qPCR verification using the formalin pain model largely correlates with the sequencing result. Therefore, I decided to perform a second round of qPCR using the capsaicin pain model, to verify that the 5 overlapping enriched genes of the two sequencings are indeed differently expressed and to confirm that there are common genes involved in processing both types of acute pain (Table 3). In this round, none of the genes were clearly enriched in either IP or lysate samples (Fig.9B).

Although most of the qPCR results of the formalin pain model fit the sequencing data, it failed to detect *c-Fos* induction in lysate. Considering the experimental shortcomings of qPCR, that I can not retrospectively check how much tissue I collected or to which lamina layer the dissection reached, I decided to switch to *in situ*

hybridization as the mean of verification, as I could decide what area to quantify, as well as visually examine the overlap between a transcript and pS6.

2.4.2 Verification by *in situ* hybridization

I continued to use the candidates from Table 1, and the formalin pain model, as qPCR indicates that many of them recapitulate the sequencing result (Fig.9A) and my aim here is to verify that the sequencing results represent the actual molecular changes. I designed and cloned *in situ* hybridization probes for *Atf3*, *Ptg*, *Pcdhb16*, *Lck*, *And6 and Meg3*, as qPCR suggested that they are enriched in ipsilateral IP samples, as well as *Cdh3* and *Cdh18*, despite that the qPCR did not detect their mRNA. In addition, I also included *Som*, *Dyn* and *MafA* as positive controls since they mark subgroups of dorsal horn neurons involved in pain processing (Xu et al., 2008; Del Barrio et al., 2013; Duan et al., 2014a; Christensen et al., 2016; Gutierrez-Mecinas et al., 2016). I then performed *in situ* hybridization on fresh frozen spinal cord cross-sections from mice sacrificed 2 hours after intraplantar formalin injection. After the *in situ* hybridization, I did immunofluorescent staining against pS6 on the same sections to visualized the cells activated by formalin-induced pain.

2.4.2.1 Co-staining of candidate and control genes with pS6

Co-stainings of candidates (*in situ* hybridization) and pS6 (immunofluorescence) on spinal cord cross-sections are shown in Fig.10A-K. *Cdh3*, *Cdh18*, *Pcdhb16*, *Meg3* and *Ano6* are not induced by peripheral painful stimuli. Their expressions were observed in both ipsi- and contra-lateral spinal cord. *Cdh3* showed a nice dorsal lamina III specific expression, while the other two cadherins, *Cdh18* and *Pcdhb16*, had a broader expression throughout the dorsal horn. *Meg3* was the most ubiquitously expressed

transcript. *Ano6* shared a similar pattern as *Cdh18*, i.e. expressed at a medium level throughout the dorsal horn. All of these genes showed partial overlap with pS6.

Atf3, *Ptg* and *c-Fos* showed ipsilateral specific expression. There were very few *Atf3* positive cells, suggesting that the sensitivity of the sequencing was good. All the *Atf3* cells were also pS6 positive. *c-Fos* also showed complete overlap with pS6. However, there were considerably more pS6-positive cells than *c-Fos*-positive neurons. The different expression dynamics (*c-Fos* mRNA is detected as early as 5 minutes after stimulation and starts to degrade after 20 minutes (S. P. Hunt et al., 1987); while pS6 expression reaches its peak 1 hour after stimulation and only start to decline after 2 hours, Fig.5E) could certainly be one explanation, but the additional pS6 positive cells raised the question whether there are other cells than neurons activated by formalin-induced pain. This thought was followed up and will be shown in the next section. The third induced gene was *Ptg*. Based on previous qPCR, I did not expect to find *Ptg* as an induced gene, as I did not detect its enrichment in the lysate. Nevertheless, *Ptg in situ* hybridization showed a clear ipsilateral specific expression through the dorsal horn, with however only limited co-localization with pS6 (white arrow). *Ptg* has not been previously reported to be a pain-induced gene.

The three dorsal spinal cord specific 'pain' genes (Som, Dyn and MafA) I selected as positive controls also showed dorsal horn expression as previously reported (Xu et al., 2008; Del Barrio et al., 2013; Duan et al., 2014a; Christensen et al., 2016; Gutierrez-Mecinas et al., 2016). After imaging the co-stainings, I continued to the quantification of them.

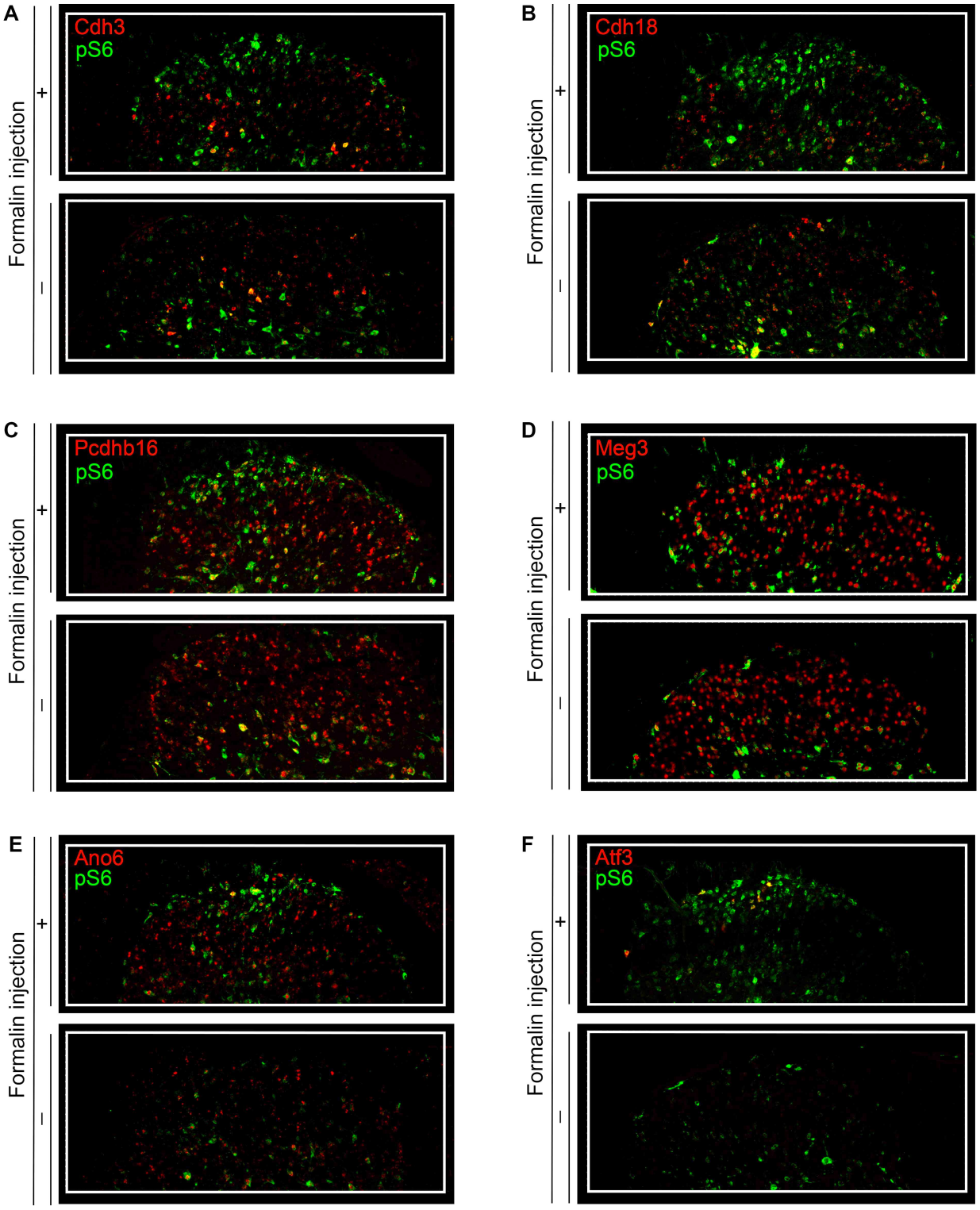
A
Cdh3
pS6
Formalin injection
+
–
B
Cdh18
pS6
Formalin injection
+
–
C
Pcdhb16
pS6
Formalin injection
+
–
D
Meg3
pS6
Formalin injection
+
–
E
Ano6
pS6
Formalin injection
+
–
F
Atf3
pS6
Formalin injection
+
–

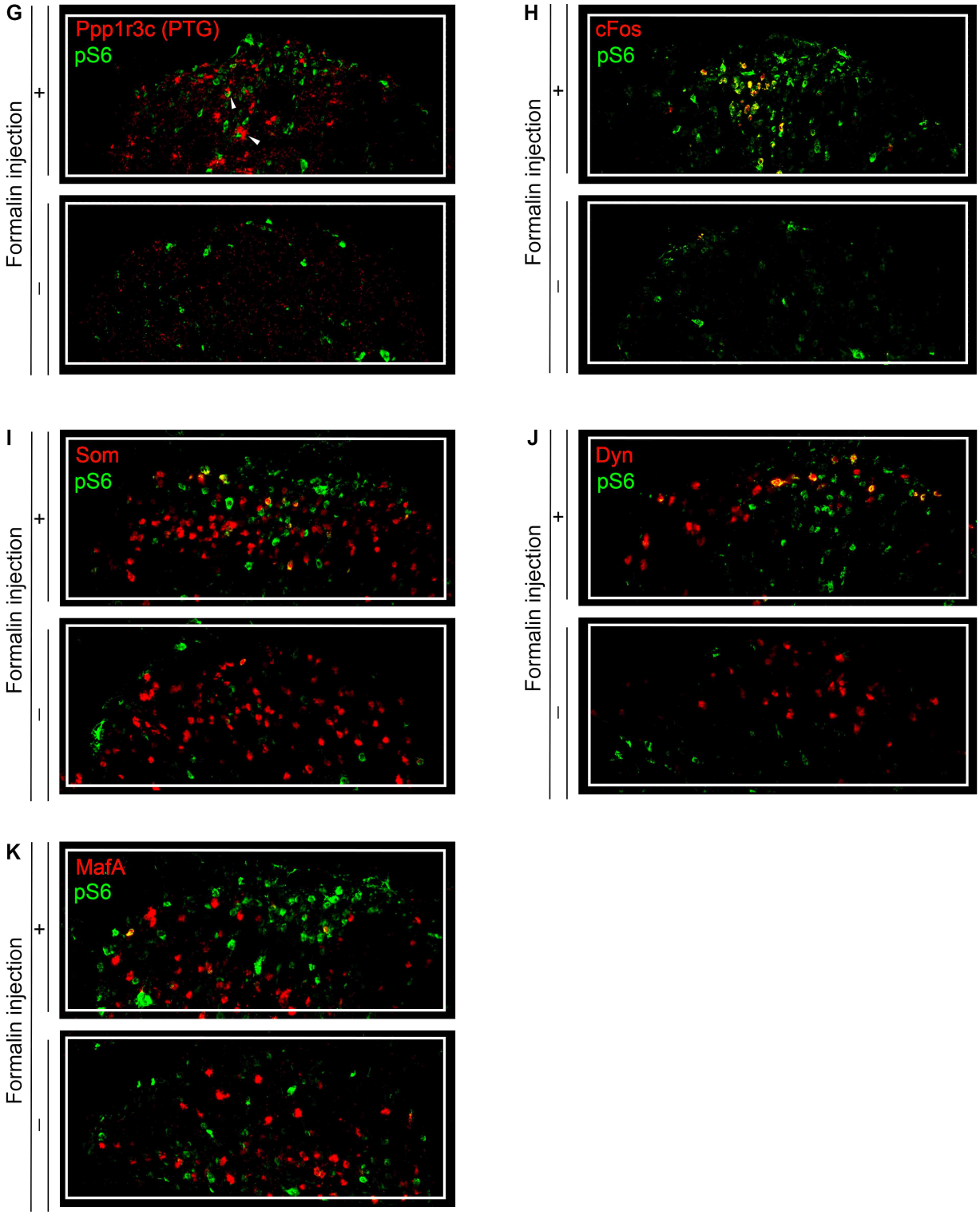

Figure 10: *In situ* hybridization verification of the sequencing results
10A-K: Expression pattern of candidate genes (red, *in situ* hybridization) and pS6 (green, immunofluorescence) in L4 dorsal spinal cord. All candidates stained showed partial or complete co-localization with pS6.
(A-C): Cadherins. *Cdh3* (10A) expression was lamina III specific while *Cdh18* and *Pcdhb16* (10B and C) spread through the dorsal horn.
(D-E): LncRNA *Meg3* (10D) and ion channel encoding *Ano6* (10E) both showed ubiquitous expression patterns.
(F-H): *Atf3*, *Ptg* and *c-Fos* were specifically induced in the ipsilateral dorsal horns.
(I-K): Known dorsal spinal cord 'pain' genes. *Som* (10I) and *MafA* (10K) spread through the dorsal horn, with most signals in lamina III. *Dyn* (10J) expression were found in lamina I and II.

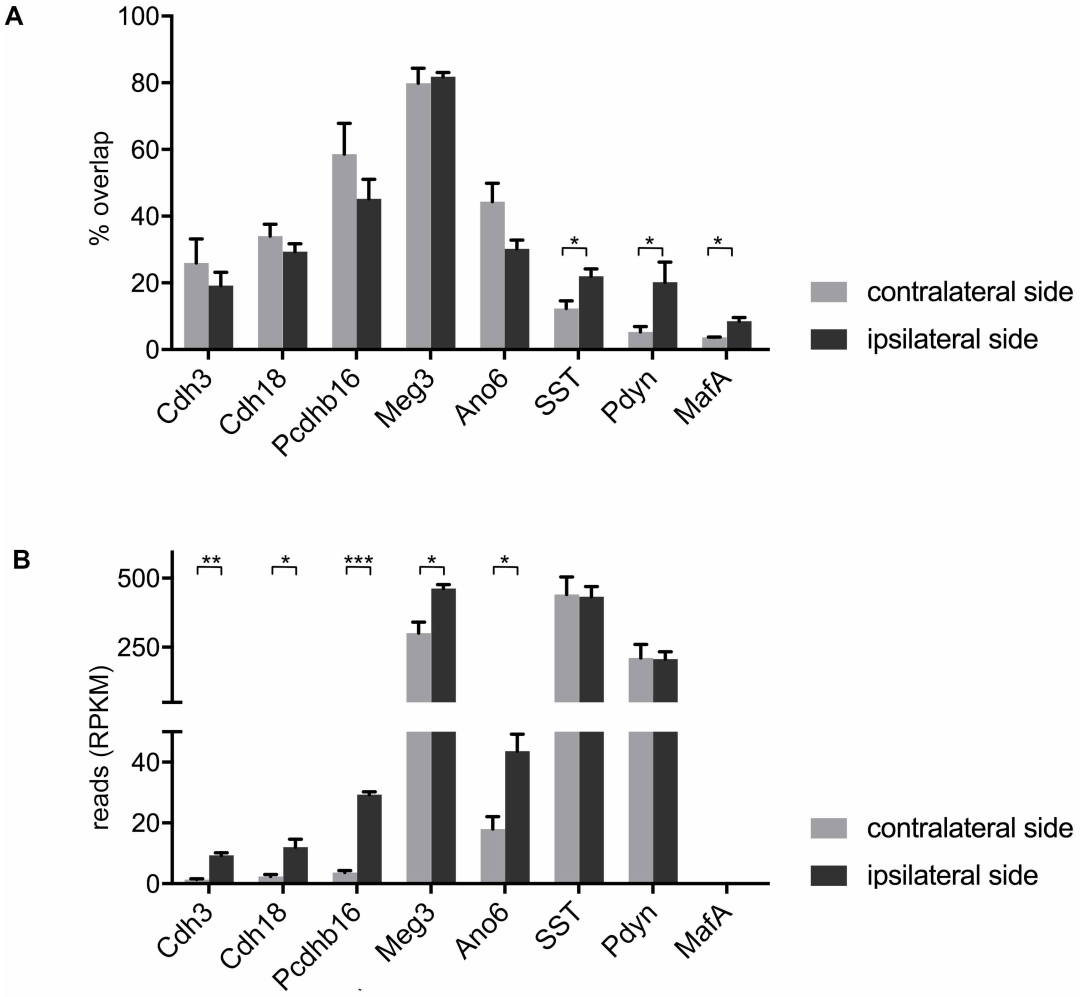

Figure 11: Quantification of in situ hybridization and sequencing results
11A: Percentage of candidate-gene expressing cells among pS6 positive cells in ipsi- and contra-lateral dorsal spinal cord were calculated, respectively. None of the candidates showed a significant ipsi-contra difference, however the 3 known dorsal horn specific genes (*Som*, *Dyn* and *MafA*) showed significant enrichment in ipsilateral sides (N=3, t-test).
11B: Reads of the same genes from sequencing. All the candidates had significantly higher reads in ipsilateral than in contralateral samples. No enrichment could be detected for the known dorsal horn 'pain' genes (N=3, t-test).

2.4.2.2 Quantifications of images and comparison to sequencing data

Atf3 and *c-Fos* showed clear co-localization with pS6 and are known activity markers, while *Ptg* showed only limited overlap with pS6, they were therefore excluded from the quantification of co-localizations.

I first counted the positive cells for all other candidates and pS6 in dorsal lamina I-III separately to avoid bias. I then overlaid the images to determine the double positive cells. Percentage was calculated as the portion of double-positive (candidate and pS6) cells in the pS6-positive population, for ipsilateral and contralateral sides, respectively. The quantification is shown in Fig11A, and normalized sequencing reads of these genes are plotted in Fig.11B.

The two graphs show contradicting results, when comparing to data shown in previous qPCR verifications. Firstly, by co-staining, the percentage of cells expressing both the candidate transcript and pS6 in the total pS6 population was not significantly different in the ipsi- and contra-lateral sides, contradicting the sequencing results, which showed significant enrichment of the candidate mRNA in the ipsilateral side. Secondly, *Som*, *Pdyn* and *MafA* were all significantly enriched in the pS6-positive cells in the ipsilateral sides over contralateral controls by *in situ* hybridization; whereas none of the three were identified by the phospho-ribosome profiling. To sum up, I was unable to verify candidate transcripts from the phospho-ribosome profiling experiment of formalin-induced pain by *in situ* hybridization. Furthermore, the method failed to identify known markers of neurons in the pain pathways. I did not achieve the goal of using pS6 immunoprecipitation to identify stable marks for spinal cells activated by peripheral painful stimuli. Possible reasons will be discussed later in the discussion part.

Nevertheless, I identified a novel transcript *Ptg*: despite its limited overlap with pS6, it was robustly induced upon painful stimuli. I therefore went on to characterize the involvement of Ptg in the spinal pain response.

2.5 Protein targeting to glycogen (Ptg) as a pain-induced transcript

I could show that *Ptg* mRNA is strongly induced on the ipsilateral side of the dorsal spinal cord by formalin-induced acute pain (Fig.12A). *Ptg* stands for protein targeting to glycogen, one of the few genes with a self-explanatory name. PTG protein is a subunit of protein phosphatase 1 (PP1) which guides PP1 to Glycogen Synthase (GYS). PP1 de-phosphorylates GYS, resulting in the activation of the latter, and glycogen is synthesized (Brady et al., 1997; Printen et al., 1997). In the brain, PTG is found predominantly in astrocytes and plays an important role in astrocytic glycogen synthesis (Allaman et al., 2000). On the other hand, abnormal excessive brain neuronal glycogen lead to the neurodegenerative Lafora disease. In Lafora disease studies, it has been reported that knocking down or out *Ptg* partially relieved the otherwise lethal symptoms (Guerrero et al., 2011; Turnbull et al., 2011; Turnbull et al., 2014).

2.5.1 Ptg localization and co-staining of Ptg with neuronal and glial markers

In order to identify the type of spinal cells in which *Ptg* is induced, I performed co-staining of *Ptg* (*in situ* hybridization) with the following cell type specific markers (immunofluorescence): GFAP (astrocytes), NeuN (neurons) and IBA1 (microglia). I continued using the formalin pain model. Fig.12B shows that filamentous GFAP signal enclosing perinuclear *Ptg*, while there was no overlap of Ptg with the neuronal marker NeuN or microglia marker IBA1. Therefore, consistent with previous study about brain *Ptg* expression (Cataldo & Broadwell, 1986), *Ptg* is induced in spinal astrocytes following formalin-induced acute pain.

- **pS6 marks reactive astrocytes**

In the co-staining of *Ptg* and pS6, I observed limited overlapping of the two signals (Fig.12A), and now with the knowledge that *Ptg* is predominantly in astrocytes, I asked whether pS6 also marks the astrocytes that are activated by formalin-induced pain i.e. reactive astrocyte? To test this, I performed co-staining of pS6 with the astrocyte marker GFAP (immunofluorescence). Fig.12C show GFAP positive filaments enclosing pS6 signals. Therefore, pS6 also marks reactive astrocytes. This might explain the above-mentioned observation that there were many more pS6-positive cells than c-Fos-positive neurons, i.e. a small fraction of pS6 cells are reactive astrocytes which does not express *c-Fos* upon activation.

But there is one more possible cause to the discrepancy of more pS6- then *c-Fos*-positive cells: the different dynamics of *c-Fos* and pS6. Although induced by the same signaling pathways, *c-Fos* mRNA is reported to be induced already 5 minutes after stimulation and would reach its peak level after 20 minutes (S. P. Hunt et al., 1987); whereas the phosphorylation of ribosome reaches its peak between between 1 hour to 2 hours after stimulation (Fig.5E). As the spinal cord tissue here was collected 2 hours after formalin injection, it is possible that some *c-Fos* mRNA has by then degraded.

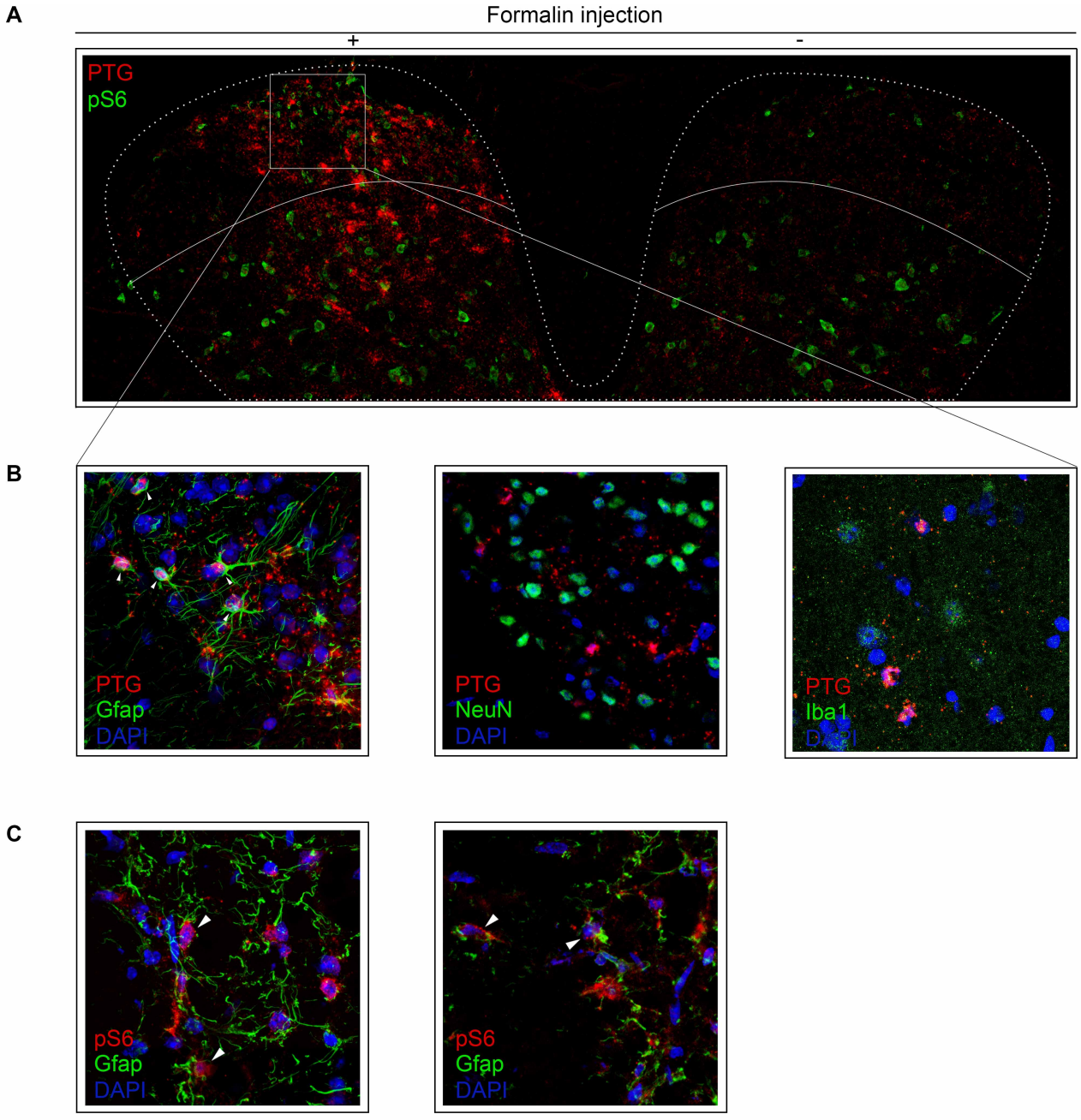

Figure 12: *Ptg* mRNA expression is induced in spinal astrocytes by formalin-induced acute pain
12A: *Ptg* mRNA (red, *in situ* hybridization) was induced at dorsal spinal cord, ipsilateral to formalin injection. The induction spread through the dorsal horn and showed limited overlap with pS6 (green, immunofluorescence).
12B: Co-stainings of *Ptg* (red, *in situ* hybridization) and cell type markers (green, immunofluorescent). *Ptg* were surrounded by filamentous astrocyte marker GFAP (left) but showed no co-localization with neuronal marker NeuN (middle) or microglia maker IBA1 (right).
12C: Immunofluorescent co-stainings of pS6 (red) and astrocyte marker GFAP (green). Partial co-expression of pS6 and GFAP were observed (white arrow).

2.5.2 Ptg RNA inductions in other forms of pain

Ptg is induced in spinal astrocytes by formalin-induced acute pain. To test whether the induction of *Ptg* is specific to formalin pain or is a general response to peripheral painful stimuli, I performed a series of *in situ* hybridization to examine the expression of *Ptg* mRNA in other acute and chronic pain models.

Apart from the previous described formalin-induced acute pain model, I also found induction of *Ptg* mRNA also by capsaicin-induced acute pain (Fig. 13A). However, when examining the samples collected at later time points after formalin pain (24 and 48 hours, Fig.13C and D), I did not find any more *Ptg* mRNA expression. Similar to the formalin model, I observed strong *Ptg* induction 2 hours post stimulation (Fig. 13B) but not after 3 days (Fig.13E). I also tested *Ptg* expression in the spared nerve injury (SNI) model. SNI is a model for neuropathic pain. SNI neuropathic pain is induced by severing two of the three branches of the sciatic nerve (the tibial nerve and the common peroneal nerve), leaving the sural nerve intact. To avoid the influence from surgical pain, I did not measure at the 2-hour time point, but examined the Ptg mRNA expression 7 days after the surgery. There was no *Ptg* mRNA detected. These data suggest that Ptg is induced within 2 hours after acute pain stimulation (formalin or capsaicin) and is transiently expressed. It is also induced in CFA inflammatory pain model, but while the pain persists for at least 7 days (Fehrenbacher et al., 2012), *Ptg* induction is observed only in the acute phase i.e. two hours after injection. Whether *Ptg* is also induced in the acute or subacute phase of SNI neuropathic pain model is, at this stage, not clear. *Ptg* inductions in different pain models are summarized in Fig. 13G.

With the above experiments, I showed that despite the unsuccessfully identification of stable markers using phospho-ribosome profiling, I identified *Ptg as* a pain-induced gene in spinal astrocytes and its transient induction was found in various pain models. In the following sections, I continued to explore the functional output of *Ptg*.

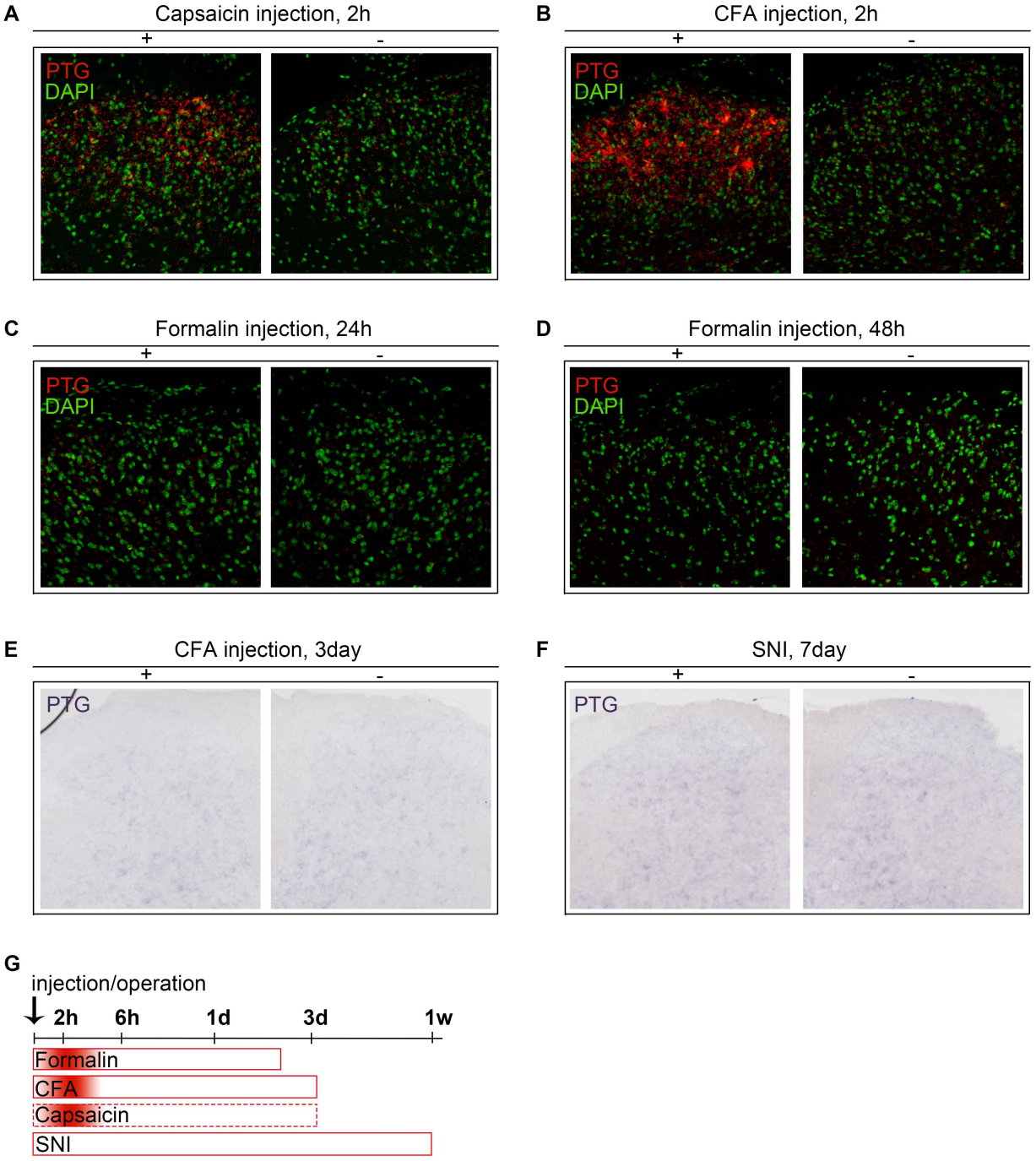

Figure 13: Ptg mRNA is transiently induced in acute and chronic pain models
13A: Capsaicin-induced acute pain. Ptg mRNA (red, *in situ* hybridization) was observed in ipsilateral dorsal spinal cord 2 hours after stimulation.
13B and E: CFA-induced inflammatory pain. Ptg mRNA expression was observed 2 hours (red, *in situ* hybridization) after intraplantar CFA injection in ipsilateral dorsal spinal cord, but not 3 days after (purple, *in situ* hybridization).
13C and D: Formalin-induced acute pain. No more Ptg mRNA expression (red, *in situ* hybridization) was detected 24 hours or 48 hours after formalin injection.
13F: SNI neuropathic pain. No Ptg mRNA expression was observed 7 days after the surgery (NBT/BCIP, in situ hybridization). No earlier time points were examined.
13G: Schematic summary of Ptg mRNA induction in different pain models. It is transiently induced at 2 hours after onset of formalin/capsaicin/CFA-induced pain.

2.6 Spinal glycogen profile of acute and chronic pain models

If *Ptg* mRNA is induced by peripheral painful stimuli, would there be a functional consequence? As *Ptg* is known as the main regulator of astrocytic glycogenesis (Ruchti et al., 2016), I studied the glycogen profiles of different pain models in order to check whether glycogen level is altered following *Ptg* mRNA induction.

2.6.1 Formalin-induced acute pain

I first examined the temporal profile of glycogen in the formalin-induced acute pain. I used an commercial kit to measure the glycogen level in the spinal cord tissue (see Material and Methods). The measurement includes two enzymatic reactions: (1) the hydrolysis of glycogen to glucose by glucoamylase and (2) the specific oxidization of glucose which produces a product that in turn reacts with OxiRed probes to generate fluorescence. The fluorescence is then measured by spectrophotometer and the glycogen level could be calculated. For this I collected dorsal spinal cord samples (ipsi- and contra-lateral) at different time points after intraplantar formalin injection, as well as from naive mice as the baseline i.e. the basal glycogen level in spinal cord. Glycogen levels were normalized to protein content and are plotted in Fig.14A. Naive mice exhibited scattered glycogen levels (detected levels ranged from 0.141 to 0.409 (μg/μL)/mg protein). Individual differences were as large as four-fold. Pairing the ipsi- and contra-lateral measurements (though no injection was admitted, the two sides are assigned ipsi- and contra-lateral for consistency and convenience) revealed comparable glycogen levels of the two sides, i.e. the mouse with high glycogen level at the ipsilateral side would also have high level at the contralateral side.

The first time point measured was two hours after injection, as it was the time when *Ptg* mRNA expression was observed. Although showing no difference between the two sides (0.188±0.022 vs 0.184±0.019 (μg/μL)/mg protein), glycogen levels at 2 hours after formalin injection seemed to have smaller individual variances, when compared to the scattered 'naive' data points.

Six hours after unilateral formalin injection into the hind paw, there was a significant difference in the glycogen levels between ipsi- and contra-lateral tissue samples: the ipsilateral glycogen levels doubled (0.400±0.015 vs 0.188±0.008 (μg/μL)/mg protein). The ipsilateral glycogen levels remained significantly higher than that of the contralateral control side at the third time point (24 hours post injection) examined (0.323±0.025 vs 0.160±0.009 (μg/μL)/mg protein).

The elevated glycogen levels dropped 3 days after injection, back to similar amount as in contralateral tissue (0.097±0.0193 vs 0.092±0.0204 (μg/μL)/mg protein).

Due to the scattered baseline, the ipsi-/contra-lateral ratio of glycogen levels was chosen to better represent the data. As previously explained, the scatter glycogen measurements of naive mice were ipsi-/contra-lateral wise paired. The ratio of glycogen levels of the ipsi- and contra-lateral tissue was calculated and shown in Fig. 14B. For naive mice, the ratios of glycogen levels in these mice were close to 1 (0.939±0.044), and similar ratios were observed two hours after formalin injection (1.026±0.093). In contrast, formalin injection caused a 2-fold increase in glycogen levels after six (2.044±0.118) and 24 hours (2.008±0.083). After 3 days, the ratio dropped back to 1 (1.078±0.062). These two plots (Fig.14A-B) showed a transient increase in glycogen level upon formalin-induced acute pain, that was delayed by approximately four hours in comparison to the *Ptg* mRNA expression. These data suggest that an acute painful stimulus triggers *Ptg* mRNA expression in dorsal spinal cord, which in turn leads to glycogen synthesis.

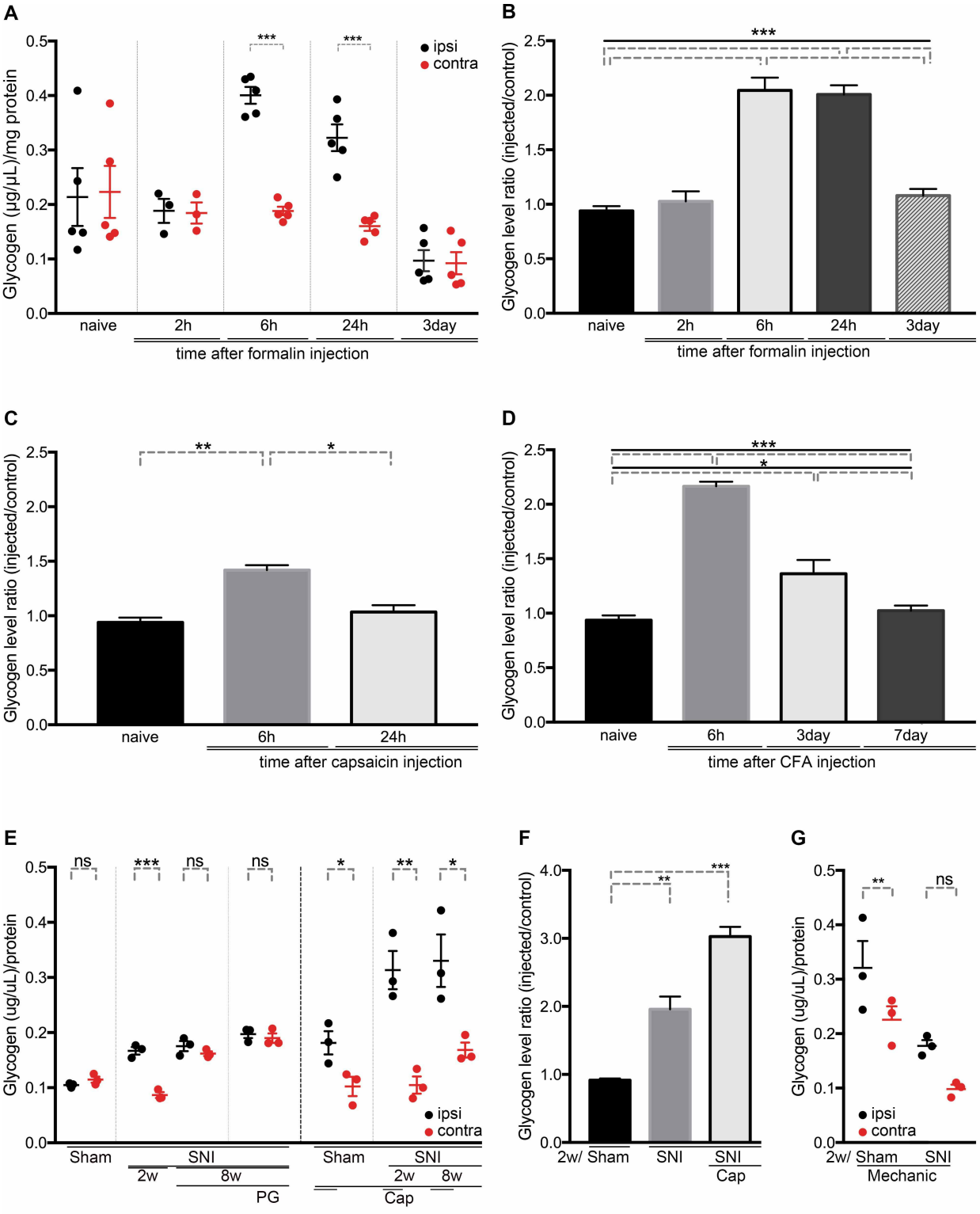

*legends on the next page

Figure 14: Spinal glycogen profiles of different pain models
Glycogen levels of ipsi- and contra-lateral dorsal spinal cord (L2 to 6) were measured.
14A and B: Formalin-induced acute pain. (A): Naive mice showed a spread in their glycogen levels but the ipsi- and contra-lateral levels of each mouse were paired (between 0.141 and 0.409 (μg/μL)/mg protein). 2 hours after formalin injection, similar glycogen levels in ipsi- and contra-lateral tissue were found (0.188±0.022 vs 0.184±0.019 (μg/μL)/mg protein), while 6 hours after injection, ipsilateral glycogen levels doubled (0.400±0.015 vs 0.188±0.008 (μg/μL)/mg protein). The ipsilateral glycogen levels remained significantly higher than that of the contralateral side 24 hours after injection (0.323±0.025 vs 0.160±0.009 (μg/μL)/mg protein). The elevated ipsilateral glycogen level dropped back to similar amounts as in contralateral tissue 3 days after (0.097±0.0193 vs 0.092±0.0204 (μg/μL)/ mg protein).
(B): Ratios of ipsi/contra-lateral glycogen levels. Corresponding to the paired ipsi-contra data in 15A, the ipsi/contra ratios of the scattered glycogen levels were around 1 in naive mice (0.939±0.044). Similar ratios were obtained 2 hours after injection (1.026±0.093). 6 hours after formalin injection, the ipsi/contra ratios increased (2.044±0.118) and remained high until 24 hours after injection (2.008±0.083). It dropped back to 1 after 3 days (1.078±0.062) (N=3 or 5, t-test).
14C: Capsaicin-induced acute pain. Ratios of ipsi/contra glycogen levels increased 6 hours after injection (1.419±0.046) and dropped 24 hours after (1.034±0.063) (N=2 or 3, t-test).
14D: CFA-induced inflammatory pain. Ratios of ipsi/contra glycogen levels rose 6 hours after injection (2.165±0.042) and were still elevated 3 days after injection (1.362±0.127). It dropped back after 7 days (1.024±0.046) (N=4, t-test).
14E-G: SNI neuropathic pain.
(E): Left: sham operated mice set the baseline glycogen levels at (0.105±0.002 and 0.115±0.006 (μg/ μL)/mg protein). Ipsilateral glycogen levels were found elevated 2 weeks after SNI surgery (0.167±0.007 (μg/μL)/mg protein), while those of contralateral sides stayed similar to baseline levels (0.087±0.005 (μg/μL)/protein). Both ipsi- and contra-lateral glycogen levels increased 8 weeks after the surgery (0.175±0.009 and 0.162±0.004 (μg/μL)/mg protein). Pregabalin (PG) treatment did not change the glycogen levels (0.197±0.007 and 0.190±0.009 (μg/μL)/mg protein). Right: Additional capsaicin injection (Cap) in SNI operated mice resulted in even higher ipsilateral glycogen levels as in sham mice (sham: 0.181±0.021, SNI 2 weeks+Cap: 0.313±0.035, SNI 8 weeks+Cap: 0.330±0.048 (μg/ μL)/mg protein). The additional capsaicin injection did not change contralateral glycogen levels (sham: 0.105±0.002, SNI 2 weeks+Cap: 0.105±0.016, SNI 8 weeks+Cap: 0.168±0.014 (μg/μL)/mg protein) (N=3, t-test).
(F): Ratio of ipsi/contra glycogen levels for sham, SNI 2 weeks and SNI 2 weeks+Cap mice from 15E. As there were no changes in glycogen levels for sham mice, the ratio stayed at 1 (0.915±0.026). Ipsilateral glycogen levels are 1.956±0.186 times higher than contralateral in SNI 2 weeks mice, while the additional additional capsaicin stimuli brought the ratio further to 3.027±0.142.
(G): Additional noxious mechanical stimuli on sham and SNI operated mice. Glycogen levels in SNI 2 weeks+Mec mice (0.178±0.010 vs 0.167±0.007 (μg/μL)/mg protein) were not different from those of SNI mice from 15E, while on the contrary, mechanic stimulation on sham operated mice resulted in elevated glycogen levels in both ipsi- and contra-lateral sides (0.321±0.0494 vs 0.226±0.025 (μg/μL)/ mg protein) (N=3, t-test) .

2.6.2 Capsaicin-induced acute pain

To study whether the observed glycogen increase is shared by other pain models, I then performed the similar experiment to obtain the spinal glycogen profile of capsaicin-induced acute pain (Fig.14C). Similar to the formalin pain model, I observed an increase in ipsilateral glycogen levels 6 hours after stimulation (ratio: 1.419±0.046), but glycogen levels already returned to the baseline 24 hours after capsaicin application (ratio: 1.034±0.063), resulting in a smaller and shorter peak than formalin acute pain. The different dynamics possibly reflects the intensity and duration of the two acute pain models.

2.6.3 CFA-induced inflammatory pain

In order to assess whether inflammatory pain model also show a similar dynamics in glycogen levels, I next tested the Complete Freund's Adjuvant (CFA) inflammatory pain model (Fig.14D). CFA inflammatory pain reaches its peak 24 hours after the injection and persists for at least 7 days (Fehrenbacher et al., 2012). Similar to the two acute pain models, increased levels of glycogen were detected in the ipsilateral samples 6 hours after CFA intraplantar injection (ratio: 2.165±0.042). I also measured glycogen levels 3 days and 7 days after the CFA injection since CFA inflammation persists for a longer time. While ipsilateral glycogen levels dropped back to baseline 3 days after formalin injection, it was still elevated 3 days after CFA injection (ratio: 1.362±0.127) but returned to baseline levels within 7 days (ratio: 1.024±0.046).

2.6.4 SNI neuropathic pain

I next asked what about the glycogen levels in chronic pain models? Glycogen levels were measured two and eight weeks after the neuropathic pain-inducing SNI surgery. Additionally I treated the mice with pregabalin, a GABA analog which is an effective medication against neuropathic pain, to determine whether suppressing chronic neuropathic pain would affect glycogen levels. I also applied an acute pain stimulus (capsaicin) in the SNI model to study the changes of glycogen level when mice are subject to two different painful stimuli (Fig.14E-G).

Although no mRNA induction were observed 7 days after surgery as previously shown, a dynamic profile of glycogen levels was uncovered. Ipsilateral glycogen levels were found elevated 2 weeks after SNI surgery (0.167±0.007 (μg/μL)/mg protein), while contralateral side stayed low (0.087±0.005 (μg/μL)/mg protein), as compared to the glycogen levels 2 weeks after sham operation (0.105±0.002 vs 0.115±0.006 (μg/μL)/mg protein). Interestingly, there was no more ipsi- to contra-lateral glycogen difference when analyzing the animals 8 weeks after the surgery (0.175±0.009 vs 0.162±0.004 (μg/μL)/mg protein). However, instead of the returning of the elevated ipsilateral glycogen levels to baseline as observed in the formalin/ capsaicin/CFA pain models, contralateral glycogen levels were increased.

Treating the animal 8 weeks after surgery with pregabalin (PG) did not change their glycogen levels (without PG: 0.175±0.009 and 0.162±0.004 vs with PG: 0.197±0.007 and 0.190±0.009 (μg/μL)/mg protein). As pregabalin alleviates pain, this result indicates that the relief of pain after its induction does not affect glycogen levels.

Both ipsilateral and contralateral glycogen levels change as SNI neuropathic pain progresses. Capsaicin was administrated into the ipsilateral hind paw and tissues were harvested 6 hours after injection. While contralateral glycogen levels were comparable to the corresponding levels in SNI animals without capsaicin injection (2

weeks SNI+Cap: 0.105±0.016 (µg/µL)/mg protein and 2 weeks SNI: 0.087±0.005 (µg/µL)/mg protein), 8 weeks SNI+Cap: 0.168±0.014 (µg/µL)/mg protein and 8 weeks SNI: 0.162±0.004 (µg/µL)/mg protein), the ipsilateral glycogen levels were significantly higher. Ipsilateral glycogen was already elevated 2 weeks after the induction of neuropathic pain, while an additional capsaicin stimulus boosted the glycogen level even higher (0.313±0.035 (µg/µL)/mg protein). The same was found for mice 8 weeks into neuropathic pain states. With some variances in the readings, an additional capsaicin stimulus also increased the glycogen levels further (0.330±0.048 (µg/µL)/mg protein). To confirm that an acute stimulation on a chronic background brings up glycogen levels further than either stimulation alone, I also applied capsaicin to sham operated animals. All four conditions (SNI, Sham, SNI+Cap and Sham+Cap) shared similar contralateral readings (Fig.14E). Highest ipsilateral glycogen levels were found in SNI+Cap mice (0.313±0.035 (µg/µL)/mg protein), mildly elevated in SNI or Sham+Cap mice (0.167±0.007 and 0.181±0.021 (µg/µL)/ mg protein, respectively) and remained unchanged in Sham mice (0.105±0.002 (µg/ µL)/mg protein) as well as in all contralateral sides.

I calculated the ipsi-/contra-lateral ratios for the ‘2 weeks after SNI’ data set. Sham mice did not have changes in their glycogen levels, thus resulting in a ratio similar as the previous ‘naive’ mice (0.915±0.026). Ipsilateral glycogen levels are 1.956±0.186 times higher than that of contralateral side in SNI mice, while applying an additional pailful chemical stimulus increased the ratio further to 3.027±0.142 (Fig.14F).

In addition to capsaicin, I tested another acute pain stimulation. SNI operated mice are known to develop mechanical hypersensitivity (Richner et al., 2011), and therefore painful mechanic stimulation was applied to the ipsilateral paw subjected to SNI surgery (Fig.14G). Glycogen levels in SNI+Mec mice were not different from plain SNI mice (0.178±0.010 vs 0.167±0.007 (µg/µL)/mg protein), while on the contrary, mechanic stimulation on Sham operated mice showed elevated glycogen levels in both ipsi- and contra-lateral sides (0.321±0.0494 and 0.226±0.025 (µg/µL)/mg protein). It would seem that painful mechanical stimulus alone can elicit glycogen

elevation, but no further increase can be observed when combining painful mechanical stimuli with existing mechanical allodynia.

In summary, in both acute (formalin and capsaicin) and inflammatory (CFA) pain models, ipsilateral glycogen levels increased about 6 hours after the induction of pain and would return to the baseline after 24 hours to 1 week, depending on the persistency of the pain. In neuropathic pain model, an increase in the ipsilateral spinal cord glycogen level was also observed, however, as the pain prolonged, the ipsilateral glycogen level did not decrease, instead, the contralateral glycogen level increased. Moreover, acute chemical pain (capsaicin) applied on mechanical allodynia background (SNI) would further increase the glycogen level, but additional acute mechanical pain did not.

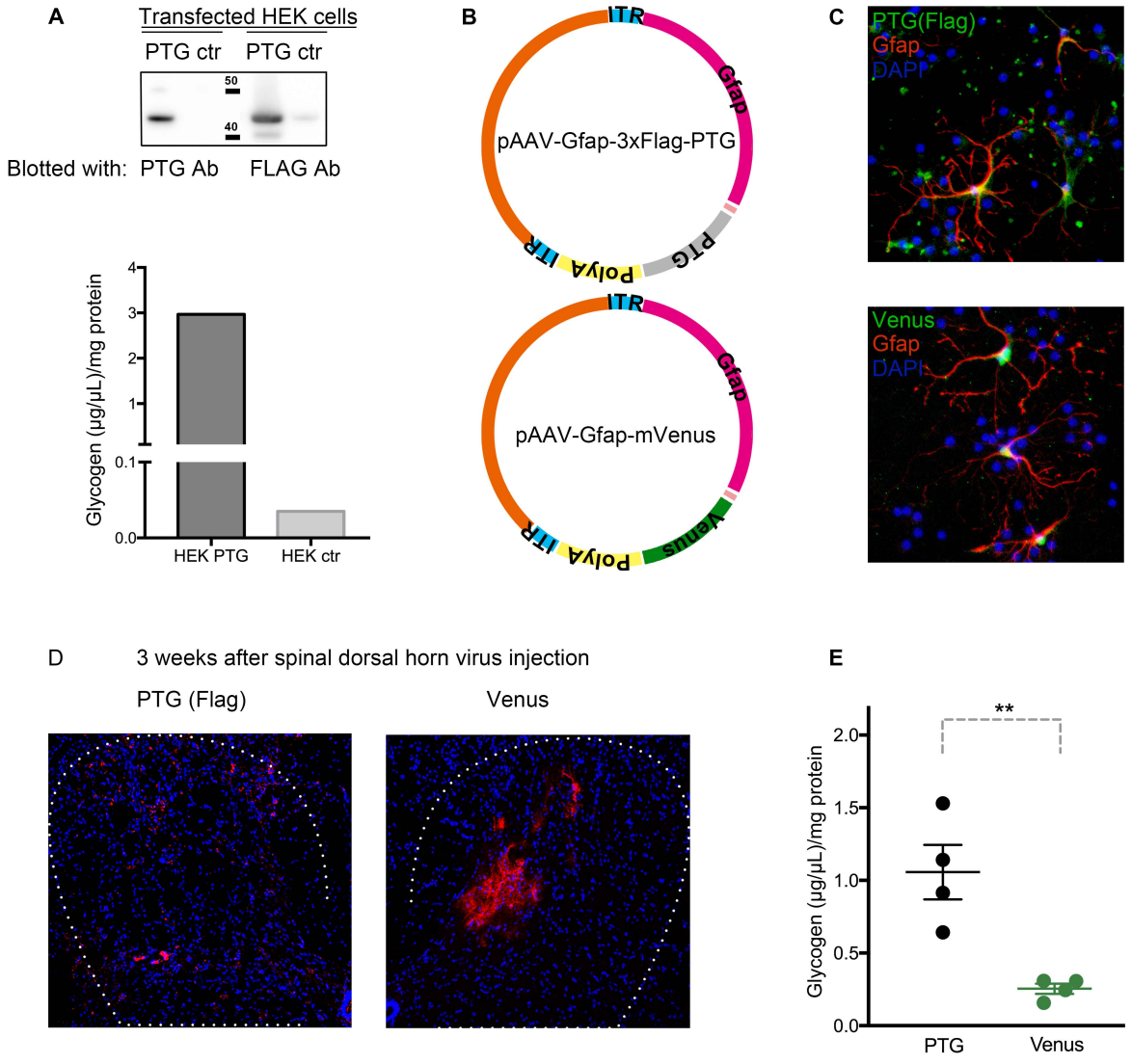

Figure 15: *in vitro* and *in vivo* PTG over-expression

15A: PTG over-expression test in HEK293 cells. Up: Ptg- and control (ctr)-transfected HEK cells were collected and loaded on a western blot and blotted with PTG (left) and FLAG (right) antibodies. In Ptg-transfected cells, both antibodies detected a band of ~40kDa which was absent from the control cells. Down: Glycogen level was greatly increased in PTG-expressing HEK cells as compared to control-transfected cells (PTG: 2.966 vs ctr: 0.035 (µg/µL)/mg protein).

15B: AAV viral constructs. 3xFlag-Ptg and Venus were under astrocytic Gfap promotor.

15C: PTG and Venus over-expression in astrocyte culture. Co-stainings of astrocyte marker GFAP (red) and PTG/Venus (green) showed astrocyte-specific expression of the two proteins respectively.

15D: PTG and Venus over-expression in dorsal spinal cord. Immunofluorescent stainings of dorsal spinal cord showed both PTG and Venus (red) expression following virus injection.

15E: Glycogen measurement after viral over-expression. The PTG over-expressing mice showed a significant increase in spinal glycogen level over Venus control mice (1.057±0.187 vs 0.254±0.036 (µg/µL)/mg protein, N=4, t-test).

2.7 The effect of glycogen levels on the pain state

I found that glycogen levels are elevated in the ipsilateral spinal cord 6 hours after acute pain stimulations or CFA induced inflammatory pain. It also increased 2 weeks after SNI surgery, and can be elevated further by the application of acute painful chemical stimulus on mechanical allodynia background. Does this additional glycogen have any effect on the extent of pain? Does it aggravate or alleviate pain? To answer these questions I next manipulated the *in vivo* expression of PTG in mouse and also blocked glycogen mobilization.

2.7.1 PTG over-expression

In order to increase glycogen levels, I over-expressed PTG using an adenoviral approach. To do this I first cloned 3xFlag-Ptg into pcDNA and tested its expression in HEK293 cells, meanwhile I cloned the 3xFlag-Ptg into an viral vector under a Gfap astrocyte-specific promotor and viral particles were produced by Karin Meyer to infect astrocytes *in vitro* and *in vivo*.

2.7.1.1 PTG over-expression in HEK cells

HEK cells were transfected with pcDNA-3xFlag-Ptg or an empty control vector and were collected 48 hours after transfection. Glycogen levels of the lysates were measured, and the remaining lysates were subjected to western blotting to detect FLAG and PTG.

Both FLAG and PTG antibodies detected a clear band at the same size (~40kDa), which was absent from the transfected negative controls (Fig.15A, up). This result

shows that, PTG was correctly expressed in HEK cells and that, since the FLAG antibody recognized a protein band of same size as PTG antibody did, FLAG could be used to report the presence of PTG.

PTG expressing HEK cells showed a strong increase in the glycogen levels compared to control transfected cells (2.966 vs 0.035 (µg/µL)/mg protein, Fig.15A, down), indicating that PTG is not only expressed, but also functional.

2.7.1.2 Testing pAAV-GFAP-3xFLAG-PTG and pAAV-GFAP-Venus viruses in cultured astrocytes

I next cloned AAV viral constructs encoding astrocytic Gfap promotor and 3xFlag-Ptg or mVenus inserts (Fig.15B). Before injecting the virus into mice, I test-infected cultured astrocytes with the above AAV virus. Mouse hippocampus primary cultures were infected with either the Ptg or Venus encoding AAV virus and kept in culture for 14 days by Dr. Anna Hertle. The cultured cells were then immuno-stained with antibodies against FLAG, Venus and GFAP. Both FLAG or Venus antibodies showed co-expression with the astrocyte marker GFAP (Fig.15C), suggesting that the GFAP promotor correctly directed the viral expression of the introduced transgender to astrocytes.

2.7.1.3 Over-expression of FLAG-PTG in mouse spinal cord

After successful test in cultures, viruses were injected in dorsal spinal cord by Dr. Manuela Simonetti. I sacrificed the mice 2 weeks after the injection and dissected the spinal cord out. I then checked for the expressions of FLAG-PTG and Venus control in spinal cord cross-sections by immunofluorescent stainings (Fig.15D). The glycogen levels of the infected dorsal spinal cord tissue were also measured. The PTG over-

expressing mice showed a significant increase in their spinal glycogen level as compared to Venus controls (1.057±0.187 vs 0.254±0.036 (µg/µL)/mg protein, Fig. 15E). This indicated the virus successfully infected astrocytes and over-expressed FLAG-PTG or Venus. The PTG over-expression resulted in elevated glycogen levels.

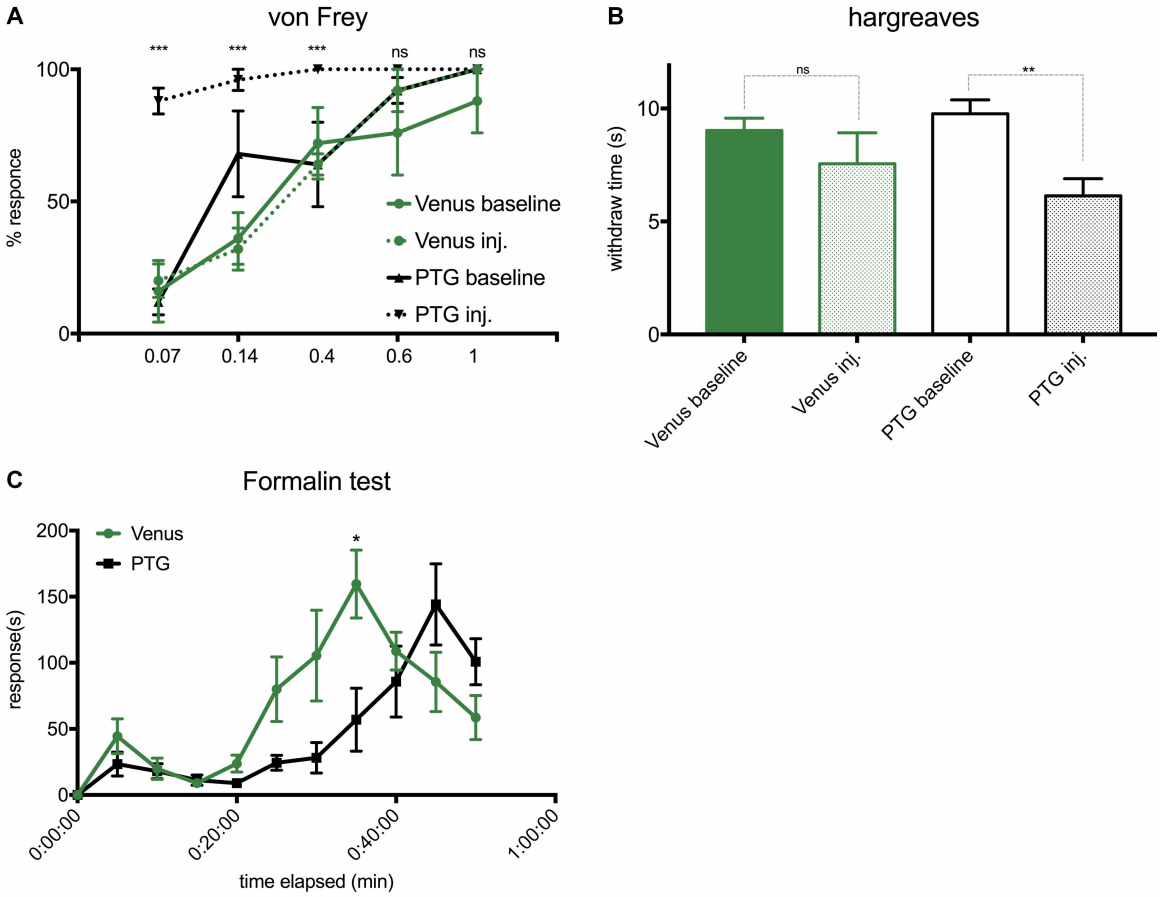

Figure 16: Altered pain thresholds in mice with spinal PTG over-expression
Mice were measured 3 weeks after virus injection, t-test, N=4.
16A: von Frey mechanical pain threshold. After PTG over-expression, the mice (black) exhibited significantly enhanced mechanical sensitivities: 0.07g filament (before:12±4.90%, after: 88±4.90%), 0.16g filament (before: 68±16.25%, after: 96±4.00%) and 0.4g filament (before: 64±16.00%, after: 100%). Venus over-expressing mice (green) showed no change before and after virus injection.
16B: Hargreaves thermal pain threshold. PTG over-expressing mice (black) showed a significantly higher thermal sensitivity (response time, before: 9.76±0.62s, after: 6.13±0.76s). Venus over-expressing mice (green) showed a non-significant drop in response time (before: 9.027±0.542, after: 7.554±1.369s).
16C: Formalin test. PTG over-expressing mice (black) showed a delayed second phase by 10 minutes, while the magnitudes of the second phase peaks did not change (PTG: 144.146±30.708s vs Venus: 159.563±25.710s).

2.7.1.4 Pain thresholds in mice over-expressing PTG

To test if high glycogen levels have an impact on mechanical and thermal pain thresholds, I performed the von Frey and Hargreaves test on the PTG over-expressing mice. The baseline was measured 3 days before virus injection and both mechanical and thermal thresholds were again measured 3 weeks after the injection (Fig.16A and B).

I did not observe a change in von Frey thresholds for the Venus injected control mice before and after the over-expression (before: 16.00±11.66%, after: 20±6.32%). In contrast to this I found that PTG over-expression significantly sensitized the animals to mechanical stimulation. Hence, spinal Ptg over-expression led to hypersensitivity upon painful mechanical stimulation (Fig.16A).

I also found a significantly increased thermal sensitivity in the PTG spinal over-expressing mice using the Hargreaves assay (Fig.16B). The response time significantly dropped from 9.76±0.62s to 6.13±0.76s, while Venus controls changed from 9.027±0.542 to 7.554±1.369s, indicating that the viral over-expression itself seems to have a slight, but non-significant, effect on thermal thresholds.

Next I measured the response to chemical pain by the formalin test in the mice over-expressing PTG or Venus. Formalin-induced pain elicits behaviors such as licking, flinching and paw lifting, and is known to have two phases (Carter & Shieh, 2010). The first phase starts immediately after the injection and lasts for 10 minutes. The second phase kicks in about 15 minutes after the injection and stays for about 50 minutes. Therefore, the behavior of the mice was video-recorded for 50 minutes after formalin injection, and their pain behaviors quantified in bins of 5 minutes (Fig.16C).

During the first phase (the first 10 minutes), PTG over-expressing mice seem to show a slight, but non-significant decrease in their response compared to control mice. During the second phase of the formalin response, PTG over-expressing mice were found to have a similar but delayed maximal response. Pain behaviors of the

control mice reached a maximum (159.6±25.7s) at 35 minutes after formalin injection, while the Ptg over-expressing mice exhibited a maximal response of similar magnitude (144.1±30.7s) at 45 minutes after injection. Both groups showed a decline of pain behaviors after reaching the peak.

2.7.2 Blocking glycogen mobilization

In the above section, I showed that elevated spinal glycogen levels following astrocytic PTG over-expression lead to altered pain sensitivity and nocifensive behaviors, I then wondered what would be the impact if the glycogen cannot be utilized? To test this, I used a potent glycogen mobilization inhibitor, 1,4-dideoxy-1,4-imino-D-arabinitol (DAB). DAB inhibits the activity of glycogen phosphorylase, the enzyme that breaks down glycogen into UDP-glucose as the first step of glycogen mobilization. DAB was administered by Dr. Manuela Simonetti via intrathecal injection 15 minutes prior to intraplantar formalin injection. Again, I recorded the behavior of the mice for 50 minutes after formalin injection, and scored their pain behaviors (Fig.17).

The DAB-injected mice showed a significantly suppressed pain behavior during the first phase (in the first 5 minutes: 2.6±0.8s vs 21.0±7.1s). There was no significant difference in the second phase of the formalin response between DAB-injected and control mice (peak at 35 minutes: 57.5±15.9s vs 67.1±23.2s). In this experiment, the mice in general exhibited weaker nocifensive reactions compared to those in the previous PTG over-expression experiment (second peak: ±67s vs ±150s). As these mice were subject to two consecutive isoflurane anesthesia within 15 minutes, the stress from short-spaced consecutive rounds of anesthesia (Hohlbaum et al., 2017) may have contributed to the reduced overall nocifensive behavior exhibited. Nevertheless, DAB seems to suppress pain behavior in the first phase of formalin test,

suggesting that the neuronal activity behind this pain behavior reply on astrocytic glycogen mobilization.

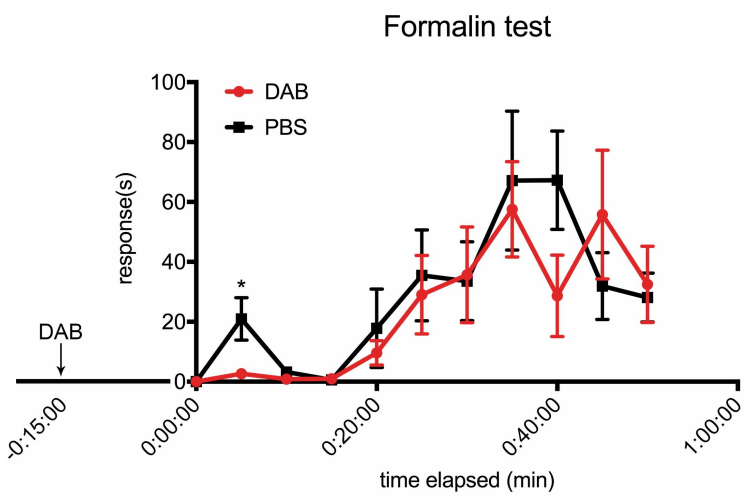

Figure 17: Intrathecal administration of glycogenolysis inhibitor DAB suppresses formalin test response
Mice received intrathecal injection of either glycogenolysis inhibitor DAB or PBS control, 15 minutes before intraplantar formalin injection. The first phase peak was significantly suppressed in DAB injected mice (DAB: 2.646±0.843s vs PBS: 20.967±7.084s). Similar second phase pain behaviors were observed in DAB or PBS injected mice (N=4, t-test).

3. Discussion

3.1 Molecular profiling of spinal dorsal horn cells activated by formalin-induced acute pain

3.1.2 pS6 marks spinal cells activated by peripheral painful stimuli: not only neurons but also astrocyte

The ribosomal subunit 6 (S6) is phosphorylated upon activation of the PI3-K/mTOR, MAPK, and PKA signaling pathways, leading to increased translational activities of the ribosome (Knight et al., 2012). The same signaling pathways are also known to lead to the expression of activity-dependent genes such as *c-Fos* (Flavell & Greenberg, 2008; Valjent et al., 2011). Several studies have reported overlapping pattern of *c-Fos* and pS6 expression in brain regions activated by fear or aggression (Dielenberg et al., 2001; D. Lin et al., 2011). In my thesis work, I used pS6 to mark spinal dorsal horn cells activated by peripheral painful stimuli, e.g. formalin-induced acute pain. After the induction of unilateral pain, immunofluorescent stainings showed specific pS6 expression in the ipsilateral superficial dorsal horn, the spinal cord region responsible for pain processing (Section 2.1). I could show that the pS6 staining overlaps not only with the neuronal activity marker *c-Fos* but also with the astrocyte marker GFAP, suggesting that pS6 marks also reactive astrocytes.

Expression of pS6 as a marker for mTOR activity has been previously reported in spinal astrocytes (Codeluppi et al., 2009; Sha et al., 2012; Kjell et al., 2014). Therefore, I propose the possible application of the phospho-ribosome profiling technique to astrocytes. One point to note is that, as illustrated in Fig.18, there are five phosphorylation sites on ribosomal protein S6 (p235,236,240,244 and 247). The phosphorylation of S6 is believed to occur in an activity-dependent sequential order i.e. N-terminal sites (p235/236) are phosphorylated with low, basal activities, while

the most C-terminal sites (p244/247) are phosphorylated only upon strong activities (Meyuhas, 2008). I used an anti-p240/244 antibody in my study while in the above-mentioned spinal astrocytes studies (Codeluppi et al., 2009; Kjell et al., 2014), an anti-p235/236 antibody was used. Knight and colleagues reported that in immunofluorescent stainings, phosphorylation at sites p235/236 and p240/244 are both stimuli-specific; however, immunoprecipitation with an anti-p240/244 antibody was proposed by Knight and colleagues to yield a more robust enrichment as it would only enrich the strongly activated neurons (Knight et al., 2012). Although the choice of antibody, among many other procedural details, needs to be optimized for the phospho-ribosome profiling to be applied to reactive astrocytes, my result shows that the technique, first of all, can be extended to astrocytes.

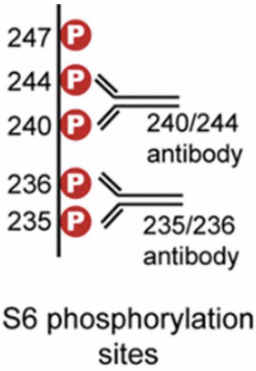

Figure 18: Five phosphorylation sites of ribosome subunit S6
The five sites of phosphorylation on ribosomal protein S6. The phosphorylation of S6 occur in an activity-dependent sequential order i.e. N-terminal sites (p235/236) are phosphorylated with low, basal activities, while the most C-terminal sites (p244/247) are phosphorylated only upon strong activities. In this study, antibodies against p240/244 were used.

3.1.2 pS6 profiling as a potential mean to decipher the molecular identities of CNS cells by their stimuli-specific activities

Based on the initial observation of specific pS6 expression in the superficial dorsal horn of the spinal cord following formalin-induced acute pain, I optimized the pS6 immunoprecipitation protocol and performed the subsequent transcriptomic analysis. With my experimental setting, an enrichment observed in the sequencing data could mean: (1) the gene is stably expressed in the pS6-positive cells, or (2) the gene is induced in the pS6-positive cells by the given stimulation.

As shown in Section 2.4.2, of the 11 genes tested by *in situ* hybridization, only the 3 induced genes *Atf3*, *Ptg* and *c-Fos* were consistently identified by both *in situ* hybridization and sequencing. Neither could the stably-expressed genes enriched by pS6 immunoprecipitation be verified by *in situ* hybridization (*Cdh3*, *Cdh18*, *Pcdhb16*, *Meg3* and *Ano6*), nor could the known dorsal horn specific 'pain' genes (*Som*, *Dyn* and *MafA*) be enriched by pS6 immunoprecipitation. At this point, I had to conclude that, this experimental setting failed to identify stable and robust maker genes for spinal cells selectively activated by formalin-induced acute pain. Nevertheless, I obtained a molecular profile of all spinal dorsal horn cells, two hours after peripheral formalin injection. Therefore, the differentially enriched genes identified in my study are those induced by formalin-induced acute pain: mostly immediate early genes, but one newly identified pain-induced gene, protein targeting to glycogen, Ptg.

Several reasons could lead to this result, as illustrated in Fig.19. First of all, I used a different p240/244 antibody from the one authors used. I used a monoclonal antibody instead of the polyclonal one used by Knight and colleagues. As previously mentioned, Knight and colleagues used an antibody against the more C-terminal p240/244 sites in order to achieve a greater enrichment. The authors further enhanced the selectivity of the antibody by pre-incubating it with a phosphopeptide containing the S6 p240 site, thereby obtaining an antibody that recognizes only p244 (Knight et al., 2012). I reasoned, that it would not be necessary to pre-incubate the monoclonal antibody that I used, since it has high specificity only to a single epitope, which reduces the probability of cross reactivity (Lipman et al., 2005). The monoclonal antibody, although showed high specificity in immunofluorescent staining, lost its selectivity to p240/244 S6 in my immuno-precipitation settings, as shown by the western blot in section 2.2.3, and most likely also recognized the more N-terminal phosphorylation sites. Nevertheless, my qPCR results suggested that *Nk1r*, *Som* and *FosB* are enriched in the ipsilateral (the stimulated side) samples and the immunoprecipitation experiment performed reasonably well, therefore I subjected my

samples to RNA sequencing. However, the pre-sequencing qPCR results unfortunately could not be confirmed by sequencing. There seems to be too little a difference in the ipsilateral stimulated and contralateral control samples to identify stimuli-specific, stable population markers.

A further possibility is that the monoclonal pS6 antibody may recognize other mRNA bound proteins with a similar epitope or nascent phosphorylation emerging from the ribosomes. These cross-reactivities would reduce signal-to-noise ratio, which in turn minimizes the ipsilateral-to-contralateral difference.

I reason that the following changes could improve my pS6 immunoprecipitation: (1) more stringent immunoprecipitation conditions to reduce unspecific binding/cross-reactivities, such as increasing detergent or salt concentration of IP buffers, increasing the numbers of washing or prolonging the washing time, 2) optimizing the ratio of total protein input to antibody, as the stoichiometry may affect immunoprecipitation efficiency and specificity (Marcon et al., 2015), or 3) using possibly a different pS6 antibody.

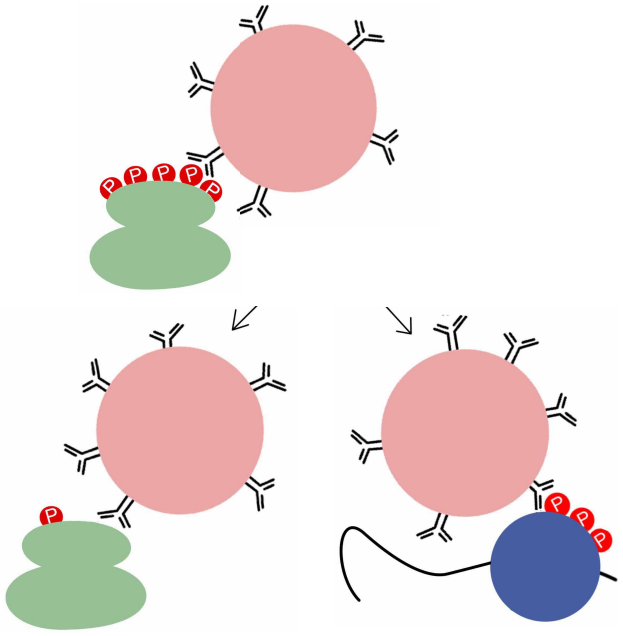

Figure 19: Possible reasons for the suboptimal phospho-ribosome profiling
Instead of a specific binding of pS6 antibody to the strongly phosphorylated ribosome (up), the antibody may also bind to (i) weakly phosphorylated ribosomes (left) or (ii) other similar phosphor-moiety in the vicinity (right).

Although I was unable to identify population marker through phospho-ribosome profiling, successful phospho-ribosome profiling as a technique has been reported once more since its first introduction by Knight and colleagues. In a study by Jiang and colleagues, subgroups of specific odorant receptors expressing olfactory neurons were successfully identified (Jiang et al., 2015). In this study, the same polyclonal anti-p240/244 S6 antibody as in the original protocol was used. The S6 p240-containing phosphopeptide was not used, as the scientists reported significantly reduced mRNA yield after a test pre-incubation and observed relatively low pS6 background in the olfactory epithelium (Jiang et al., 2015). I speculate this low basal level of may be another factor that could have possibly facilitated their experiment, and should be taken into consideration in future phospho-ribosome profiling experiment design.

With optimal experimental settings, I believe phospho-ribosome profiling could still be a powerful tool to study spinal pain processing. As I could show that pS6 marks both active neurons and reactive astrocytes, one future application could be to obtain separate transcriptomes of these two cell populations. Protocols to isolate neurons and different glial cells from CNS tissue, mostly brain, have been previously established (Cahoy et al., 2008; Guez-Barber et al., 2012; Saxena et al., 2012; Srinivasan et al., 2016). Applying pS6 phospho-ribosome profiling to analyze isolated neurons or astrocytes moves forward from the conventional cell type specific sequencing and provides an additional activity/function-specific entry point to identify cells types responsible for specific functions.

Nevertheless, the phospho-ribosome profiling led to the discovery that the expression of Ptg mRNA is induced by peripheral formalin-induced acute pain.

3.2 Ptg induction and the dynamic glycogen level following peripheral painful stimuli

I could show that Ptg co-localizes with the astrocyte marker GFAP. This shows that *Ptg* is induced in spinal astrocytes, which is in line with previous reports that *Ptg* mRNA is expressed in cortical astrocytes (Allaman et al., 2000; Lovatt et al., 2007). *Ptg* regulates glycogen synthesis by mediating the de-phosphorylation of glycogen synthase by protein phosphatase 1. Once de-phosphorylated, glycogen synthase becomes active and synthesizes glycogen (Brady et al., 1997; Printen et al., 1997; Greenberg et al., 2006; Jurczak et al., 2007). A basal expression of *Ptg* mRNA is maintained in cortical astrocytes to meet the metabolic demand under physiological conditions (Lovatt et al., 2007), and an elevated expression can be stimulated by the neurotransmitter noradrenalin (NA) and the peptide hormone vasoactive intestinal peptide (VIP) in cultured astrocytes (Allaman et al., 2000). In my experiments, I could show that the induction of astrocytic *Ptg* mRNA was transient (i.e. induction at 2 hours and gone by 24 hours) and independent of the type or persistency of pain stimulus (formalin/capsaicin/CFA, see section 2.5). This result suggests that it is more likely a general pain-triggered induction than specific to certain categories of noxious stimulations. Therefore, when I examined the spinal cord 3 days after spared nerve injury (SNI), a neuropathic pain model, I could not observe the ipsilateral (operated) *Ptg* induction. Similarly, a recent transcriptomic study using another neuropathic pain model, spinal cord injury (SCI), failed to detect the induction of *Ptg* (Shi et al., 2017). The brief, transient induction could potentially explain the absence, as these studies were performed at least 1 day after the injury (Chen et al., 2013; Shi et al., 2017). It is likely that I would observe an induction of *Ptg* in the SNI model if I would examine the spinal cord 2 hours after operation, but at such short time after surgery, the nociceptive input would come from both the surgical wound and the damaged nerves.

Although the *Ptg* mRNA induction is transient and independent of the pain model used, I found surprising differences in the functional outcome (i.e. the synthesis/

accumulation of glycogen) (see section 2.6). When comparing the glycogen profiles of the pain models studied, an interesting correlation was observed: in formalin/ capsaicin/CFA pain models, although the glycogen elevations in the ipsilateral spinal cord, i.e. the stimulated side, were observed around the same time (6 hours after stimulation), the extent of glycogen increase and the duration of elevated glycogen levels seem to correlate with the severity and persistency of pain.

The shortest-lasting capsaicin-induced acute pain led to a 1.4 times more ipsilateral glycogen, which dropped back to the same levels as the contralateral control side after 24 hours. Formalin induced a higher, 2-fold glycogen increase in the ipsilateral spinal cord, which stayed elevated for 24 hours. The CFA model, which induces longer lasting pain (Fehrenbacher et al., 2012), let to elevated glycogen levels for more than 3 days. And in the case of chronic SNI neuropathic pain, I observed a 2-fold higher glycogen levels even 2 weeks after the surgery.

To briefly recapitulate: (1) a transient Ptg mRNA induction (<1day) in spinal astrocytes is triggered by peripheral painful stimuli; (2) glycogen level increases in the ipsilateral spinal cord following peripheral painful stimuli; (3) the length and magnitude of the elevated ipsilateral glycogen level correlates with the severity and persistency of pain. How could this be explained?

The central terminals of nociceptors release a pool of signaling molecules into dorsal horn laminae I and II when activated, including peptide hormone VIP (Dickinson & Fleetwood-Walker, 1999). VIP has been reported to stimulate *Ptg* mRNA expression through the cAMP signaling cascade in several studies using in cortical astrocyte culture (Sorg & Magistretti, 1992; Allaman et al., 2000; Ruchti et al., 2016). While these previous studies were all conducted *in vitro*, I believe the same mechanism may also apply *in vivo*, i.e. as nociceptors are activated by peripheral painful stimuli, they release VIP into superficial dorsal horn, where it is taken up by spinal astrocytes to trigger new transcription through cAMP signaling, and *Ptg* mRNA

expression is thereby induced. Following VIP stimulation, Allaman and colleagues detected an increase in *Ptg* mRNA expression in cultured astrocytes as early as 2 hours after application of VIP, *Ptg* expression reached a maximum at 4 hours and returned to basal level by 24 hours. I found similar *Ptg* mRNA dynamics in my study, although I can not say when the peak was reached as I did not include any time points between 2 and 24 hours.

VIP also affects the glycogen levels in astrocytes. It exerts a biphasic effect on glycogen levels via cAMP signaling, i.e. a rapid Ptg-independent glycogen mobilization (minutes) and a delayed Ptg-dependent glycogen re-synthesis (hours) to replenish the glycogen reserves (Sorg & Magistretti, 1992; Allaman et al., 2000; Ruchti et al., 2016). In the study by Sorg and Magistretti, scientists mapped the glycogen level of cortical astrocyte cultures following VIP stimulation: (1) the rapid glycogen mobilization led to a near depletion 1 hour after application of VIP, and (2) as the re-synthesis starts, glycogen level rose back to the basal level 2 hours later, and continued to rise until they reached the peak 8 hours after VIP stimulation, and (3) returned to basal level 48 hours later. For the later time points, I observed similar dynamics in formalin/capsaicin/CFA models (Fig.14): a peak at 6 hours and the subsequent return to base line. According to Sorg and Magistretti, the glycogen level first dropped then recovered during the first 2 hour. As I did not include a 1 hour time point in my time series, I propose two scenarios here: (1) the *in vivo* condition reflects the *in vitro* observation, and the spinal glycogen level significantly drops 1 hour after peripheral painful stimulation or (2) while VIP application virtually affect all the astrocytes in culture, in *in vivo* condition, the number of astrocytes activated by a given painful stimuli may be relatively small, and the depletion of their glycogen storage may not significantly affect the *total* spinal dorsal horn glycogen level. As my current glycogen measurement does not render cellular resolution, one potential future experiment is to apply anti-glycogen antibody to visualize the drop of glycogen levels during the early phase i.e. 0-2 hours after the stimulation.

Astrocytic glycogen metabolism is linked with neuronal activity (Magistretti & Allaman, 2007). Although astrocytic glycogen was long considered as just an emergency energy source, in case of hypoglycemia or ischemia (Obel et al., 2012), more and more compelling evidence are suggesting the involvement of astrocytic glycogen in neuronal functions under physiological condition (Belanger et al., 2011): (1) increased levels of glycogen was found in the sleeping brain, indicating that increased neuronal activity in the awake brain consumes glycogen (Magistretti et al., 1993; Brown, 2004); and (2) decreased glycogen levels were found associated with increased neuronal activity, demonstrating the coupling of neuronal activity and glycogen mobilization (Swanson et al., 1992; Dienel et al., 2007). As discussed in the paragraph above, I hypothesize a decrease in glycogen levels immediately following painful stimuli. This decrease would be concurrent with the activation of spinal pain neurons, as shown by *c-Fos* and pS6 stainings (Fig.5), i.e. the nociceptors activate spinal neurons as well as the spinal astrocytes. In contrast to previous *in vivo* brain astrocytic glycogen studies (Swanson et al., 1992; Magistretti et al., 1993; Brown, 2004; Dienel et al., 2007), but in accordance with the *in vitro* study by Sorg and Magistretti, I report a delayed but sustained glycogen re-synthesis. The possible reasons for the massive, sustained glycogen re-synthesis will be discussed later in light of the possible roles of astrocytic glycogen in pain processing.

Sorg and Magistretti also reported a correlation between stimulus intensity/ concentration and the magnitude of the Ptg-dependent glycogen re-synthesis. Although they did not test if a stronger stimulus would lead to a longer state of elevated glycogen, it is a reasonable speculation (Sorg & Magistretti, 1992). This partially explains the correlation between the length and magnitude of the elevated ipsilateral glycogen level and the severity and persistency of pain I observed. With my current dataset, I propose a scenario that (1) within a narrow dynamic range (up to 2 fold), the stronger the pain is, more astrocytes are activated, and higher the ipsilateral glycogen level increases, and (2) once the elevated glycogen level reaches the upper limit of 2 fold, the longer the pain persists, the longer the glycogen level remains

elevated. This hypothesis is supported by (1) a higher ipsilateral glycogen is reached 6 hours after the stronger formalin-induced pain than that after the milder capsaicin-induced pain (2 fold vs 1.4 fold) and (2) formalin/CFA/SNI-pain all resulted in a 2-fold ipsilateral glycogen increase, but it took longer for the elevated ipsilateral glycogen to return to baseline after CFA injection than it did after formalin injection (>3 days vs 1 day). Furthermore, it was still 2-fold higher 2 weeks after the chronic pain inducing SNI surgery. The 2-fold high glycogen level seems to be the upper limit evoked by a single stimulus, as injecting capsaicin to mice already under SNI neuropathic pain brought ipsilateral glycogen a further 50% higher i.e. a 3-fold increase from contralateral/baseline. Since capsaicin-pain and SNI neuropathic pain recruit different nociceptors, and likely different astrocytes as well, the newly activated astrocytes by capsaicin-pain contribute to the additional rise. This is also consistent with the result that additional painful mechanical stimulus did not further increase glycogen levels of mice already with mechanical allodynia. A more complete glycogen profile of these pain models would reveal more details about the dynamics of glycogen re-synthesis while immunofluorescent staining of the activity marker pS6 in combination with neuronal marker NeuN could be used to map the exact duration of neuronal activities in different pain models. Based on the graded glycogen level changes, one additional interesting question would be: is the glycogen change specific to painful stimuli? or is it a more general activity triggered process? Testing the glycogen levels following innocuous stimuli such as gentle mechanical brushing would shed more light in this regard.

There remains, however, a missing link to account for the different time spans of *Ptg* mRNA and elevated glycogen level. The mRNA is degraded within a day (Fig.13) (Allaman et al., 2000), while ipsilateral glycogen levels remain elevated as long as the pain persists (Fig.14). For the initial phase, the first 24 hour, pain-induced Ptg mRNA expression results in new PTG protein synthesis and glycogen synthesis is thereby activated. While 2 weeks into SNI neuropathic pain, it is still an open question

whether PTG protein is around to mediate the activity of glycogen synthase anymore, as there unfortunately lacks a working antibody against PTG. Alternatively, the involvement of PTG could be indirectly tested via the visualization of the de-phosphorylated (active) and the phosphorylated (inactive) forms of glycogen synthase by immunofluorescent staining.

On the other hand, as reduced but still significant amount of glycogen was found in the brain of PTG knock-out mice (Turnbull et al., 2011; Turnbull et al., 2014), existence of PTG-independent glycogen synthesis pathway(s) has been proposed: (1) insulin or glutamate have been reported to mediate glycogen levels in astrocytes through PTG-independent mechanism (Swanson et al., 1990; Dringen & Hamprecht, 1992; Hamai et al., 1999; Allaman et al., 2000), and (2) additional CNS glycogen targeting proteins PPP16, PPP1R3F and PPP1R3G (Armstrong et al., 1997; Kelsall et al., 2011; Zhang et al., 2014) may sustain normal CNS glycogen synthesis in the absence of PTG. One or a combination of these modulators may account for the continued glycogen synthesis after the pain-induced *Ptg* mRNA and the subsequently synthesized PTG protein have been degraded or down-regulated and the study of their expression in the presence and absence of PTG may reveal more details of the complementary metabolic glycogen pathways.

Before I go on to the roles of astrocytic glycogen in pain processing, I would like to mention one more intriguing observation regarding glycogen levels. Eight weeks after SNI surgery, the contralateral glycogen levels doubled while the ipsilateral glycogen level was still 2-fold elevated. A study by Decosterd and Woolf showed that SNI produces only ipsilateral mechanical allodynia but not in the contralateral side (Decosterd & Woolf, 2000). However, studies have shown development of bilateral mechanical allodynia following unilateral SNI surgery (Swartjes et al., 2011) and bilateral increase of the pro-inflammatory cytokine TNF-α and microglia activation following other unilateral nerve damages (Hatashita et al., 2008; Jancalek et al., 2010). Therefore, it is possible that these mice developed contralateral mechanical

allodynia, which could be tested in future experiments with the von Frey assay. Both increased general metabolic activity and glucose consumption in contralateral spinal cord following unilateral forms of nerve injury has been reported (Price et al., 1991; Won & Lee, 2015), which are consistent with my observation.

3.3 The role of astrocytic glycogen in pain processing

Following peripheral painful stimuli, I showed an induction of astrocytic *Ptg* mRNA and a dynamic pain state-dependent glycogen profile. What does this glycogen do and why would the astrocytes synthesize more glycogen during the re-synthesis?

Two generally accepted hypothesizes of how astrocytic glycogen benefits neurons are the inter-cellular transport of glycogen-derived lactate as source of energy and glycogen-derived neurotransmitter glutamate (Gibbs et al., 2007; Suzuki et al., 2011; Obel et al., 2012; Sickmann et al., 2012; Waitt et al., 2017).

- **Astrocytic glycogen as the source of lactate**

Neurons have been, until recently, believed to obtain their energy through their own oxidative metabolism of glucose. Emerging evidences are showing that neurons can efficiently utilize lactate and, actually, have a preference for lactate if both glucose and lactate are present (Hertz et al., 2007). Upon activation, neurons shift their energy source from glucose to lactate (Parsons & Hirasawa, 2010). According to the astrocyte-to-neuron lactate shuttle hypothesis (ANLS), glucose is taken up by astrocytes and converted to lactate, which is then transported to neurons via monocarboxylate transporters (MCT). Lactate then enters the neuronal tricarboxylic acid (TCA) cycle to produce ATP (Pellerin & Magistretti, 2012). Moreover, neurons have been reported to rely heavily on lactate as their energy source during intense

neuronal activity (Pellerin & Magistretti, 2012; Brown & Ransom, 2015). To meet the increasing lactate demand during periods of intense stimulation, astrocytic glycogen is first broken down by glycogen phosphorylase (GP), which then gets stepwise converted to lactate to sustain neuronal activity (Fig.20A) (Brown et al., 2005; Tekkok et al., 2005; Falkowska et al., 2015). It is possible that astrocytes synthesize a surplus of glycogen in prevention of running out energy supply.

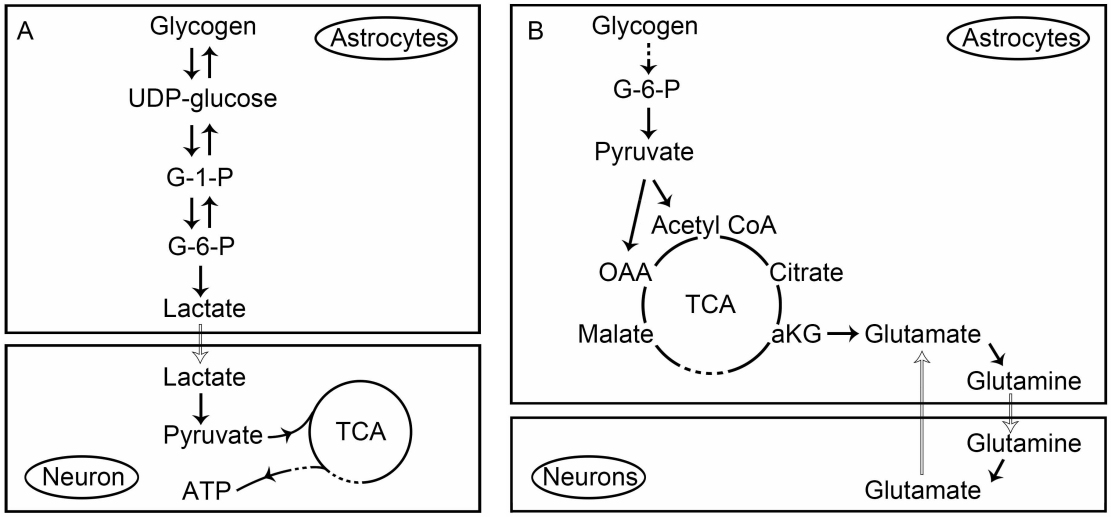

Figure 20: Current knowledge of glycogen-lactate and glycogen-glutamate pathways
20A: Glycogen-lactate pathway: astrocytic glycogen is broken down to uridine diphosphate glucose (UDP-glucose), which is converted first to glucose 1-phosphate (G-1-P), then glucose 6-phosphate (G-6-P), and finally lactate. Astrocytic lactate is then transported to neurons, where it gets converted to pyruvate and enters neuronal tricarboxylic acid (TCA) cycle to generate energy.
20B: Glycogen-glutamate pathway: astrocytic glycogen is first converted stepwise to G-6-P, then to pyruvate, which enters astrocytic TCA cycle as both oxaloacetic acid (OAA) and Acetyl CoA. The two molecules form first citrate and then α-ketoglutarate (αKG). αKG is transaminated to form glutamate, which is subsequently amidated to glutamine. The glutamic is then transported to neurons and converted to neurotransmitter glutamate. Direct transport of astrocytic glutamate to neuron has also been reported. Adapted from (Falkowska et al., 2015).

- **Astrocytic glycogen as the precursor of glutamate**

Astrocytes are responsible for the replenishment of brain glutamate (Belanger et al., 2011; Falkowska et al., 2015). In a study by Gibbs and colleagues, it was shown that astrocytic glycogen was the preferred precursor of the neurotransmitter glutamate

(Gibbs et al., 2007). Astrocytic glycogen is converted to glutamine, which is transported to neurons to produce the neurotransmitter glutamate and maintain synaptic excitability (Fig.20B). Direct release of glutamate from astrocytes has also been reported. Chiang and colleagues proposed that in exaggerated pain states, e.g. hyperalgesia and allodynia, reactive astrocytes may release glutamate as glio-transmitter (Chiang et al., 2012). The glycogen-derived glutamate hypothesis is supported by several studies that show significantly suppressed neuronal activity upon inhibiting the above-described pathway (Chiang et al., 2007; Chiang et al., 2008; Mozrzymas et al., 2011; Sickmann et al., 2012). In other words, if astrocytes run out of glycogen, neurons are unable to sustain their activities due to the subsequent shortage of glutamine/glutamate. This is another possible explanation why astrocytes synthesize extra glycogen following stimulation.

Measurement of lactate and glycogen levels at different time points after peripheral painful stimulus would map out their changes following the stimulation. As previously proposed, the glycogen level may show an initial decrease followed by a sustained re-synthesis. The levels of lactate and glutamate, the potential end products of glycogen, may exhibit an initial (within the first hour) increase as glycogen is being actively mobilized. And in longer term, lactate and glutamate levels may stay elevated as long as there are ample glycogen supply.

3.4 Manipulation of pain through glycogen

Astrocytic glycogen metabolism correlates with neuronal activity (Cruz & Dienel, 2002; Magistretti & Allaman, 2007). Therefore, I hypothesized that manipulating astrocytic glycogen metabolism would have an impact on pain processing. Indeed, I report primary results that (1) increased mechanical and thermal pain sensitivity as well as delayed second phase nocifensive behavior in formalin test were observed in mice with high spinal glycogen level driven by local PTG over-expression, and (2)

suppressed first phase nocifensive behavior in the formalin test were found after halting glycogen mobilization by pharmacologically inhibiting the activity of glycogen phosphorylase (GP).

I could show that viral over-expression of PTG led to high spinal glycogen levels (Fig.14E), which is consistent with previous *in vitro* experiments, where a massive glycogen increase was observed following PTG over-expression in cultured astrocytes (Ruchti et al., 2016) or adipocytes (Greenberg et al., 2003; Greenberg et al., 2006; Jurczak et al., 2007). But what is the link between high glycogen levels and the observed mechanical and thermal pain hypersensitivity? I hypothesize two possible scenarios here: (I) The accumulated glycogen is actively mobilized and contributes directly to the hypersensitivity. In the brain, highest glycogen levels are found in areas with greatest synaptic densities (Phelps, 1972; Brown & Ransom, 2007), suggesting the involvement of glycogen in synaptic transmission. Furthermore, glycogen-derived glutamate is believed to promote neuronal activity by maintaining normal synaptic excitability, while glycogen-derived lactate acts as fuel for neurons upon intense or prolonged stimulation (Gibbs et al., 2007; Suh et al., 2007; Obel et al., 2012; Brown & Ransom, 2015; Falkowska et al., 2015; Swanson, 2015). Assuming the accumulated glycogen is actively mobilized to glutamine/glutamate and lactate, a reasonable speculation is that the excess of glutamate and lactate would prime the neurons to be more readily excitable or even hypersensitive. (II) The hypersensitivity is not directly linked to glycogen. Glycogen surplus however drives astrocytes into a reactive state, and pain hypersensitivity is the result of other glycogen-independent astrocytic activity. A recent study by Nam and colleagues reported mechanical and thermal hypersensitivity after optogenetic activation of spinal astrocytes (Nam et al., 2016). In this study, Nam and colleagues proposed that the release of ATP and proalgesic mediators from activated spinal astrocytes are responsible for the increased pain response.

I propose the following experiments to test the two hypotheses: (1) immuno-fluorescent stainings of glycogen phosphorylase and astrocyte activity marker e.g. p-JNK to determine if accumulation of glycogen leads to active glycogen mobilization and astrocyte activation; (2) biochemical measurement to determine whether lactate and/or glutamate is the end product of the mobilized glycogen; (3) spinal cord interstitial fluid analysis to check for changes in ATP and proalgesic mediator levels; (4) electrophysiological measurement or immunofluorescent stainings of neuronal activity marker *c-Fos* to test for the excitability/activity of spinal neurons. I found that the induction of mechanical allodynia is greater than the induction of thermal hyperalgesia similar to observations by Nam and colleagues (Nam et al., 2016). In contrast to hypothesis (I) that dorsal horn neurons as a whole are more easily excitable upon a surplus of glycogen-derived lactate or glutamate, Nam and colleagues speculated that the pain hypersensitivity is the result of the inhibition of GABAergic inhibitory interneurons following astrocyte activation. The GABAergic pathway has been associated with the development of mechanical allodynia, but not with thermal hyperalgesia (Polgar et al., 2003; Nam et al., 2016). Therefore, it is possible that thermal sensitivity is less affected following the optogenetic (Nam et al., 2016) or the presumed glycogen-driven activation of spinal astrocytes.

Apart from thermal and mechanical pain, the behavioral response to chemical pain was also tested, using the formalin test. In contrast to mechanical or thermal pain, formalin chemical pain and the corresponding behavioral response have two phases: the first acute phase (0-10min) as the result of nociceptor activation and the second tonic phase (15-50min) coming from the sensitization of spinal dorsal horn neurons (Tjolsen et al., 1992; Abbadie et al., 1997; McNamara et al., 2007). The PTG over-expression mice showed similar first and second peaks as the control mice. However, I found a delay of the second phase. This would suggest that the acute phase, i.e. the activation of nociceptors as well as the dorsal horn neurons they project to, is not affected by the high spinal glycogen level. This would contradict hypothesis (I), in which dorsal horn neurons as a whole become more excitable with the surplus of

glycogen-derived lactate and glutamate, but may fit hypothesis (II). As suggested by Nam and colleagues, the activated astrocytes act to inhibit certain subgroups of inhibitory neurons, leading to disinhibition of excitatory spinal interneurons. Although the inhibitory pathway involved in formalin chemical pain is yet not clear, I speculate that similar as in the case of thermal pain, it could be less affected by the inhibition of inhibitory neurons following astrocyte activation. I used 3xFLAG-tagged PTG in my over-expression experiments, but if I substitute the FLAG with a fluorescent protein, the affected interneurons which are next to the astrocytes could potentially be characterized by slice electrophysiological measurements combined with single-cell qPCR.

The second phase on the other hand, though of same magnitude and duration as in control mice, is delayed. The second phase involves sensitization/plasticity of dorsal horn neurons. Previous studies have shown that memory formation, which also involves neuronal plasticity, is critically dependent on the transfer of astrocytic glycogen-derived lactate to neurons (Suzuki et al., 2011; Boury-Jamot et al., 2016). Does a readily accessible rich reservoir of glycogen facilitate this process? My result suggests otherwise, high glycogen level, instead, seems to delay the second phase. I suggest a serial titrated viral over-expressions to confirm a dose-dependent correlation between the delay and the level of glycogen elevation. Intrathecal administration of exogenous lactate or glutamate could potentially reveal which end product(s) of glycogen mobilization may be contributing to the delay.

In addition to increasing spinal glycogen level by PTG over-expression, I pharmacologically blocked spinal glycogen mobilization by intrathecally injecting 1,4-dideoxy-1,4-imino-D-arabinitol (DAB). DAB is a potent inhibitor of glycogen phosphorylase (GP), the first enzyme in the glycogenolysis process which breaks glycogen down to smaller UDP-glucose molecules. Subsequent formalin test showed a significantly suppressed first phase and an unchanged second phase. The suppressed first phase supports the hypothesis that astrocytic glycogen plays an essential role in neuronal activity. The behavior response is significantly suppressed, but not

abolished, indicating that (1) a certain level of neuronal activity is sustained, and (2) there exists additional, probably less efficient energy supply than astrocytic glycogen-derived lactate. *C-Fos* stainings could be used to examine whether there are fewer neurons activated or the neurons fire weaker. A study by Dienel and colleagues showed an compensatory increase of glucose utilization upon the inhibition of GP activity during normal brain activity (Dienel et al., 2007). As glycogen is a better source of energy than glucose for sudden, intense activity (Berg et al., 2002), I speculate that the compensatory glucose metabolism does not suffice the large energy demand following formalin-induced acute pain, therefore the nocifensive behavior is attenuated. In addition, I suggest that the nocifensive response would be abolished if astrocytic metabolism is inhibited by an astrocyte-specific TCA cycle blocker fluorocitrate, which achieves its specificity by inhibiting the astrocyte-specific utilization of acetate (Hassel et al., 1992; Meller et al., 1994; Swanson & Graham, 1994).

As the second phase, which involves neuronal plasticity, is critically dependent on the astrocytic glycogen-derived lactate, as the above-mentioned studies suggested (Suzuki et al., 2011; Boury-Jamot et al., 2016), I would predict a significantly suppressed second phase by DAB as well. Strikingly, the second phase was found unchanged in the DAB injected mice and the controls. As the role of DAB as GP inhibitor has long been established, I think the most plausible explanation here is that the intrathecally injected DAB has been diffused and/or degraded. As glycogen mobilization resumes, the nocifensive response is also recovered. In previous *in vivo* studies, DAB was administrated directly into the tissue, such as the intra-hippocampus injections employed by Matsui and colleagues as well as by Suzuki and colleagues, which showed an effective time of 1 hour (Suzuki et al., 2011; Matsui et al., 2017). It is a reasonable speculation that the circulation of cerebral spinal fluid expedited the diffusion of DAB, shortening its effective time in my experimental setting. A spinal cord cassette could be implanted to facilitate an intra-spinal DAB

injection, which should provide longer effective time to cover the second phase of formalin test and shed more light on the impact of glycogen on spinal pain processing.

3.5 Summary and perspectives

In this study, I identified protein targeting to glycogen (*Ptg*) as a pain-induced gene. The *Ptg* mRNA induction in spinal astrocytes is transient, but glycogen levels were elevated from 24h to several weeks depending on the different pain models. There seems to be a correlation between the magnitude and duration of elevated glycogen levels and the persistency of pain. Over-expression of PTG in spinal astrocytes significantly increased local glycogen levels and led to the development of both mechanical and thermal hypersensitivity. Inhibition of spinal glycogenolysis, on the other hand, suppressed the pain behavior during the first phase of formalin test.

The mechanism of how exactly glycogen is involved in spinal pain processing remain unresolved: whether the glycogen is broken down to lactate for energy or to glutamate for signaling. To understand glycogen metabolism in pain, both acute and chronic, would be one direction for future studies.

The involvement of astrocytes in (chronic) pain is attracting more and more attention. However, changes in metabolic states, either of astrocytes or neurons, have not been addressed in the context of pain. *Ptg* and glycogen open up a new angle to investigate the role of astrocytic and neuronal metabolism in pain processing. While the adverse side effects of current pain-suppressing drugs come from the fact that they act on our nervous system, understanding the metabolic changes in (chronic) pain may provide an alternative direction of for pain medication discovery. One potential hurdle in interfering with metabolic activities is the difficulty to achieve specificity. Many substances used to interfere with one metabolic activity often interact with other

pathways. DAB, a widely used glycogen phosphorylase inhibitor employed in this study, has reported interaction also with glycogen synthase (Walls et al., 2008). Specific inhibitor of PTG and/or careful maneuver of the metabolic state of chronic pain patients may be one promising therapeutic possibility.

4. Material and methods

4.1 Mice

Housing: Animal housing and experiments were conducted following the animal welfare and use guidelines (Regierungspräsidium Karlsruhe, Germany). C57BL/6J mice were bred at the animal facility of University of Heidelberg (Interfakultäre Biomedizinische Forschungseinrichtung, IBF) or purchased from Javier Labs. Both male and female mice were used for the experiments. Prior to experiments, mice were given 24-72h to habituate in the lab.

Pain models:
Formalin pain model: 36.5% formaldehyde solution (Sigma, F8775) was diluted with 0.9% NaCl sterile saline (B.Braun, 190/150936) to a 5% solution shortly before injection. Formalin-induced pain was induced by intraplantar injection of 15µL of the 5% formaldehyde solution into the hind paw of the mouse, under shallow anesthesia by isoflurane.
Capsaicin pain model: 0.6% capsaicin/DMSO solution (obtained from Rohini Kuner lab) was diluted with sterile saline to a 0.06% suspension shortly before injection. Capsaicin-induced pain was induced by intraplantar injection of 20µL of the 0.06% capsaicin solution into the hind paw of the mouse, under shallow anesthesia by isoflurane.
CFA pain model: 10µL of Complete Freund's Adjuvant (Sigma, F5881) was injected into the hind paw while mouse was under shallow anesthesia by isoflurane to induce the inflammatory pain.
SNI pain model: The SNI surgery was performed by severing two of the three branches of the sciatic nerve (the tibial nerve and the common peroneal nerve). The mice were under isoflurane anesthesia during the surgery and were let to recover for at lease one week before subjected to any measurement/experiments.

4.2 Immunofluorescence Staining

Sample preparation: At different time points after intraplantar injection of formalin, the mice were perfused first with PBS (Sigma, D8537) then 4% Paraformaldehyde/ PBS (Sigma, 16005). After perfusion, the mice were dissected to collect the lumbar spinal cord. The spinal cord piece was incubated in 20% sucrose/PBS (Sigma S0389) overnight at 4ºC with gentle shaking for the purpose of cryoprotection and embedded in OCT (Tissue-Tek® O.C.T. Compound, Sakura, 4583). The sample was sectioned to 12µM on a Leica CM3050S Research Cryostat and collected on glass slides (HistoBond, 0810001). The sections were stored in -80ºC until further experiment.
Staining: Immunofluorescent staining was performed on spinal cord sections collected as above described. The sections were first let to warm up to room temperature and then washed in PBST (0.1% TritonX(Merck, 108603)/PBS) for 2 times, 5 minutes each. Blocking was performed with 1% goat serum in PBST for 1 hour at room temperature. The sections were incubated with primary antibody (pS6 Cell Signaling

2215, 1:2000) in blocking buffer overnight at 4ºC. After washing in PBST 3 times, 10 minutes each, secondary antibody (1:1000 in blocking buffer) was applied to the sections and let to incubate at room temperature for 1 hour. The sections were mounted in Immu-Mount (Thermo Scientific, 9990402) after another washing in PBST (3 times, 10 minutes each) and preserved in 4ºC.

4.3 Wholemount immunofluorescent staining

Sample preparation: Mice were sacrificed 2 hours after intraplantar formalin injection and immediately perfused as previously described. After perfusion, the spinal cord was dissected out and subject to 4 hours of post-fixation in 4% Paraformaldehyde/ PBS at 4ºC with gentle rotation. The tissue piece was then washed in PBS for 10 minutes and put into Dent's Bleach (10% H_2O_2(Merck, 107209), 13.3% DMSO(Sigma, D2438) and 53.3% Methanol(Honeywell, 32213)) for 24 hours at 4ºC with gentle rotation. After bleaching, the tissue piece was subject to dehydration with methanol at room temperature for 5 times, 2 minutes each. The sample was then fixed in Dent's Fix (20% DMSO, 80% Methanol) for 24 hours at 4ºC with general rotation. The tissue was stored in Dent's Fix at 4ºC until use.

Staining: The processed tissue was rinsed with PBS 3 times, 20 minutes each to wash off the Dent's Fix and then incubated with primary antibody in blocking buffer (same as in section 4.2) at 4ºC with gentle rotation for 5 days. After primary antibody incubation, the tissue sample was washed with PBS at room temperature for 6 times, 30 minutes each. Secondary antibody was diluted in blocking solution (as in section 4.3) and the tissue piece was let to incubate for 2 days at room temperature with gentle rotation. After the incubation, the tissue piece was again washed with PBS for 6 times, 30 minutes each at room temperature.

Clearing: After staining, the spinal cord piece was dehydrated and cleared before imaging. First dehydration was performed by incubating the tissue piece in 50%methanol/PBS for 5 minutes at room temperature, followed by 20 minutes of incubation in 100% methanol, changing the solution twice during the incubation. After dehydration, the piece was cleared in BABB (1 part benzyl alcohol(Sigma, 108006) and 2 parts benzyl benzoate(Sigma, B6630)) for 5 minutes and stored in BABB till imaging.

4.4 Western blot

Sample preparation

spinal cord tissue: two hours after intraplantar injection of formalin, the mice were sacrificed and the lumbar spinal cord was quickly dissected in ice cold PBS. The whole spinal cord or the dorsal horn laminae I-III spinal cord was collected and snap froze immediately. The spinal cord tissue piece was kept in -80ºC until homogenization. Homogenization buffer was freshly prepared (NP40-RIPA buffer: 50mM pH 7.4 Tris (Roth, 4855), 1% NP40(Sigma, I8896), 0.5% sodium deoxycholate(Sigma, D6750), 150mM NaCl(Bernd Kraft, 04160.5600), 1mM EDTA(Roth, X986.2), 0.1% SDS(Roth, 2326), 1x cOmplete™ Protease Inhibitor

Cocktail(Roche, 11697498001), 1x PhosSTOP phosphatase inhibitor tablet(Roche, 04906845001)).
HEK293 cell culture: after harvest, the cell culture medium was removed and the cells were collected in cold PBS. Excessive PBS was removed after pelleting cells by centrifugation at 1000rpm, 10 minutes. The cells were re-suspended and lysed in 2x Laemmli buffer, supplemented with 2-mercaptoethanol. The cell lysis was incubated at 95ºC for 5 minutes and let to cool down on ice. The lysate was directly loaded on to the western blot gel or stored in -20ºC until use.
Blotting: Depending on the number of wells, 10-20µL tissue or cell lysates were loaded into each well (Life Technologies, NP0321). The gel was let run for 1/1.5 hour at 180/120V. The transfer to PVDF membranes (Roche, 03010040001) was performed at 30V for 50 minutes. The transfer chamber was placed in ice during the transfer.
Protein visualization: After the proteins were transferred to the nitrocellulose membrane, blocking with 5% milk/PBST (milk powder, Roth, T145.2, 0.1% Tween, Roth, 9127, in PBS) was performed for 1 hour at room temperature with gentle rotation. After blocking, the membrane was briefly rinsed with PBST and placed in primary antibody (pS6 Cell Signaling 5364 1:10000, β-ACTIN 1:5000, GFP Nacalai Tesque 04404-84, 1:1500, PTG Abnova D03P 1:1000, FLAG Sigma F1804 1:3000, in 3%BSA(Roth, T844.4)/PBST) at 4ºC overnight. The next day, the membrane was washed 3 times, 10 minutes each with PBST at room temperature and subject to secondary antibody incubation (1:1000, in 3%BSA/PBST) for 1 hour at room temperature. The membranes were washed again 3 times, 10 minutes each with PBST before developing. GE Amersham ECL Prime Western Blotting Detection Reagent (RPN2232) was used for detection.

4.5 Immunoprecipitation/Ribosome capture

Sample preparation: For sequencing experiments, 5 mice were pooled for each sample. Three samples of each conditions were prepared. Immunoprecipitation was performed based on the protocol developed by Knight and colleagues (Knight et al., 2012). The mice were sacrificed 2 hours after formalin injection and quickly dissected in ice cold freshly prepared buffer B (1xHBSS(Life Technologies, 14185-045), 4mM $NaHCO_3$(AppliChem, 131638.1211), 2.5mM pH7.4 HEPES(Roth, 9105.4), 35mM Glucose(Merck, 08337), 100 µg/ml cycloheximide(Sigma, C7698)). The tissue was snap froze and kept in -80ºC. The tissues were kept frozen until homogenization.
Homogenization: Tissue was resuspended in 1350µL freshly prepared buffer C (10mM pH7.4 HEPES, 150 mM KCl(Sigma, P9541), 5 mM $MgCl_2$(Sigma, M2670), 1x PhosSTOP phosphatase inhibitor tablet, 1x cOmplete™ Protease Inhibitor Cocktail, 2mM DTT(Sigma, 10197777), 100U/ml RNasin(Promega N2515), 100 µg/ml cycloheximide) and homogenized at 4ºC. The homogenates were centrifuged at 2000g for 10 minutes at 4ºC and the supernatants (~1mL) were transferred to new tubes on ice. 90µL 10% NP40 and 90µL 1,2-diheptanoyl-sn-glycero-3-phosphocholine (DHPC, Avanti Polar Lipids, 850306, 100mg/0.69mL, freshly prepared) were added to each tube. The new mix was centrifuged at 17000g for 10 minutes at 4ºC and the supernatant was collected in a clean tube. A small aliquot of

the supernatant was taken for western blot (“Ly”) and the rest were used for immunoprecipitation.
Antibody coating: 3µg of pS6 Cell Signaling 5364 antibody and 50µL Protein A Dynabeads (Invitrogen 1001D) were used for each immunoprecipitation. Antibody was incubated with Dynabeads in 1mL buffer A (0.1% TritonX/PBS) for 10 minutes at room temperature with gentle rotation. The coated beads were equilibrated in buffer C till immunoprecipitation.
Immunoprecipitation: Immunoprecipitation was performed by applying the supernatant to pS6 coated protein A Dynabeads and rotated at 4ºC for 10 minutes. After immunoprecipitation, the liquid were collected for western blot (“SN”). The beads were washed for four times in 500µL buffer D (10mM pH7.4 HEPES, 350mM KCl, 5mM MgCl2, 2mM DTT, 1% NP40, 100 U/ml RNasin, and 100 µg/ml cycloheximide). During the third wash, the beads were transferred to a new tube and let to incubate at room temperature for 10 minutes. Phospho-ribosomes were eluted with 350µL RLT (or 50µL 2x laemmli for western blot, “IP”). The eluates were immediately processed to RNA extraction for test qPCR or deep sequencing.

4.6 qPCR

RNA extraction: RNA extraction was performed using RNAeasy micro kit (QIAGEN, 74004), following the manufacturer’s instruction. The elution volume was 10µL. The RNA was reverse transcribed using SuperScript III Reverse Transcriptase (Thermo Fisher, 18080044) and Oligod(T)23VN (NEB, S1327) following the manufacturer’s instruction for SuperScript First-Strand Synthesis System (Thermo Fisher).
Primer design: qPCR primers were designed using the commercial software OLIGO (version 7). Primers used:

Calb2-Fw: AATGAACTGGACGCCCTC;	Dyn-Fw: AAGCTCTTGGAACCCGTCCTG;
Calb2-Rv: GGCCAAGGACATGACACTCT;	Dyn-Rv: TTTCCGTTGCCAAAGCTGCTG;
Som-Fw: GAGGACCTGCGACTAGACTGA;	NK1R-Fw: ACAACCCCATCATCTACTGCT;
Som-Rv: CAGGACAGCATCTTCCTTGC;	NK1R-Rv: TTCCAGCCCCTCATAATCACC;
Gad67-Fw: TCTTCCAGCCAGACAAGCAG;	FosB-Fw: GGCCTAGAAGACCCCGAGAA;
Gad67-RV: AGCCAGAACTTGAAGATGTCC;	FosB-Rv: TTTCCGCCTGAAGTCGATCTGT

qPCR: qPCR were performed using the FastStart Essential DNA Green Master (Roche, 06402712001) and Roche LightCycler® 96 Instrument, following the manufacturer's instruction.

4.7 RNA sequencing

RNA extraction: RNA were extracted from IP eluates as described in section 4.6. The obtained RNA were snap frozen and kept at -80ºC till use.

Reverse transcription and amplification: cDNA synthesis and amplification was performed following the SMART-Seq2 protocol described by Picelli and colleagues (Picelli et al., 2014) and optimized by EMBL Genecore. 2µL of RNA was used as the starting material and a 18 cycles of amplification was performed.
Quality control: The amplified cDNA from the step above was subject to concentration measurement by Qubit dsDNA HS Assay kit (Thermo Fisher, Q32854) and then quality check on a bioanalyzer (Agilent High Sensitivity DNA Kit, 5067-4626). A small aliquot the amplified cDNA was used for test qPCR testing while the remaining were kept at -20ºC until further process. qPCR primers used:

Atf3-Fw: AGGAAGAGCCAAAGATAACCAC

Atf3-Rv: TCCCACAATGCAGATGCCT

Ppp1r3c-Fw: GGTGACTCATCTTTCTGCCACA

Ppp1r3c-Rv: CAAGACAAAATTAGGCACGAGA

Pcdhb16-Fw: ACTGAATACACCCGACATAGCAA

Pcdhb16-Rv: CCAGTAGAGGCCAAATAAAGCAA

Lck-Fw: ACATGTGTCTTATACCTGTGGAGC

Lck-Rv: AGAGACACGCATCAATCGCAGA

Ano6-Fw: GTCCTGAACATGCTCCCTC

Ano6-Rv: AAGCACAGAAAAGGAGCTCT

Meg3-Fw: TCCCCTTGAGTAGAGAGACCC

Meg3-Rv: CAGTGAAGACACAACAGCCTT

Gab1-Fw: CTGGCCTGCTCTTACTCC

Gab1-Rv: CGCACACTAACTGAAGCACT

Rem2-Fw: TCTCCCGGAAAGACACTCCA

Rem2-Rv: AGGCATGTTCCGAGTACCAA

Actb-Fw: ATCAAGATCATTGCTCCTCC

Actb-Rv: GACTCATCGTACTCCTGCTT

Klf15-Fw: CTTTGTGCCTTCCTGCCAG

Klf15-Rv: AAAACACTTCTTCCCCAGCAA

MVK-Fw: TGAGACCACCCGACACACC

MVK-Rv: CCATCTCAGAAGACCCCACA

Sez6l-Fw: AGCCTTTGAAGCCAGCTC

Sez6l-Rv: TACGGTTCCTGAAGCTACCCAT

MMD-Fw: GACATAACTTCGCTACATGCCTT

MMD-Rv: TCGCCATGATTCAGAAAGCTC

Library preparation, barcoding and sequencing: Library preparation and barcoding were performed following the standard protocol of EMBL Genecore (Nextera XT DNA Library Preparation Kit, FC-131-1096 and Nextera XT Index Kit v2 Set A, FC-131-2001), using 125pg amplified cDNA as input. The sequencing was performed by EMBL Genecore on Illumina MiSeq platform.
Data analysis: The sequencing reads were aligned by EMBL Genecore to mouse genome Mm10. FastQC was used for quality check and the differential expression analysis was performed with R following the Bioconductor RNA-Seq workflow developed by Love and colleagues (Love et al., 2015). The following packages were used during the data analysis: DESeq2, Rsamtools, GenomicFeatures, TxDb.Mmusculus.UCSC.mm10.ensGene, GenomicAlignments, AnnotationDbi, org.Mm.eg.db.

4.8 In situ hybridization

Sample preparation: Spinal cord were dissected 2 hours after intraplantar formalin injection in ice cold PBS and immediately embedded into OCT and frozen using dry ice/isopropanol. 20µm sections were prepared using Leica CM3050S cryostat and stored at -80 °C until staining.

Probe design and synthesis: In situ hybridization probes were designed using commercial software OLIGO (version 7). Primers used:

Cdh3-fw: gacGTCGACCAAGTGCTGAACATCACTGACA

Cdh3-rv: gacGCGGCCGCCATAGTCCTGGTCCTCTTCACC

Cdh18-fw: gacCTCGAGGCCACCACTCTTTTCTATGCC

Cdh18-rv: gacGCGGCCGCCATTCTCTCGCACATCCTCC

Pcdhb16-fw: gacCTCGAGAAGTGCGATTGAAAGAACACC

Pcdhb16-rv: gacGCGGCCGCTAGTGCCACCCTTCTGCAT

Meg3-fw: gacCTCGAGATTGCTGTAGACAAAGCCACCT

Meg3-rv: gacGCGGCCGCCCTTTCCTGATCACGCCAT

Ano6 (pool of 3 used)

fw1: gacCTCGAGTGCCTCCTTGAACTGACCAC

rv1: gacGCGGCCGCACCAGCCTTTCCCATAACCC

fw2: gacCTCGAGCCTAGCGAGCGTTACCTCC

rv2: gacGCGGCCGCTAGTGCCACCCTTCTGCAT

fw3: gacCTCGAGTGCCTCCTTGAACTGACCAC

rv3: gacGCGGCCGCCTGCGTGAGGTATTTCTCCC

Atf3-fw: gacCTCGAGCTCCTTTTCCACCCCACACC

Atf3-rv: gacGCGGCCGCGCTCTTCCTGCCCTGTCAC

Ppp1r3c-fw: gacGTCGACAAGAACTTTGTCTGCCTCGAGA

Ppp1r3c-rv: gacGCGGCCGCTACCACAGCGTTCCATCACC

Probe sequences were amplified from spinal cord cDNA, molecularly cloned into pBlueScript plasmids and bacterially amplified. DIG-labeled in situ probes were subsequently synthesized (POD: Roche, 11207733910, AP: Roche, 11093274910). c-Fos, Som, Dyn and MafA probes were produced and provided by Dr. Hong Wang and Dr. Hagen Wende.

AP/fluorescent in situ hybridization: stainings were performed using the protocols (AP and fluorescent) optimized in the Jan Siemens lab and described in the recent publication by Song and colleagues (Song et al., 2016). All probes were used at 1:100 dilution.

Immunofluorescent-in situ hybridization double staining: single color fluorescent in situ hybridization was performed following the same protocol as above, after the single color fluorescent in situ hybridization was completed, the sections were subject to antibody immunofluorescent staining (pS6 Cell Signaling 2215 1:1000, GFAP Cell

Signaling 3670 1:500, NeuN Cell Signaling D4G40 1:2000, IBA1 Wako, 019-19741, 1:500) using the protocol described in 4.2.

4.9 Glycogen assay

Sample preparation: Spinal cord dorsal horn was dissected in ice cold PBS and immediately snap froze. The samples were kept in -80ºC till measurement.

Glycogen measurement: Spinal cord tissue was sonicated in 120µL ddH_2O and incubated at 99ºC for 10 minutes at 350rpm to inactivate enzymes. After heat inactivation, the homogenates were centrifuged at 18000g for 10 minutes at 4ºC. The supernatants (100-110µL) were collected to clean tubes. Two aliquots of the collected supernatants (35µL each) were mixed with 15µL hydrolysis buffer, with (sample) and without (negative control) 1µL hydrolysis enzyme, respectively. The remaining steps were performed following the manufacturer's instruction. Glycogen standard curve was prepared in every experiment to counter the kit to kit variances. 25µL of the remaining supernatants were used for protein measurement (Pierce™ BCA Protein Assay Kit, 23225). After glycogen and protein measurements, the glycogen level of each sample were calculated by extracting that of the corresponding negative control, multiplied by the dilution factor (35µL/120µL) and normalized to the protein contents.

4.10 Viral-mediated PTG over-expression

Cloning of pAAV-GFAP-3xFLAG-PTG and pAAV-GFAP-Venus: Dr. Anna Hertle provided the GFAP multi-cloning-site AAV plasmid. 3xFLAG and PTG sequences were PCR amplified from a 3xFlag containing plasmid from Charlotte Rostock and spinal cord cDNA respectively, and cloned into GFAP plasmid using In-Fusion® HD Cloning Kit (Clonetech, 121416). Venus sequence was digested from a Venus containing plasmid from Dr. Hagen Wende and ligated into the GFAP AAV plasmid. The plasmids were bacterial amplified and sequenced to confirm the correct inserts.

PTG test expression: After the AAV plasmids were correctly produced, the 3xFLAG-PTG insert was digested out and ligated into pcDNA. HEK293 cells were transfected with pcDNA-3xFLAG-PTG and pBlueScript control plasmids. 48 hours after transfection, the cells were collected for western blot analysis. The western blot detection of PTG and FLAG was performed as described in section 4.4.

Virus production: The AAV viruses were produced by Karin Meyer in Rohini Kuner's lab using AAV serotype 1 and 2. The cleaned supernatants were collected and kept at -80ºC until injection.

Virus test on astrocyte culture: astrocyte culture was prepared by Dr. Anna Hertle. 14 days after infection with PTG and Venus viruses respectively, the cultured cells were fixed with 4% Paraformaldehyde/PBS. The cultures were incubated with GFAP antibody (Cell Signaling 3670 1:500) to visualize the astrocytes and with FLAG (Sigma F1804 1:500) antibody to mark the PTG over-expression. Venus over-expression was detected by its own fluorescence.

Spinal cord over-expression: Spinal cord virus injection was performed by Dr. Manuela Simonetti. For each mouse, bilateral injection of 1μL of virus mixed with equal amount of mannitol was perform at dorsal horns of lumbar section L2. The mice were let to recover for 3 weeks before behavioral testings.

4.11 von Frey and Hargreaves tests

Mice were habituated for 3 days before the testing. Both von Frey and Hargreaves tests were performed following standard protocols of the Interdisciplinary Neurobehavioral Core at University of Heidelberg. In short, a filament set of 0.07g, 0.14g, 0.4g, 0.6g, and 1.0g were used in the von Frey measurement. 5 measurements were performed for each filament and the response is calculated as the percentage (number of response/5). For Hargreaves test, the lamp was set to 40Lux.

4.12 DAB-mediated glycogen mobilization inhibition

1,4-dideoxy-1,4-imino-D-Arabinitol (DAB, Cayman Chemicals, 20939) was dissolved in sterile PBS and 100pmol working dilution was prepared. 10μL DAB/PBS or PBS control solution was intrathecally injected by Dr. Manuela Simonetti 15 minutes before intraplantar formalin injection. The mice were video recorded for 55 minutes for formalin test behavioral quantification.

5. Appendix

A1 Characterization of *MafA* knock-out mouse line

Introduction

The *Maf* family acts as transcriptional factors (Wende et al., 2012). Studies have revealed spinal cord neuronal subtypes identified by different members of the Maf family, such as *MafA*, *c-Maf*, and *Maf-B* (Bourane et al., 2009). *c-Maf* is distinctively expressed at lamina III (Fig.A1-A, down), whereas the expression of *MafA* expands also to the more superficial laminae I and II (Fig.A1-A, up) where nociceptive afferents come in, indicating an additional role of *MafA* in nociception. In this side project, I performed initial molecular and behavioral characterizations a *MafA* knock-out mouse line produced by Dr. Hagen Wende, in the context of pain.

Results

In order to determine whether the *MafA*-expressing spinal cord neurons are excitatory or inhibitory, I first performed double fluorescent in situ hybridization of *MafA* with excitatory (*vGlut2* and *vGlut3*) and inhibitory (*Gad65* and *Gad67*) neuron markers. Quantification of the stainings is shown in Fig.A1-B. The majority of *MafA*-expressing neurons are excitatory.

As I speculated a potential involvement of *MafA* in pain processing for its superficial dorsal horn expression, I performed von Frey test to test the mechanical pain

threshold (Fig.A1-C). The knock-out mice showed no difference in mechanical pain thresholds as the heterozygote controls.

I further tested if a phenotype would emerge when the mice are under chronic pain. I performed SNI surgery to induce neuropathic pain and measured the mechanical pain threshold before and after the surgery (Fig.A1-D). The *MafA* knock-out mice showed an interesting phenotype, i.e. under neuropathic pain, the MafA knock-out mice developed hypersensitivity in both ipsilateral (operated) and contralateral (un-operated) paw. Whereas the control mice only developed hypersensitivity in the operated paw.

Discussion

Nociceptive inputs from the peripheral are processed at spinal cord superficial dorsal horn (Basbaum et al., 2009). The laminae I and II expression of *MafA* points to its potential involvement in pain processing. In this side project, I found that under chronic neuropathic pain, *MafA* knock-out mice developed hypersensitivity for mechanical pain in the un-operated control paw. Previous studies have reported development of mirror pain in the contralateral paw in certain knock-out mouse lines following SNI surgery (Racz et al., 2008; La Porta et al., 2013). Racz and colleagues also observed an enhanced activity of contralateral spinal dorsal horn astrocytes as the pain developed in the contralateral paw (Racz et al., 2008). I hypothesize a potential inhibitory role of *MafA*-expressing neurons in the cross-talking of spinal cord pain circuits, i.e. *MafA*-expressing neurons act to prevent the activation of the pain processing neurons on the contralateral side. Further thorough investigations would be needed to elaborate the exact connections and mechanisms of the observed phenotype.

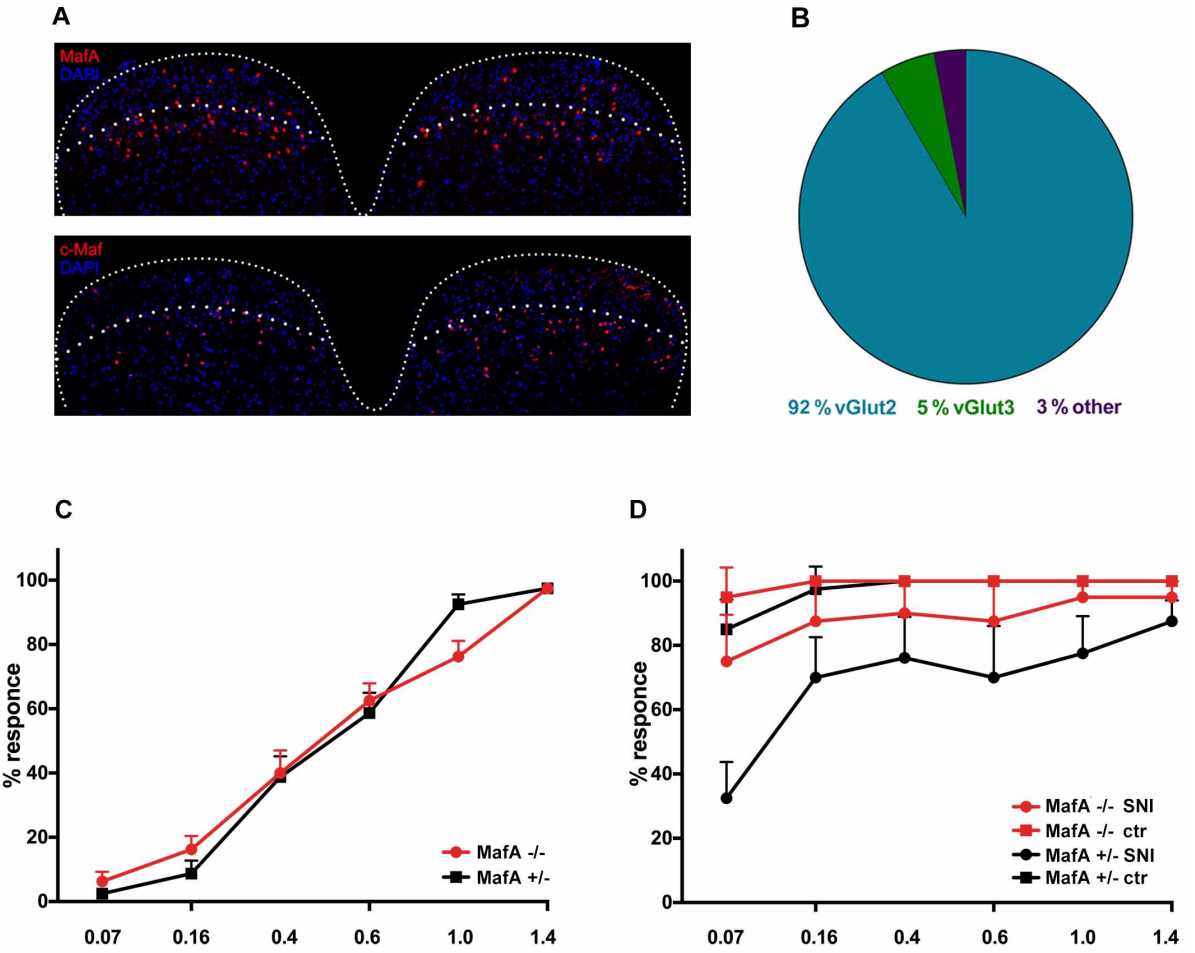

Figure A1: Molecular and behavioral characterization of MafA knock-out mouse
A: Up: *MafA* (*in situ* hybridization) expression spread from laminae I to III while Down: *c-Maf* (*in situ* hybridization) showed specific lamina III expression.
B: Quantification of *MafA*-expressing spinal neurons. 92% of *MafA*-possitive neurons co-express *vGlut2* and 5% express *vGlut3*.
C: von Frey test of *MafA* knock-out mice and heterozygote controls. *MafA* knock-out mice did not show altered mechanical sensitivity (N=8 each).
D: von Frey test of *MafA* knock-out mice and heterozygote controls after SNI surgery. *MafA* knock-out mice developed mechanical hypersensitivity in both operated paw and the un-operated paw; while heterozygous control mice only developed hypersensitivity in the operated side.

Reference

Abbadie, C., Taylor, B. K., Peterson, M. A., & Basbaum, A. I. (1997). Differential contribution of the two phases of the formalin test to the pattern of c-fos expression in the rat spinal cord: studies with remifentanil and lidocaine. *Pain, 69*(1-2), 101-110.

Abraira, V. E., Kuehn, E. D., Chirila, A. M., Springel, M. W., Toliver, A. A., Zimmerman, A. L., . . . Ginty, D. D. (2017). The Cellular and Synaptic Architecture of the Mechanosensory Dorsal Horn. *Cell, 168*(1-2), 295-310 e219. doi:10.1016/j.cell.2016.12.010

Aimone, J. B., Leasure, J. L., Perreau, V. M., Thallmair, M., & Christopher Reeve Paralysis Foundation Research, C. (2004). Spatial and temporal gene expression profiling of the contused rat spinal cord. *Exp Neurol, 189*(2), 204-221. doi:10.1016/j.expneurol.2004.05.042

Aldskogius, H., & Kozlova, E. N. (1998). Central neuron-glial and glial-glial interactions following axon injury. *Prog Neurobiol, 55*(1), 1-26.

Allaman, I., Pellerin, L., & Magistretti, P. J. (2000). Protein Targeting to Glycogen mRNA Expression Is Stimulated by Noradrenaline in Mouse Cortical Astrocytes. *Glia*(30), 382-391.

Armstrong, C. G., Browne, G. J., Cohen, P., & Cohen, P. T. (1997). PPP1R6, a novel member of the family of glycogen-targetting subunits of protein phosphatase 1. *FEBS Lett, 418*(1-2), 210-214.

Bas-Orth, C., Tan, Y. W., Lau, D., & Bading, H. (2017). Synaptic Activity Drives a Genomic Program That Promotes a Neuronal Warburg Effect. *J Biol Chem, 292*(13), 5183-5194. doi:10.1074/jbc.M116.761106

Basbaum, A. I., Bautista, D. M., Scherrer, G., & Julius, D. (2009). Cellular and molecular mechanisms of pain. *Cell, 139*(2), 267-284. doi:10.1016/j.cell.2009.09.028

Bear, M. F., Connors, B. W., & Paradiso, M. A. (2007). "The somatic sensory system" *Neuroscience: exploring the brain* (3rd ed.). Philadelphia, PA: Lippincott Williams & Wilkins.

Belanger, M., Allaman, I., & Magistretti, P. J. (2011). Brain energy metabolism: focus on astrocyte-neuron metabolic cooperation. *Cell Metab, 14*(6), 724-738. doi:10.1016/j.cmet.2011.08.016

Benarroch, E. E. (2015). Ion channels in nociceptors: recent developments. *Neurology, 84*(11), 1153-1164. doi:10.1212/WNL.0000000000001382

Berg, J. M., Tymoczko, J. L., Stryer, L., & Stryer, L. (2002). *Chapter 21: Glycogen Metabolism* (5th ed.). New York: W.H. Freeman.

Bourane, S., Garces, A., Venteo, S., Pattyn, A., Hubert, T., Fichard, A., . . . Carroll, P. (2009). Low-threshold mechanoreceptor subtypes selectively express MafA and are specified by Ret signaling. *Neuron, 64*(6), 857-870. doi:10.1016/j.neuron.2009.12.004

Boury-Jamot, B., Carrard, A., Martin, J. L., Halfon, O., Magistretti, P. J., & Boutrel, B. (2016). Disrupting astrocyte-neuron lactate transfer persistently reduces conditioned responses to cocaine. *Mol Psychiatry, 21*(8), 1070-1076. doi:10.1038/mp.2015.157

Bove, G. M., & Swenson, R. S. (2007). Chapter 129 – Nociceptors and Peripheral Sources of Pain. Philadelphia: Saunders/Elsevier.

Brady, M. J., Printen, J. A., Mastick, C. C., & Saltiel, A. R. (1997). Role of protein targeting to glycogen (PTG) in the regulation of protein phosphatase-1 activity. *J Biol Chem, 272*(32), 20198-20204.

Brown, A. M. (2004). Brain glycogen re-awakened. *J Neurochem, 89*(3), 537-552. doi:10.1111/j.1471-4159.2004.02421.x

Brown, A. M., & Ransom, B. R. (2007). Astrocyte glycogen and brain energy metabolism. *Glia, 55*(12), 1263-1271. doi:10.1002/glia.20557

Brown, A. M., & Ransom, B. R. (2015). Astrocyte glycogen as an emergency fuel under conditions of glucose deprivation or intense neural activity. *Metab Brain Dis, 30*(1), 233-239. doi:10.1007/s11011-014-9588-2

Brown, A. M., Sickmann, H. M., Fosgerau, K., Lund, T. M., Schousboe, A., Waagepetersen, H. S., & Ransom, B. R. (2005). Astrocyte glycogen metabolism is required for neural activity during aglycemia or intense stimulation in mouse white matter. *J Neurosci Res, 79*(1-2), 74-80. doi:10.1002/jnr.20335

Cahoy, J. D., Emery, B., Kaushal, A., Foo, L. C., Zamanian, J. L., Christopherson, K. S., . . . Barres, B. A. (2008). A transcriptome database for astrocytes, neurons, and oligodendrocytes: a new resource for understanding brain development and function. *J Neurosci, 28*(1), 264-278. doi:10.1523/JNEUROSCI.4178-07.2008

Carter, M., & Shieh, J. C. (2010). Nociception *Guide to research techniques in neuroscience* (pp. xxiv, 376 p.). Amsterdam ; Boston: Elsevier/Academic Press.

Cataldo, A. M., & Broadwell, R. D. (1986). Cytochemical identification of cerebral glycogen and glucose-6-phosphatase activity under normal and experimental conditions. II. Choroid plexus and ependymal epithelia, endothelia and pericytes. *J Neurocytol, 15*(4), 511-524.

Chen, K., Deng, S., Lu, H., Zheng, Y., Yang, G., Kim, D., . . . Wu, J. Q. (2013). RNA-seq characterization of spinal cord injury transcriptome in acute/subacute phases: a resource for understanding the pathology at the systems level. *PLoS One, 8*(8), e72567. doi:10.1371/journal.pone.0072567

Cheng, L., Duan, B., Huang, T., Zhang, Y., Chen, Y., Britz, O., . . . Ma, Q. (2017). Identification of spinal circuits involved in touch-evoked dynamic mechanical pain. *Nat Neurosci, 20*(6), 804-814. doi:10.1038/nn.4549

Chiang, C. Y., Li, Z., Dostrovsky, J. O., Hu, J. W., & Sessle, B. J. (2008). Glutamine uptake contributes to central sensitization in the medullary dorsal horn. *Neuroreport, 19*(11), 1151-1154. doi:10.1097/WNR.0b013e3283086781

Chiang, C. Y., Sessle, B. J., & Dostrovsky, J. O. (2012). Role of astrocytes in pain. *Neurochem Res, 37*(11), 2419-2431. doi:10.1007/s11064-012-0801-6

Chiang, C. Y., Wang, J., Xie, Y. F., Zhang, S., Hu, J. W., Dostrovsky, J. O., & Sessle, B. J. (2007). Astroglial glutamate-glutamine shuttle is involved in central sensitization of nociceptive neurons in rat medullary dorsal horn. *J Neurosci, 27*(34), 9068-9076. doi:10.1523/JNEUROSCI.2260-07.2007

Cho, H., Yang, Y. D., Lee, J., Lee, B., Kim, T., Jang, Y., . . . Oh, U. (2012). The calcium-activated chloride channel anoctamin 1 acts as a heat sensor in nociceptive neurons. *Nat Neurosci, 15*(7), 1015-1021. doi:10.1038/nn.3111

Christensen, A. J., Iyer, S. M., Francois, A., Vyas, S., Ramakrishnan, C., Vesuna, S., . . . Delp, S. L. (2016). In Vivo Interrogation of Spinal Mechanosensory Circuits. *Cell Rep, 17*(6), 1699-1710. doi:10.1016/j.celrep.2016.10.010

Codeluppi, S., Svensson, C. I., Hefferan, M. P., Valencia, F., Silldorff, M. D., Oshiro, M., . . . Pasquale, E. B. (2009). The Rheb-mTOR pathway is upregulated in reactive astrocytes of the injured spinal cord. *J Neurosci, 29*(4), 1093-1104. doi:10.1523/JNEUROSCI.4103-08.2009

Cohen, J. L., Glover, M. E., Pugh, P. C., Fant, A. D., Simmons, R. K., Akil, H., . . . Clinton, S. M. (2015). Maternal Style Selectively Shapes Amygdalar Development and Social Behavior in Rats Genetically Prone to High Anxiety. *Dev Neurosci, 37*(3), 203-214. doi:10.1159/000374108

Cruz, N. F., & Dienel, G. A. (2002). High glycogen levels in brains of rats with minimal environmental stimuli: implications for metabolic contributions of working astrocytes. *J Cereb Blood Flow Metab, 22*(12), 1476-1489. doi:10.1097/01.WCB.0000034362.37277.C0

Cui, L., Miao, X., Liang, L., Abdus-Saboor, I., Olson, W., Fleming, M. S., . . . Luo, W. (2016). Identification of Early RET+ Deep Dorsal Spinal Cord Interneurons in Gating Pain. *Neuron, 91*(5), 1137-1153. doi:10.1016/j.neuron.2016.07.038

Damann, N., Voets, T., & Nilius, B. (2008). TRPs in our senses. *Curr Biol, 18*(18), R880-889. doi:10.1016/j.cub.2008.07.063

Decosterd, I., & Woolf, C. J. (2000). Spared nerve injury: an animal model of persistent peripheral neuropathic pain. *Pain, 87*(2), 149-158.

Del Barrio, M. G., Bourane, S., Grossmann, K., Schule, R., Britsch, S., O'Leary, D. D., & Goulding, M. (2013). A transcription factor code defines nine sensory interneuron subtypes in the mechanosensory area of the spinal cord. *PLoS One, 8*(11), e77928. doi:10.1371/journal.pone.0077928

Dickinson, T., & Fleetwood-Walker, S. M. (1999). VIP and PACAP: very important in pain? *Trends Pharmacol Sci, 20*(8), 324-329.

Dielenberg, R. A., Hunt, G. E., & McGregor, I. S. (2001). "When a rat smells a cat": the distribution of Fos immunoreactivity in rat brain following exposure to a predatory odor. *Neuroscience, 104*(4), 1085-1097.

Dienel, G. A., Ball, K. K., & Cruz, N. F. (2007). A glycogen phosphorylase inhibitor selectively enhances local rates of glucose utilization in brain during sensory stimulation of conscious rats: implications for glycogen turnover. *J Neurochem, 102*(2), 466-478. doi:10.1111/j.1471-4159.2007.04595.x

Dougherty, K. J., Zagoraiou, L., Satoh, D., Rozani, I., Doobar, S., Arber, S., . . . Kiehn, O. (2013). Locomotor rhythm generation linked to the output of spinal shox2 excitatory interneurons. *Neuron, 80*(4), 920-933. doi:10.1016/j.neuron.2013.08.015

Dringen, R., & Hamprecht, B. (1992). Glucose, insulin, and insulin-like growth factor I regulate the glycogen content of astroglia-rich primary cultures. *J Neurochem, 58*(2), 511-517.

Duan, B., Cheng, L., Bourane, S., Britz, O., Padilla, C., Garcia-Campmany, L., . . . Ma, Q. (2014a). Identification of spinal circuits transmitting and gating mechanical pain. *Cell, 159*(6), 1417-1432. doi:10.1016/j.cell.2014.11.003

Duan, B., Cheng, L., Bourane, S., Britz, O., Padilla, C., Garcia-Campmany, L., . . . Ma, Q. (2014b). Identification of spinal circuits transmitting and gating mechanical pain. *Cell, 159*(6), 1417-1432. doi:10.1016/j.cell.2014.11.003

Duan, B., Cheng, L., & Ma, Q. (2017). Spinal Circuits Transmitting Mechanical Pain and Itch. *Neurosci Bull*. doi:10.1007/s12264-017-0136-z

Dubin, A. E., & Patapoutian, A. (2010). Nociceptors: the sensors of the pain pathway. *J Clin Invest, 120*(11), 3760-3772. doi:10.1172/JCI42843

Edvardson, S., Elbaz-Alon, Y., Jalas, C., Matlock, A., Patel, K., Labbe, K., . . . Elpeleg, O. (2016). A mutation in the THG1L gene in a family with cerebellar ataxia and developmental delay. *Neurogenetics, 17*(4), 219-225. doi:10.1007/s10048-016-0487-z

Falkowska, A., Gutowska, I., Goschorska, M., Nowacki, P., Chlubek, D., & Baranowska-Bosiacka, I. (2015). Energy Metabolism of the Brain, Including the Cooperation between Astrocytes and Neurons, Especially in the Context of Glycogen Metabolism. *Int J Mol Sci, 16*(11), 25959-25981. doi:10.3390/ijms161125939

Fehrenbacher, J. C., Vasko, M. R., & Duarte, D. B. (2012). Models of inflammation: Carrageenan- or complete Freund's Adjuvant (CFA)-induced edema and hypersensitivity in the rat. *Curr Protoc Pharmacol, Chapter 5*, Unit5 4. doi:10.1002/0471141755.ph0504s56

Fiacco, T. A., Agulhon, C., & McCarthy, K. D. (2009). Sorting out astrocyte physiology from pharmacology. *Annu Rev Pharmacol Toxicol, 49*, 151-174. doi:10.1146/annurev.pharmtox.011008.145602

Flavell, S. W., & Greenberg, M. E. (2008). Signaling mechanisms linking neuronal activity to gene expression and plasticity of the nervous system. *Annu Rev Neurosci, 31*, 563-590. doi:10.1146/annurev.neuro.31.060407.125631

Foster, E., Wildner, H., Tudeau, L., Haueter, S., Ralvenius, W. T., Jegen, M., . . . Zeilhofer, H. U. (2015). Targeted ablation, silencing, and activation establish glycinergic dorsal horn neurons as key components of a spinal gate for pain and itch. *Neuron, 85*(6), 1289-1304. doi:10.1016/j.neuron.2015.02.028

Gangadharan, V., & Kuner, R. (2013). Pain hypersensitivity mechanisms at a glance. *Dis Model Mech, 6*(4), 889-895. doi:10.1242/dmm.011502

Gao, Y.-J., & Ji, R.-R. (2010). Targeting Astrocyte Signaling for Chronic Pain. *Neurotherapeutics*.

Garrison, C. J., Dougherty, P. M., Kajander, K. C., & Carlton, S. M. (1991). Staining of glial fibrillary acidic protein (GFAP) in lumbar spinal cord increases following a sciatic nerve constriction injury. *Brain Res, 565*(1), 1-7.

Ghiretti, A. E., Moore, A. R., Brenner, R. G., Chen, L. F., West, A. E., Lau, N. C., . . . Paradis, S. (2014). Rem2 is an activity-dependent negative regulator of dendritic complexity in vivo. *J Neurosci, 34*(2), 392-407. doi:10.1523/JNEUROSCI.1328-13.2014

Gibbs, M. E., Lloyd, H. G., Santa, T., & Hertz, L. (2007). Glycogen is a preferred glutamate precursor during learning in 1-day-old chick: biochemical and behavioral evidence. *J Neurosci Res, 85*(15), 3326-3333. doi:10.1002/jnr.21307

Gorlov, I. P., Meyer, P., Liloglou, T., Myles, J., Boettger, M. B., Cassidy, A., . . . Amos, C. I. (2007). Seizure 6-like (SEZ6L) gene and risk for lung cancer. *Cancer Res, 67*(17), 8406-8411. doi: 10.1158/0008-5472.CAN-06-4784

Greenberg, C. C., Danos, A. M., & Brady, M. J. (2006). Central role for protein targeting to glycogen in the maintenance of cellular glycogen stores in 3T3-L1 adipocytes. *Mol Cell Biol, 26*(1), 334-342. doi: 10.1128/MCB.26.1.334-342.2006

Greenberg, C. C., Meredith, K. N., Yan, L., & Brady, M. J. (2003). Protein targeting to glycogen overexpression results in the specific enhancement of glycogen storage in 3T3-L1 adipocytes. *J Biol Chem, 278*(33), 30835-30842. doi:10.1074/jbc.M303846200

Greenhaff, P. L., Soderlund, K., Ren, J. M., & Hultman, E. (1993). Energy metabolism in single human muscle fibres during intermittent contraction with occluded circulation. *J Physiol, 460*, 443-453.

Grudt, T. J., & Perl, E. R. (2002). Correlations between neuronal morphology and electrophysiological features in the rodent superficial dorsal horn. *J Physiol, 540*(Pt 1), 189-207.

Guan, Z., Kuhn, J. A., Wang, X., Colquitt, B., Solorzano, C., Vaman, S., . . . Basbaum, A. I. (2016). Injured sensory neuron-derived CSF1 induces microglial proliferation and DAP12-dependent pain. *Nat Neurosci, 19*(1), 94-101. doi:10.1038/nn.4189

Guerrero, R., Vernia, S., Sanz, R., Abreu-Rodriguez, I., Almaraz, C., Garcia-Hoyos, M., . . . Gomez-Garre, P. (2011). A PTG variant contributes to a milder phenotype in Lafora disease. *PLoS One, 6*(6), e21294. doi:10.1371/journal.pone.0021294

Guez-Barber, D., Fanous, S., Harvey, B. K., Zhang, Y., Lehrmann, E., Becker, K. G., . . . Hope, B. T. (2012). FACS purification of immunolabeled cell types from adult rat brain. *J Neurosci Methods, 203*(1), 10-18. doi:10.1016/j.jneumeth.2011.08.045

Gutierrez-Mecinas, M., Furuta, T., Watanabe, M., & Todd, A. J. (2016). A quantitative study of neurochemically defined excitatory interneuron populations in laminae I-III of the mouse spinal cord. *Mol Pain, 12*. doi:10.1177/1744806916629065

Hains, B. C., & Waxman, S. G. (2006). Activated microglia contribute to the maintenance of chronic pain after spinal cord injury. *J Neurosci, 26*(16), 4308-4317. doi:10.1523/JNEUROSCI.0003-06.2006

Halassa, M. M., Fellin, T., Takano, H., Dong, J. H., & Haydon, P. G. (2007). Synaptic islands defined by the territory of a single astrocyte. *J Neurosci, 27*(24), 6473-6477. doi:10.1523/JNEUROSCI. 1419-07.2007

Hald, A., Nedergaard, S., Hansen, R. R., Ding, M., & Heegaard, A. M. (2009). Differential activation of spinal cord glial cells in murine models of neuropathic and cancer pain. *Eur J Pain, 13*(2), 138-145. doi:10.1016/j.ejpain.2008.03.014

Hamai, M., Minokoshi, Y., & Shimazu, T. (1999). L-Glutamate and insulin enhance glycogen synthesis in cultured astrocytes from the rat brain through different intracellular mechanisms. *J Neurochem, 73*(1), 400-407.

Han, Y., Ren, J., Lee, E., Xu, X., Yu, W., & Muegge, K. (2017). Lsh/HELLS regulates self-renewal/ proliferation of neural stem/progenitor cells. *Sci Rep, 7*(1), 1136. doi:10.1038/s41598-017-00804-6

Harris, J. A. (1998). Using c-fos as a neural marker of pain. *Brain Res Bull, 45*(1), 1-8.

Hassel, B., Paulsen, R. E., Johnsen, A., & Fonnum, F. (1992). Selective inhibition of glial cell metabolism in vivo by fluorocitrate. *Brain Res, 576*(1), 120-124.

Hatashita, S., Sekiguchi, M., Kobayashi, H., Konno, S., & Kikuchi, S. (2008). Contralateral neuropathic pain and neuropathology in dorsal root ganglion and spinal cord following hemilateral nerve injury in rats. *Spine (Phila Pa 1976), 33*(12), 1344-1351. doi:10.1097/BRS.0b013e3181733188

Haueter, S. (2016). PKCγ and CCK expressing neurons in the spinal processing of somatosensory information. *Doctoral thesis, ETH, Switzerland*. doi:org/10.3929/ethz-a-010616057

Hertz, L., Peng, L., & Dienel, G. A. (2007). Energy metabolism in astrocytes: high rate of oxidative metabolism and spatiotemporal dependence on glycolysis/glycogenolysis. *J Cereb Blood Flow Metab, 27*(2), 219-249. doi:10.1038/sj.jcbfm.9600343

Hohlbaum, K., Bert, B., Dietze, S., Palme, R., Fink, H., & Thone-Reineke, C. (2017). Severity classification of repeated isoflurane anesthesia in C57BL/6JRj mice-Assessing the degree of distress. *PLoS One, 12*(6), e0179588. doi:10.1371/journal.pone.0179588

Hunt, S., P., & Mantyh, P., W. (2001). The molecular dynamics of pain control. *Nat Rev Neurosci, 2*(2), 83-91. doi:10.1038/35053509

Hunt, S. P., Pini, A., & Evan, G. (1987). Induction of c-fos-like protein in spinal cord neurons following sensory stimulation. *Nature, 328*(6131), 632-634. doi:10.1038/328632a0

Jacobsen, K. S., Zeeberg, K., Sauter, D. R., Poulsen, K. A., Hoffmann, E. K., & Schwab, A. (2013). The role of TMEM16A (ANO1) and TMEM16F (ANO6) in cell migration. *Pflugers Arch, 465*(12), 1753-1762. doi:10.1007/s00424-013-1315-z

Jancalek, R., Dubovy, P., Svizenska, I., & Klusakova, I. (2010). Bilateral changes of TNF-alpha and IL-10 protein in the lumbar and cervical dorsal root ganglia following a unilateral chronic constriction injury of the sciatic nerve. *J Neuroinflammation, 7*, 11. doi:10.1186/1742-2094-7-11

Ji, R.-R., Chamessian, A., & Zhang, Y.-Q. (2016). Pain regulation by non-neuronal cells and inflammation. *Science, 354*(6312), 572-577.

Ji, R.-R., & Wen, Y.-R. (2006). Neural-glial interaction in the spinal cord for the development and maintenance of nerve injury-induced neuropathic pain. *Drug Development Research, 67*(4), 331-338. doi:10.1002/ddr.20097

Jiang, Y., Gong, N. N., Hu, X. S., Ni, M. J., Pasi, R., & Matsunami, H. (2015). Molecular profiling of activated olfactory neurons identifies odorant receptors for odors in vivo. *Nat Neurosci, 18*(10), 1446-1454. doi:10.1038/nn.4104

Julius, D., & Basbaum, A., I. (2001). Molecular mechanisms of nociception. *Nature, 413*(6852), 203-210. doi:10.1038/35093019

Junghans, D., Heidenreich, M., Hack, I., Taylor, V., Frotscher, M., & Kemler, R. (2008). Postsynaptic and differential localization to neuronal subtypes of protocadherin beta16 in the mammalian central nervous system. *Eur J Neurosci, 27*(3), 559-571. doi:10.1111/j.1460-9568.2008.06052.x

Jurczak, M. J., Danos, A. M., Rehrmann, V. R., Allison, M. B., Greenberg, C. C., & Brady, M. J. (2007). Transgenic overexpression of protein targeting to glycogen markedly increases adipocytic glycogen storage in mice. *Am J Physiol Endocrinol Metab, 292*(3), E952-963. doi:10.1152/ajpendo.00559.2006

Kelsall, I. R., Voss, M., Munro, S., Cuthbertson, D. J., & Cohen, P. T. (2011). R3F, a novel membrane-associated glycogen targeting subunit of protein phosphatase 1 regulates glycogen synthase in astrocytoma cells in response to glucose and extracellular signals. *J Neurochem, 118*(4), 596-610. doi:10.1111/j.1471-4159.2011.07345.x

Kjell, J., Codeluppi, S., Josephson, A., & Abrams, M. B. (2014). Spatial and cellular characterization of mTORC1 activation after spinal cord injury reveals biphasic increase mainly attributed to microglia/macrophages. *Brain Pathol, 24*(6), 557-567. doi:10.1111/bpa.12135

Knight, Z. A., Tan, K., Birsoy, K., Schmidt, S., Garrison, J. L., Wysocki, R. W., . . . Friedman, J. M. (2012). Molecular profiling of activated neurons by phosphorylated ribosome capture. *Cell, 151*(5), 1126-1137. doi:10.1016/j.cell.2012.10.039

Koch, S. C., Acton, D., & Goulding, M. (2017). Spinal Circuits for Touch, Pain, and Itch. *Annu Rev Physiol*. doi:10.1146/annurev-physiol-022516-034303

Koehn, L. M., Noor, N. M., Dong, Q., Er, S. Y., Rash, L. D., King, G. F., . . . Habgood, M. D. (2016). Selective inhibition of ASIC1a confers functional and morphological neuroprotection following traumatic spinal cord injury. *F1000Res, 5*, 1822. doi:10.12688/f1000research.9094.2

Kohno, T. (2010). Neuropathic pain and neuron-glia interactions in the spinal cord. *J Anesth, 24*(2), 325-327. doi:10.1007/s00540-010-0918-1

Korhonen, J. M., Said, F. A., Wong, A. J., & Kaplan, D. R. (1999). Gab1 mediates neurite outgrowth, DNA synthesis, and survival in PC12 cells. *J Biol Chem, 274*(52), 37307-37314.

Kreutzberg, G. W. (1996). Microglia: a sensor for pathological events in the CNS. *Trends Neurosci, 19*(8), 312-318.

Kuhn, P. H., Colombo, A. V., Schusser, B., Dreymueller, D., Wetzel, S., Schepers, U., . . . Lichtenthaler, S. F. (2016). Systematic substrate identification indicates a central role for the metalloprotease ADAM10 in axon targeting and synapse function. *Elife, 5*. doi:10.7554/eLife.12748

La Porta, C., Bura, S. A., Aracil-Fernandez, A., Manzanares, J., & Maldonado, R. (2013). Role of CB1 and CB2 cannabinoid receptors in the development of joint pain induced by monosodium iodoacetate. *Pain, 154*(1), 160-174. doi:10.1016/j.pain.2012.10.009

LaMotte, R. H., Shimada, S. G., & Sikand, P. (2011). Mouse models of acute, chemical itch and pain in humans. *Exp Dermatol, 20*(10), 778-782. doi:10.1111/j.1600-0625.2011.01367.x

Lim, H., Lee, H., Noh, K., & Lee, S. J. (2017). IKK/NF-kappaB-dependent satellite glia activation induces spinal cord microglia activation and neuropathic pain after nerve injury. *Pain, 158*(9), 1666-1677. doi:10.1097/j.pain.0000000000000959

Lin, D., Boyle, M. P., Dollar, P., Lee, H., Lein, E. S., Perona, P., & Anderson, D. J. (2011). Functional identification of an aggression locus in the mouse hypothalamus. *Nature, 470*(7333), 221-226. doi: 10.1038/nature09736

Lin, J., Wang, C., & Redies, C. (2014). Restricted expression of classic cadherins in the spinal cord of the chicken embryo. *Front Neuroanat, 8*, 18. doi:10.3389/fnana.2014.00018

Lipman, N. S., Jackson, L. R., Trudel, L. J., & Weis-Garcia, F. (2005). Monoclonal versus polyclonal antibodies: distinguishing characteristics, applications, and information resources. *ILAR J, 46*(3), 258-268.

Liu, Q., Zheng, J., Yin, D. D., Xiang, J., He, F., Wang, Y. C., . . . Han, H. (2012). Monocyte to macrophage differentiation-associated (MMD) positively regulates ERK and Akt activation and TNF-alpha and NO production in macrophages. *Mol Biol Rep, 39*(5), 5643-5650. doi:10.1007/s11033-011-1370-5

Liu, Y., & Ma, Q. (2011). Generation of somatic sensory neuron diversity and implications on sensory coding. *Curr Opin Neurobiol, 21*(1), 52-60. doi:10.1016/j.conb.2010.09.003

Lovatt, D., Sonnewald, U., Waagepetersen, H. S., Schousboe, A., He, W., Lin, J. H., . . . Nedergaard, M. (2007). The transcriptome and metabolic gene signature of protoplasmic astrocytes in the adult murine cortex. *J Neurosci, 27*(45), 12255-12266. doi:10.1523/JNEUROSCI.3404-07.2007

Love, M. I., Anders, S., Kim, V., & Huber, W. (2015). RNA-Seq workflow: gene-level exploratory analysis and differential expression. *F1000Res, 4*, 1070. doi:10.12688/f1000research.7035.1

Lu, Y., Dong, H., Gao, Y., Gong, Y., Ren, Y., Gu, N., . . . Xiong, L. (2013). A feed-forward spinal cord glycinergic neural circuit gates mechanical allodynia. *J Clin Invest, 123*(9), 4050-4062. doi:10.1172/JCI70026

Lumpkin, E. A., & Caterina, M. J. (2007). Mechanisms of sensory transduction in the skin. *Nature, 445*(7130), 858-865. doi:10.1038/nature05662

Magistretti, P. J., & Allaman, I. (2007). Glycogen: a Trojan horse for neurons. *Nat Neurosci, 10*(11), 1341-1342. doi:10.1038/nn1107-1341

Magistretti, P. J., Sorg, O., Yu, N., Martin, J. L., & Pellerin, L. (1993). Neurotransmitters regulate energy metabolism in astrocytes: implications for the metabolic trafficking between neural cells. *Dev Neurosci, 15*(3-5), 306-312.

Mantyh, P., W., Rogers, S., D., Honore, P., Allen, B., J., Ghilardi, J., R., Li, J., . . . Simone, D., A. (1997). Inhibition of Hyperalgesia by Ablation of Lamina I Spinal Neurons Expressing the Substance P Receptor. *Science, 278*, 275–279.

Marcon, E., Jain, H., Bhattacharya, A., Guo, H., Phanse, S., Pu, S., . . . Edwards, A. M. (2015). Assessment of a method to characterize antibody selectivity and specificity for use in immunoprecipitation. *Nat Methods, 12*(8), 725-731. doi:10.1038/nmeth.3472

Matsui, T., Omuro, H., Liu, Y. F., Soya, M., Shima, T., McEwen, B. S., & Soya, H. (2017). Astrocytic glycogen-derived lactate fuels the brain during exhaustive exercise to maintain endurance capacity. *Proc Natl Acad Sci U S A, 114*(24), 6358-6363. doi:10.1073/pnas.1702739114

McNamara, C. R., Mandel-Brehm, J., Bautista, D. M., Siemens, J., Deranian, K. L., Zhao, M., . . . Fanger, C. M. (2007). TRPA1 mediates formalin-induced pain. *Proc Natl Acad Sci U S A, 104*(33), 13525-13530. doi:10.1073/pnas.0705924104

Medzhitov, R. (2008). Origin and physiological roles of inflammation. *Nature, 454*(7203), 428-435. doi:10.1038/nature07201

Meller, S. T., Dykstra, C., Grzybycki, D., Murphy, S., & Gebhart, G. F. (1994). The possible role of glia in nociceptive processing and hyperalgesia in the spinal cord of the rat. *Neuropharmacology, 33*(11), 1471-1478.

Meyuhas, O. (2008). Physiological roles of ribosomal protein S6: one of its kind. *Int Rev Cell Mol Biol, 268*, 1-37. doi:10.1016/S1937-6448(08)00801-0

Mickle, A. D., Shepherd, A. J., & Mohapatra, D. P. (2016). Nociceptive TRP Channels: Sensory Detectors and Transducers in Multiple Pain Pathologies. *Pharmaceuticals (Basel), 9*(4). doi:10.3390/ph9040072

Miller, G. (2005). Neuroscience. The dark side of glia. *Science, 308*(5723), 778-781. doi:10.1126/science.308.5723.778

Morgan, J. I., & Curran, T. (1991). Stimulus-transcription coupling in the nervous system: involvement of the inducible proto-oncogenes fos and jun. *Annu Rev Neurosci, 14*, 421-451. doi:10.1146/annurev.ne.14.030191.002225

Mozrzymas, J., Szczesny, T., & Rakus, D. (2011). The effect of glycogen phosphorolysis on basal glutaminergic transmission. *Biochem Biophys Res Commun, 404*(2), 652-655. doi:10.1016/j.bbrc.2010.12.033

Nam, Y., Kim, J. H., Kim, J. H., Jha, M. K., Jung, J. Y., Lee, M. G., . . . Suk, K. (2016). Reversible Induction of Pain Hypersensitivity following Optogenetic Stimulation of Spinal Astrocytes. *Cell Rep, 17*(11), 3049-3061. doi:10.1016/j.celrep.2016.11.043

Obel, L. F., Muller, M. S., Walls, A. B., Sickmann, H. M., Bak, L. K., Waagepetersen, H. S., & Schousboe, A. (2012). Brain glycogen-new perspectives on its metabolic function and regulation at the subcellular level. *Front Neuroenergetics, 4*, 3. doi:10.3389/fnene.2012.00003

Ohtsuka, T., Shimojo, H., Matsunaga, M., Watanabe, N., Kometani, K., Minato, N., & Kageyama, R. (2011). Gene expression profiling of neural stem cells and identification of regulators of neural differentiation during cortical development. *Stem Cells, 29*(11), 1817-1828. doi:10.1002/stem.731

Omri, B., Crisanti, P., Marty, M. C., Alliot, F., Fagard, R., Molina, T., & Pessac, B. (1996). The Lck tyrosine kinase is expressed in brain neurons. *J Neurochem, 67*(4), 1360-1364.

Parsons, M. P., & Hirasawa, M. (2010). ATP-sensitive potassium channel-mediated lactate effect on orexin neurons: implications for brain energetics during arousal. *J Neurosci, 30*(24), 8061-8070. doi:10.1523/JNEUROSCI.5741-09.2010

Patapoutian, A., Tate, S., & Woolf, C. J. (2009). Transient receptor potential channels: targeting pain at the source. *Nat Rev Drug Discov, 8*(1), 55-68. doi:10.1038/nrd2757

Peirs, C., Williams, S. P., Zhao, X., Walsh, C. E., Gedeon, J. Y., Cagle, N. E., . . . Seal, R. P. (2015). Dorsal Horn Circuits for Persistent Mechanical Pain. *Neuron, 87*(4), 797-812. doi:10.1016/j.neuron.2015.07.029

Pellerin, L., & Magistretti, P. J. (2012). Sweet sixteen for ANLS. *J Cereb Blood Flow Metab, 32*(7), 1152-1166. doi:10.1038/jcbfm.2011.149

Perl, E. R. (2007). Ideas about pain, a historical view. *Nat Rev Neurosci, 8*(1), 71-80. doi:10.1038/nrn2042

Petitjean, H., Pawlowski, S. A., Fraine, S. L., Sharif, B., Hamad, D., Fatima, T., . . . Sharif-Naeini, R. (2015). Dorsal Horn Parvalbumin Neurons Are Gate-Keepers of Touch-Evoked Pain after Nerve Injury. *Cell Rep, 13*(6), 1246-1257. doi:10.1016/j.celrep.2015.09.080

Phelps, C. H. (1972). Barbiturate-induced glycogen accumulation in brain. An electron microscopic study. *Brain Res, 39*(1), 225-234.

Picelli, S., Faridani, O. R., Bjorklund, A. K., Winberg, G., Sagasser, S., & Sandberg, R. (2014). Full-length RNA-seq from single cells using Smart-seq2. *Nat Protoc, 9*(1), 171-181. doi:10.1038/nprot.2014.006

Polgar, E., Hughes, D. I., Riddell, J. S., Maxwell, D. J., Puskar, Z., & Todd, A. J. (2003). Selective loss of spinal GABAergic or glycinergic neurons is not necessary for development of thermal hyperalgesia in the chronic constriction injury model of neuropathic pain. *Pain, 104*(1-2), 229-239.

Prescott, S. A., Ma, Q., & De Koninck, Y. (2014). Normal and abnormal coding of somatosensory stimuli causing pain. *Nat Neurosci, 17*(2), 183-191. doi:10.1038/nn.3629

Price, D. D., Mao, J. R., Coghill, R. C., d'Avella, D., Cicciarello, R., Fiori, M. G., . . . Hayes, R. L. (1991). Regional changes in spinal cord glucose metabolism in a rat model of painful neuropathy. *Brain Res, 564*(2), 314-318.

Printen, J. A., Brady, M. J., & Saltiel, A. R. (1997). PTG, a protein phosphatase 1-binding protein with a role in glycogen metabolism. *Science, 275*(5305), 1475-1478.

Qin, M., Wang, J. J., Cao, R., Zhang, H., Duan, L., Gao, B., . . . Rao, Z. R. (2006). The lumbar spinal cord glial cells actively modulate subcutaneous formalin induced hyperalgesia in the rat. *Neurosci Res, 55*(4), 442-450. doi:10.1016/j.neures.2006.04.017

Qin, R., Chen, Z., Ding, Y., Hao, J., Hu, J., & Guo, F. (2013). Long non-coding RNA MEG3 inhibits the proliferation of cervical carcinoma cells through the induction of cell cycle arrest and apoptosis. *Neoplasma, 60*(5), 486-492. doi:10.4149/neo_2013_063

Racz, I., Nadal, X., Alferink, J., Banos, J. E., Rehnelt, J., Martin, M., . . . Maldonado, R. (2008). Crucial role of CB(2) cannabinoid receptor in the regulation of central immune responses during neuropathic pain. *J Neurosci, 28*(46), 12125-12135. doi:10.1523/JNEUROSCI.3400-08.2008

Raghavendra, V., Tanga, F. Y., & DeLeo, J. A. (2004). Complete Freunds adjuvant-induced peripheral inflammation evokes glial activation and proinflammatory cytokine expression in the CNS. *Eur J Neurosci, 20*(2), 467-473. doi:10.1111/j.1460-9568.2004.03514.x

Richner, M., Bjerrum, O. J., Nykjaer, A., & Vaegter, C. B. (2011). The spared nerve injury (SNI) model of induced mechanical allodynia in mice. *J Vis Exp*(54). doi:10.3791/3092

Ronald, M., & Patrick, D., Wall. (1965). Pain Mechanisms: A New Theory. *Science, 150*.

Ruchti, E., Roach, P. J., DePaoli-Roach, A. A., Magistretti, P. J., & Allaman, I. (2016). Protein targeting to glycogen is a master regulator of glycogen synthesis in astrocytes. *IBRO Reports, 1*, 46-53. doi: 10.1016/j.ibror.2016.10.002

Saxena, A., Wagatsuma, A., Noro, Y., Kuji, T., Asaka-Oba, A., Watahiki, A., . . . Carninci, P. (2012). Trehalose-enhanced isolation of neuronal sub-types from adult mouse brain. *Biotechniques, 52*(6), 381-385. doi:10.2144/0000113878

Schmidt, R., Schmelz, M., Forster, C., Ringkamp, M., Torebjork, E., & Handwerker, H. (1995). Novel classes of responsive and unresponsive C nociceptors in human skin. *J Neurosci, 15*(1 Pt 1), 333-341.

Schuster, P., Fontana, W., Stadler, P. F., & Hofacker, I. L. (1994). From sequences to shapes and back: a case study in RNA secondary structures. *Proc Biol Sci, 255*(1344), 279-284. doi:10.1098/rspb. 1994.0040

Segerdahl, A. R., Mezue, M., Okell, T. W., Farrar, J. T., & Tracey, I. (2015). The dorsal posterior insula subserves a fundamental role in human pain. *Nat Neurosci, 18*(4), 499-500. doi:10.1038/nn.3969

Sha, L. Z., Xing, X. L., Zhang, D., Yao, Y., Dou, W. C., Jin, L. R., . . . Xu, Q. (2012). Mapping the spatio-temporal pattern of the mammalian target of rapamycin (mTOR) activation in temporal lobe epilepsy. *PLoS One, 7*(6), e39152. doi:10.1371/journal.pone.0039152

Shi, L. L., Zhang, N., Xie, X. M., Chen, Y. J., Wang, R., Shen, L., . . . Lu, H. Z. (2017). Transcriptome profile of rat genes in injured spinal cord at different stages by RNA-sequencing. *BMC Genomics, 18*(1), 173. doi:10.1186/s12864-017-3532-x

Sickmann, H. M., Waagepetersen, H. S., Schousboe, A., Benie, A. J., & Bouman, S. D. (2012). Brain glycogen and its role in supporting glutamate and GABA homeostasis in a type 2 diabetes rat model. *Neurochem Int, 60*(3), 267-275. doi:10.1016/j.neuint.2011.12.019

Siemiatkowska, A. M., van den Born, L. I., van Hagen, P. M., Stoffels, M., Neveling, K., Henkes, A., . . . Collin, R. W. (2013). Mutations in the mevalonate kinase (MVK) gene cause nonsyndromic retinitis pigmentosa. *Ophthalmology, 120*(12), 2697-2705. doi:10.1016/j.ophtha.2013.07.052

Sofroniew, M. V., & Vinters, H. V. (2010). Astrocytes: biology and pathology. *Acta Neuropathol, 119*(1), 7-35. doi:10.1007/s00401-009-0619-8

Soh, H., Pant, R., LoTurco, J. J., & Tzingounis, A. V. (2014). Conditional deletions of epilepsy-associated KCNQ2 and KCNQ3 channels from cerebral cortex cause differential effects on neuronal excitability. *J Neurosci, 34*(15), 5311-5321. doi:10.1523/JNEUROSCI.3919-13.2014

Song, K., Wang, H., Kamm, G. B., Pohle, J., Reis, F. C., Heppenstall, P., . . . Siemens, J. (2016). The TRPM2 channel is a hypothalamic heat sensor that limits fever and can drive hypothermia. *Science, 353*(6306), 1393-1398. doi:10.1126/science.aaf7537

Sorg, O., & Magistretti, P. J. (1992). Vasoactive intestinal peptide and noradrenaline exert long-term control on glycogen levels in astrocytes: blockade by protein synthesis inhibition. *J Neurosci, 12*(12), 4923-4931.

Srinivasan, K., Friedman, B. A., Larson, J. L., Lauffer, B. E., Goldstein, L. D., Appling, L. L., . . . Hansen, D. V. (2016). Untangling the brain's neuroinflammatory and neurodegenerative transcriptional responses. *Nat Commun, 7*, 11295. doi:10.1038/ncomms11295

Suh, S. W., Bergher, J. P., Anderson, C. M., Treadway, J. L., Fosgerau, K., & Swanson, R. A. (2007). Astrocyte glycogen sustains neuronal activity during hypoglycemia: studies with the glycogen phosphorylase inhibitor CP-316,819 ([R-R*,S*]-5-chloro-N-[2-hydroxy-3-(methoxymethylamino)-3-oxo-1-(phenylmethyl)pro pyl]-1H-indole-2-carboxamide). *J Pharmacol Exp Ther, 321*(1), 45-50. doi: 10.1124/jpet.106.115550

Suzuki, A., Stern, S. A., Bozdagi, O., Huntley, G. W., Walker, R. H., Magistretti, P. J., & Alberini, C. M. (2011). Astrocyte-neuron lactate transport is required for long-term memory formation. *Cell, 144*(5), 810-823. doi:10.1016/j.cell.2011.02.018

Swanson, R. A. (2015). Brain glycogen--vestigial no more. Foreword. *Metab Brain Dis, 30*(1), 251-253. doi:10.1007/s11011-014-9596-2

Swanson, R. A., & Graham, S. H. (1994). Fluorocitrate and fluoroacetate effects on astrocyte metabolism in vitro. *Brain Res, 664*(1-2), 94-100.

Swanson, R. A., Morton, M. M., Sagar, S. M., & Sharp, F. R. (1992). Sensory stimulation induces local cerebral glycogenolysis: demonstration by autoradiography. *Neuroscience, 51*(2), 451-461.

Swanson, R. A., Yu, A. C., Chan, P. H., & Sharp, F. R. (1990). Glutamate increases glycogen content and reduces glucose utilization in primary astrocyte culture. *J Neurochem, 54*(2), 490-496.

Swartjes, M., Morariu, A., Niesters, M., Brines, M., Cerami, A., Aarts, L., & Dahan, A. (2011). ARA290, a peptide derived from the tertiary structure of erythropoietin, produces long-term relief of neuropathic pain: an experimental study in rats and beta-common receptor knockout mice. *Anesthesiology, 115*(5), 1084-1092. doi:10.1097/ALN.0b013e31822fcefd

Takashima, M., Ogawa, W., Hayashi, K., Inoue, H., Kinoshita, S., Okamoto, Y., . . . Kasuga, M. (2010). Role of KLF15 in regulation of hepatic gluconeogenesis and metformin action. *Diabetes, 59*(7), 1608-1615. doi:10.2337/db09-1679

Takazawa, T., & MacDermott, A. B. (2010). Synaptic pathways and inhibitory gates in the spinal cord dorsal horn. *Ann N Y Acad Sci, 1198*, 153-158. doi:10.1111/j.1749-6632.2010.05501.x

Tanga, F. Y., Raghavendra, V., Nutile-McMenemy, N., Marks, A., & Deleo, J. A. (2006). Role of astrocytic S100beta in behavioral hypersensitivity in rodent models of neuropathic pain. *Neuroscience, 140*(3), 1003-1010. doi:10.1016/j.neuroscience.2006.02.070

Tekkok, S. B., Brown, A. M., Westenbroek, R., Pellerin, L., & Ransom, B. R. (2005). Transfer of glycogen-derived lactate from astrocytes to axons via specific monocarboxylate transporters supports mouse optic nerve activity. *J Neurosci Res, 81*(5), 644-652. doi:10.1002/jnr.20573

Tjolsen, A., Berge, O. G., Hunskaar, S., Rosland, J. H., & Hole, K. (1992). The formalin test: an evaluation of the method. *Pain, 51*(1), 5-17.

Todd, A. J. (2010). Neuronal circuitry for pain processing in the dorsal horn. *Nat Rev Neurosci, 11*(12), 823-836. doi:10.1038/nrn2947

Todd, A. J. (2017). Identifying functional populations among the interneurons in laminae I-III of the spinal dorsal horn. *Mol Pain, 13*, 1744806917693003. doi:10.1177/1744806917693003

Torsney, C., & MacDermott, A. B. (2006). Disinhibition opens the gate to pathological pain signaling in superficial neurokinin 1 receptor-expressing neurons in rat spinal cord. *J Neurosci, 26*(6), 1833-1843. doi:10.1523/JNEUROSCI.4584-05.2006

Turnbull, J., DePaoli-Roach, A. A., Zhao, X., Cortez, M. A., Pencea, N., Tiberia, E., . . . Minassian, B. A. (2011). PTG depletion removes Lafora bodies and rescues the fatal epilepsy of Lafora disease. *PLoS Genet, 7*(4), e1002037. doi:10.1371/journal.pgen.1002037

Turnbull, J., Epp, J. R., Goldsmith, D., Zhao, X., Pencea, N., Wang, P., . . . Minassian, B. A. (2014). PTG protein depletion rescues malin-deficient Lafora disease in mouse. *Ann Neurol, 75*(3), 442-446. doi:10.1002/ana.24104

Valjent, E., Bertran-Gonzalez, J., Bowling, H., Lopez, S., Santini, E., Matamales, M., . . . Fisone, G. (2011). Haloperidol regulates the state of phosphorylation of ribosomal protein S6 via activation of PKA and phosphorylation of DARPP-32. *Neuropsychopharmacology, 36*(12), 2561-2570. doi:10.1038/npp.2011.144

Vilchez, D., Ros, S., Cifuentes, D., Pujadas, L., Valles, J., Garcia-Fojeda, B., . . . Guinovart, J. J. (2007). Mechanism suppressing glycogen synthesis in neurons and its demise in progressive myoclonus epilepsy. *Nat Neurosci, 10*(11), 1407-1413. doi:10.1038/nn1998

Waitt, A. E., Reed, L., Ransom, B. R., & Brown, A. M. (2017). Emerging Roles for Glycogen in the CNS. *Front Mol Neurosci, 10*, 73. doi:10.3389/fnmol.2017.00073

Walls, A. B., Sickmann, H. M., Brown, A., Bouman, S. D., Ransom, B., Schousboe, A., & Waagepetersen, H. S. (2008). Characterization of 1,4-dideoxy-1,4-imino-d-arabinitol (DAB) as an inhibitor of brain glycogen shunt activity. *J Neurochem, 105*(4), 1462-1470. doi:10.1111/j.1471-4159.2008.05250.x

Weisshaar, C. L., & Winkelstein, B. A. (2014). Ablating spinal NK1-bearing neurons eliminates the development of pain and reduces spinal neuronal hyperexcitability and inflammation from mechanical joint injury in the rat. *J Pain, 15*(4), 378-386. doi:10.1016/j.jpain.2013.12.003

Wende, H., Lechner, S. G., Cheret, C., Bourane, S., Kolanczyk, M. E., Pattyn, A., . . . Birchmeier, C. (2012). The transcription factor c-Maf controls touch receptor development and function. *Science, 335*(6074), 1373-1376. doi:10.1126/science.1214314

Won, R., & Lee, B. H. (2015). Contralateral Metabolic Activation Related to Plastic Changes in the Spinal Cord after Peripheral Nerve Injury in Rats. *Neural Plast, 2015*, 438319. doi:10.1155/2015/438319

Woolf, C., J., & Salter, M., W. (2000). Neuronal plasticity: increasing the gain in pain. *Science, 288*(5472), 1765-1768. doi:10.1126/science.288.5472.1765

Xu, Y., Lopes, C., Qian, Y., Liu, Y., Cheng, L., Goulding, M., . . . Ma, Q. (2008). Tlx1 and Tlx3 coordinate specification of dorsal horn pain-modulatory peptidergic neurons. *J Neurosci, 28*(15), 4037-4046. doi:10.1523/JNEUROSCI.4126-07.2008

Yamamoto, T., Higo, N., Sato, A., Nishimura, Y., Oishi, T., Murata, Y., . . . Kojima, T. (2011). SPP1 expression in spinal motor neurons of the macaque monkey. *Neurosci Res, 69*(1), 81-86. doi:10.1016/j.neures.2010.09.010

Yang, L., Liu, C. C., Zheng, H., Kanekiyo, T., Atagi, Y., Jia, L., . . . Bu, G. (2016). LRP1 modulates the microglial immune response via regulation of JNK and NF-kappaB signaling pathways. *J Neuroinflammation, 13*(1), 304. doi:10.1186/s12974-016-0772-7

Zeilhofer, H. U., Wildner, H., & Yevenes, G. E. (2012). Fast synaptic inhibition in spinal sensory processing and pain control. *Physiol Rev, 92*(1), 193-235. doi:10.1152/physrev.00043.2010

Zhang, Y., Chen, K., Sloan, S. A., Bennett, M. L., Scholze, A. R., O'Keeffe, S., . . . Wu, J. Q. (2014). An RNA-sequencing transcriptome and splicing database of glia, neurons, and vascular cells of the cerebral cortex. *J Neurosci, 34*(36), 11929-11947. doi:10.1523/JNEUROSCI.1860-14.2014

献给莉娜和阿莹

知我者，谓我心忧，不知我者，谓我何求